



Keele  
University

This work is protected by copyright and other intellectual property rights and duplication or sale of all or part is not permitted, except that material may be duplicated by you for research, private study, criticism/review or educational purposes. Electronic or print copies are for your own personal, non-commercial use and shall not be passed to any other individual. No quotation may be published without proper acknowledgement. For any other use, or to quote extensively from the work, permission must be obtained from the copyright holder/s.

# **Development of a novel doxorubicin delivery system for pancreatic cancer**



Jenan Jasim Mohammed AL-AMERI

**A thesis submitted in partial fulfilment of the  
requirements of Keele University for the degree of  
Doctor of Philosophy at the School of Pharmacy**

**March 2020**

## **ABSTRACT**

Pancreatic cancer is considered as the 4<sup>th</sup> most aggressive cancer in the Western world. There is a direct link between pancreatic cancer diagnosis and patient age with high occurrence of the disease happening in the 65-75-year age group. The majority of cases are diagnosed at the advanced stages, making curing of this disease unattainable and leading to high mortality rates. Problems related to treatment of cancer using traditional systemically delivered drugs are as a result of an ineffective absorption, bioavailability or high systemic toxicity resulting in unwanted side effects. Thus there is an unmet need for better, more efficient delivery systems causing an increased patient quality of life.

In this work a poly(allylamine) graft polymer modified with 5-(4-chlorophenyl)-1,3,4-oxadiazole-2-thiol hydrophobic pendant groups was developed. This polymer was capable of incorporation of metallic hybrid iron oxide-gold nanoparticles. The resultant magnetomicelles were capable not only of laser triggered heating but also carrying lipophilic drug molecules which we exploited in this work. In order to produce a heat triggered drug delivery system, a two new analogues of doxorubicin was created modifying the molecule with spermine or lipoic acid forming DOX-SP and DOX-LA respectively.

Magnetomicelle synthesis was confirmed using nuclear magnetic resonance spectroscopy, inductively coupled spectra – optical emission spectroscopy and fourier transform infrared spectroscopy. The aggregation behaviour was confirmed using photon correlation spectroscopy. Reversible drug incorporation was realised via linkage between the drug analogue linkers and the hybrid nanoparticle surface in the magnetomicelle. The magnetomicelles developed exhibited up to 59.21% drug release noticed at 44 °C after 24 h.

Cytotoxicity of the doxorubicin analogue formulations was tested on human pancreatic adenocarcinoma (BxPC3) cells. The unloaded nano-aggregates were incubated for 24 h with the cells and the cell viability was compared to control wells. The result revealed that 50% of the total cell number was viable (IC<sub>50</sub>) at 50  $\mu\text{g mL}^{-1}$  (PAA-Ox5-HNPs). These values revealed that the incorporation of the metallic HNPs

into the polymer backbone did not result in any significant increase in toxicity ( $p>0.001$ ).

“This thesis is the result of the author's original research. The copyright of this thesis belongs to the author under the terms of the United Kingdom Copyright Acts as qualified by Keele University. Due acknowledgment must always be made of the use of any material contained in, or derived from, this thesis.”

## **Acknowledgements**

I would like to express my true gratitude to Dr. Clare Hoskins, for being such an amazing supervisor and for her constant guidance and support throughout my Ph.D. and thesis preparation. Also, I would like to express my profound thanks to my co-supervisor, Dr. Anthony Curtis for his caring approach and the invaluable advice he has given to me.

I would also like to thank my late father for his constant support, who was unable to see the final result of my hard work.

I also would like to convey my thanks to the Iraqi Ministry of Higher Education and Scientific Research for giving me the opportunity to take this research project and for the constant support.

My special thanks will go to my husband and to my children (Ali and Noor) for their love, support, kindness and mostly for being patience. Special thanks to my family (parents, sisters and brothers) for showing loving patience and encouragement.

I would also like to share my thanks with Karrar Arab and Ali Alsuraifi for their kind help. I would also like to share my thanks with Mark, Simon, Reg, Gayle, Neil, Lisa, Karen and Melissa for their kind help and training.

I am also appreciative to all former and current members of the Nanopharmaceutics group, for their different kinds of support during my graduate studies and wish to express my thanks to them.

# Contents

CHAPTER ONE .....	1
1 GENERAL INTRODUCTION .....	1
1.1 General Introduction .....	2
1.1.1 Cancer.....	2
1.1.1.1 Pancreatic cancer .....	2
1.1.1.2 Types of pancreatic cancer .....	6
1.1.1.2.1 Adenosquamous carcinoma .....	6
1.1.1.3 Clinical presentation.....	7
1.1.1.4 Treatment of pancreatic cancer.....	8
1.1.1.5 Metastasis of evolution pancreatic cancer .....	10
1.1.2 Nanomedicine .....	10
1.1.3 Drug Solubility.....	14
1.1.4 Polymers for drug delivery .....	15
1.1.5 Types of polymeric constructs .....	16
1.1.5.1 Polymer–drug conjugates.....	16
1.1.5.2 Amphiphilic polymers.....	17
1.1.5.3 Block copolymer.....	19
1.1.5.4 Graft polymers .....	21
1.1.5.5 Star shaped polymers.....	24
1.1.5.6 Dendrimers.....	27
1.1.5.7 Stimuli response polymers (smart polymers).....	31
1.1.6 Magnetomicelles.....	32
1.1.7 Research Aim .....	35
CHAPTER TWO .....	37

2	SYNTHESIS, CHARACTERISATION AND OPTIMISATION OF POLYMERIC AMPHIPHILES FOR DRUG DELIVERY .....	37
2.1	Introduction .....	38
2.2	Aims and Objectives .....	42
2.3	Materials and method .....	43
2.3.1	Materials.....	43
2.3.2	Method .....	43
2.3.2.1	PAA-Ox5 Synthesis .....	43
2.3.2.2	Nuclear magnetic resonance spectroscopy (NMR) .....	44
2.3.2.3	Fourier transform infrared spectroscopy (FTIR) .....	44
2.3.2.4	Photon correlation spectroscopy and zeta potential measurement (PCS,ZS) .....	45
2.3.2.5	Critical aggregation concentration (CAC) as a function of PAA molecular weight .....	45
2.3.2.5.1	Critical aggregation concentration using methyl orange hydrophobic probe .....	45
2.3.2.5.2	Surface tension .....	46
2.3.2.6	Drug loading.....	46
2.3.2.6.1	Quantification of Propofol .....	47
2.3.2.6.2	Quantification of griseofulvin .....	48
2.3.2.7	<i>In vitro</i> drug release from nano-aggregates .....	49
2.4	Results .....	50
2.4.1	Synthesis and Characterisation of PAA-Ox5 .....	50
2.4.2	Critical aggregation concentration (CAC) .....	60
2.4.2.1	Methyl orange .....	60
2.4.2.2	Surface tension .....	61
2.4.3	Drug loading.....	65
2.4.3.1	Propofol .....	65
2.4.3.2	Griseofulvin.....	74

2.4.4	Drug release .....	81
2.4.4.1	Drug release of Propofol and Griseofulvin .....	81
2.5	Discussion .....	84
2.6	Conclusion.....	89
CHAPTER THREE .....		90
3	MAGNETIC IRON OXIDE GOLD HYBRID NANOPARTICLE FABRICATION AND MAGNETOMICELLE FORMATION .....	90
3.1	Introduction .....	91
3.1.1	Hybrid iron oxide core gold shell nanoparticles (HNPs) .....	92
3.2	Research aims .....	94
3.3	Materials and methods .....	95
3.3.1	Materials used .....	95
3.3.2	Synthesis of iron oxide nanoparticles .....	96
3.3.2.1	Coating of iron oxide nanoparticles with Poly(ethylenimine) .....	96
3.3.2.2	Gold seeding step.....	97
3.3.2.3	Gold coating process .....	98
3.3.3	Hybrid nanoparticle characterisation .....	98
3.3.3.1	Transmission electron microscopy (TEM) .....	98
3.3.3.2	Inductively coupled plasma –optical emission spectroscopy .....	98
3.3.3.3	UV/Visible spectroscopy.....	99
3.3.3.4	Photon correlation spectroscopy and zeta potential measurement .....	99
3.3.4	Incorporation of HNPs into PAA-Ox5 .....	99
3.3.5	Characterisation of PAA-Ox5 and PAA-Ox5-HNP Nano-aggregates .....	100
3.4	Results .....	100

3.4.1	Inductively Coupled Plasma-Optical Emission Spectroscopy (ICP- OES)	100
3.4.2	UV/Visible spectroscopy.....	101
3.4.3	Characterisation using TEM.....	102
3.4.4	Characterisation of PAA-Ox5-HNP .....	105
3.4.4.1	Surface tension .....	105
3.4.4.2	Photon correlation spectroscopy.....	106
3.5	Discussion .....	108
3.6	Conclusion.....	111
CHAPTER FOUR .....		112
4	SYNTHESIS AND CHARACTERISATION OF DOXORUBICIN ANALOGUES.....	112
4.1	Introduction .....	113
4.1.1	Doxorubicin.....	113
4.1.2	Polyamines.....	115
4.1.2.1	Spermine .....	117
4.1.3	Lipoic acid .....	118
4.2	Aims and Objectives .....	119
4.3	Materials and Methods .....	119
4.3.1	Materials.....	119
4.3.2	Method .....	120
4.3.2.1	Coupling of doxorubicin to spermine.....	120
4.3.2.2	Coupling of lipoic acid to doxorubicin .....	121
4.3.2.2.1	Activated the lipoic acid (step 1).....	121
4.3.2.2.2	Doxorubicin coupling to lipoic acid (step2) .....	121

4.3.2.3	Characterisation of Doxorubicin analogues .....	122
4.3.2.3.1	Melting point .....	122
4.3.2.3.2	Thin Layer Chromatography (TLC).....	123
4.3.2.3.3	<sup>13</sup> C NMR Spectrum .....	124
4.3.2.3.4	Mass Spectrometry .....	125
4.4	Result .....	125
4.4.1	Characterisation of doxorubicin -spermine derivative .....	125
4.4.1.1	TLC analyses of doxorubicin-spermine.....	125
4.4.1.2	FT-IR spectrum of doxorubicin – spermine .....	126
4.4.1.3	<sup>1</sup> H NMR spectrum of Doxorubicin with spermine.....	128
4.4.1.4	Mass Spectrometry .....	128
4.4.1.5	<sup>13</sup> C NMR Spectrum of DOX- SP .....	129
4.4.2	Characterisation of Doxorubicin – lipoic acid derivative .....	130
4.4.2.1	TLC analyses of doxorubicin-lipoic acid.....	130
4.4.2.2	FTIR spectrum of Doxorubicin – lipoic acid .....	131
4.4.2.3	<sup>1</sup> H NMR spectrum of DOX-LA.....	133
4.4.2.4	<sup>13</sup> C NMR Spectrum of Doxorubicin-lipoic acid (DOX-LA) .....	133
4.4.2.5	Mass Spectrometry .....	134
4.5	Discussion .....	135
4.6	Conclusion.....	136
CHAPTER FIVE.....		138
5	INCORPORATION OF ANALOGUES INTO POLYMERIC SYSTEMS AND POTENTIAL IN CANCER THERAPY .....	138
5.1	Introduction .....	139
5.1.1	MTT assay .....	141
5.2	Research aims .....	142
5.3	Materials and Methods .....	143

5.3.1	Materials used .....	143
5.3.2	Methods .....	144
5.3.2.1	Drug conjugation.....	144
5.3.2.2	HNP-DOX-Spermine and HNP-DOX-Lipoic acid loading into polymer.....	144
5.3.2.3	Quantification of doxorubicin.....	144
5.3.2.4	<i>In vitro</i> drug release study in aqueous media.....	145
5.3.3	Biological characterisation of nano-aggregates and formulation .....	146
5.3.3.1	MTT([3-(4,5-Dimethylthiazol-2-yl)2,5DiphenyltetrazoliumBromide]) cytotoxicity assay .....	146
5.3.3.2	<i>In vitro</i> thermo-responsive cytotoxicity assay .....	147
5.4	Results .....	147
5.4.1	Drug conjugation.....	147
5.4.2	Drug release of PAA-Ox5-HNPs- DOX-SP at different temperatures.....	148
5.4.3	Drug release of PAA-Ox5-HNPs- DOX-LA at different temperatures....	150
5.4.4	Biological characterisation of nano-aggregates and formulation .....	152
5.5	Discussion .....	155
5.6	Conclusion.....	160
CHAPTER SIX.....		162
6	GENERAL CONCLUSION.....	162
6.1	General Conclusion .....	163
REFERENCES.....		169

## List of figures

Figure 1-1: The pancreas location inside the body (Mayo foundation for medical education and research).....	3
Figure 1-2: Pancreatic cancer and its development.....	5
Figure 1-3: H&E staining with the typical trabecular pattern of a well-differentiated pNEN (Hruban & Wilentz. 2009). ....	7
Figure 1-4: Schematic diagram representing the mode of action of targeted multifunctional nanoparticle (NP) (Srinivasan <i>et al.</i> 2015). ....	12
Figure 1-5: Schematic representation of the varied architectures of block copolymers .....	19
Figure 1-6: Schematic representation of a graft polymer. ....	22
Figure 1-7: Schematic representation of star shaped polymers (Iatridi & Tsitsilianis,2011). ....	24
Figure 1-8: Structure of the PCL-PEEP star-shaped copolymer and micelles' development (Fonseca (2015 :11)). ....	26
Figure 1-9: Schematic representation of dendrimer structure (Science Photo Library / Alamy Stock Photo,2016) .....	28
Figure 1-10: The conjugate of Dox to a biodegradable dendrimer (Wang <i>et al.</i> 2012). 30	
Figure 1-11: Cataloguing of stimuli responsive polymers. (Ganesh,2014). ....	31
Figure 1-12: Schematic explanation of the nano-sized thermo-sensitive magnetic micelle for drug delivery.....	34
Figure 1-13: Fabrication of novel doxorubicin analogues for enhanced pancreatic cancer therapy. ....	36

Figure 2-1: Schematic explaining the micellization of copolymers and drug encapsulation inside polymeric micelle ( Hussein & Youssry, 2018). .....	39
Figure 2-2: Chemical structure of propofol, 2,6-diisopropylphenol (C <sub>12</sub> H <sub>18</sub> O) M.W (178.27 g/mol).....	41
Figure 2-3: Chemical structural of 7-Chloro-2',4,6-trimethoxy-6'B-methylspiro[ benzofuran-2( 3H)J '[ 21 cyclohexene ] -3,4'-dione(griseofulvin).....	41
Figure 2-4 Calibration curve of propofol at 229 nm. ....	48
Figure 2-5: Standard curve of griseofulvin .....	49
Figure 2-6: Chemical synthesis of PAA-Ox5.....	50
Figure 2-7: The spectra of 1H NMR spectroscopy of (A1) PAA 15kDa , (A2) PAA-Ox5 15 kDa carried out on 400MHz NMR at 25 °C .....	52
Figure 2-8: The spectra of 1H NMR spectroscopy of (B1) PAA 17.5 kDa, (B2)PAA-Ox5 17.5 kDa carried out on 400MHz NMR at 25 °C. ....	53
Figure 2-9: The spectra of 1H NMR spectroscopy of (C1) PAA 120 kDa, (C2)PAA-Ox5 .	54
Figure 2-10: The spectra of 1H NMR spectroscopy of (D1) PAA 900 kDa, (D2)PAA-Ox5 900 kDa carried out on 400MHz NMR at 25 °C. ....	55
Figure 2-11: The spectra of (A1) PAA 15kDa and (A2) PAA-Ox5 15kDa polymer structure using diamond tripped ATR-FTIR (64scan) .....	56
Figure 2-12: The spectra of (B1) PAA 17.5 kDa and (B2) PAA-Ox5 17.5 kDa polymer structure using diamond tripped ATR-FTIR (64scan) .....	57
Figure 2-13: The spectra of(C1) PAA 120 kDa and (C2)PAA-Ox5 120 kDa polymer structure using diamond tripped ATR-FTIR (64scan) .....	58
Figure 2-14: The spectra of (D1) PAA 900 kDa and (D2) PAA-Ox5 900 kDa polymer structure using diamond tripped ATR-FTIR (64scan) .....	59

Figure 2-15: Effect of PAA-Ox5 (15 kDa, 17.5 kDa ,120 kDa and 900 kDa on the peak absorbance of methyl orange at 465 nm (n=3, ave $\pm$ SD) .....	61
Figure 2-16: Surface Tension results for $\blacklozenge$ PAA 15 kDa , $\blacksquare$ PAA 17.5 kDa, $\blacktriangle$ PAA 120 kDa and $\times$ 900 kDa at 25 $^{\circ}$ C, (n=3, ave $\pm$ SD) .....	64
Figure 2-17: Drug loading of propofol representative spectra using HPLC.....	65
Figure 2-18: Drug loading of propofol in 0.25 % with Poly (allylamine) PAA (15 kDa) at RT (n=3).....	66
Figure 2-19: Drug loading of propofol in 0.25 % with Poly (allylamine) PAA (17.5 kDa) at RT (n=3).....	67
Figure 2-20: Drug loading of propofol in 0.25 % with Poly (allylamine) PAA (120kDa) at RT (n=3 ).....	68
Figure 2-21: Zeta potential and size of PAA 17.5 kDa (n=3) .....	69
Figure 2-22: Drug loading of Griseofulvin in 0.25 % with Poly(allylamine) PAA (15kDa) at room temperature, (n=3) .....	74
Figure 2-23: Drug loading of griseofulvin in 0.25 % with Poly (allylamine) PAA (17.5 kDa) at R. T, (n=3) .....	75
Figure 2-24: Drug loading of Griseofulvin in 0.25 % with Poly(allylamine) PAA (120kDa) at R . T, (n=3, $\pm$ SD) .....	76
Figure 2-25: The percentages of drug release of PAA 15 kDa ,PAA 17.5 kDa and 120 kDa with propofol at R .T , (n=3, $\pm$ SD) .....	81
Figure 2-26: The percentages of drug release of PAA 17.5 kDa at deferent temperature with propofol, (n=3, $\pm$ SD) .....	82
Figure 2-27: The percentages of drug release of PAA 15000 with griseofulvin at room temperature, (n=3).....	83

Figure 2-28: The percentages of drug release of griseofulvin with PAA-OX5-17.5 kDa from formulation at different temperatures(n=3).....	83
Figure 2-29: Mechanism of hydrophobic drug molecule encapsulation A) propofol and B) griseofulvin .....	84
Figure 2-30: Drug loading of propofol and griseofulvin in 0.25 % with Poly (allylamine) PAA at R.T, (n=3, $\pm$ SD).....	86
Figure 3-1: Schematic representation of gold Iron oxide hybrid nanoparticles.....	92
Figure 3-2: Schematic diagram of iron oxide NPS coated with PEI.....	97
Figure 3-3: ICP/OES standard calibration curves for A ) Fe and B) Au .....	100
Figure 3-4: A graph viewing the concentrations of Au and Fe in HNPs identified by ICP-OES.....	101
Figure 3-5: UV –Vis absorbance spectra of Fe <sub>3</sub> O <sub>4</sub> , Au seed , Fe <sub>3</sub> O <sub>4</sub> -PEI and HNPs .....	102
Figure 3-6: TEM images of A) iron oxide core.....	103
Figure 3-7: TEM images of iron core-PEI coating.....	103
Figure 3-8: TEM image of gold seeded iron NPs.....	104
Figure 3-9: TEM image of final HNPs.....	105
Figure 3-10: Surface tension (N/m) of PAA-Ox5-HNP(n=3, ave $\pm$ SD).....	106
Figure 3-11: TEM image of PAA-Ox5-HNPs nano-aggregates .....	108
Figure 3-12: Explain PEI-coated iron oxide core .....	109
Figure 4-1: Structure of doxorubicin .....	114
Figure 4-2 Doxorubicin intraction into DNA structure (Freeman ,2012). .....	114
Figure 4-3: Structures of naturally occurring polyamines: A spermine ,B spermidine and C putrescine .....	116
Figure 4-4: Chemical structure of lipoic acid .....	118

Figure 4-5: Synthesis of doxorubicin –spermine Reagents and conditions: deionized water, stirrer, 24 h.....	120
Figure 4-6: Activated the lipoic acid , Reagents and conditions: ethanol absolute reflux, stirrer, 24 h.....	121
Figure 4-7: Reaction between doxorubicin and lipoic acid, Reagents and conditions: ethanol absolute reflux, stirrer, 24 h .....	122
Figure 4-8: Diagram of TLC procedure .....	124
Figure 4-9: TLC plate of doxorubicin coupling to spermine (DOX-SP) post workup ....	126
Figure 4-10: FT-IR spectra obtained for the DOX-Spermine.....	127
Figure 4-11: <sup>1</sup> H NMR spectrum of doxorubicin with spermine in DMSO carried out using 400MHz NMR at 25 °C.....	128
Figure 4-12: Doxorubicin coupling to spermine .....	129
Figure 4-13: Mass spectra of DOX-SP .....	129
Figure 4-14: <sup>13</sup> C NMR spectrum of (c) DOX-SP (c), (a) Aliphatic hydrocarbons, (b) Amide group of DOX in DMSO- carried out using 400MHz NMR at 25 °C.....	130
Figure 4-15: Chromatogram of TLC plate of DOX-LA,(A) step 1,(B) step 2.....	131
Figure 4-16: FT-IR spectra of doxorubicin with lipoic acid (DOX-LA) .....	132
Figure 4-17: <sup>1</sup> H NMR spectrum of doxorubicin-lipoic acid in DMSO carried out using 400 MHz NMR machine at 20 °C .....	133
Figure 4-18: <sup>13</sup> C NMR spectrum of (c) DOX-LA (c), (a) Aliphatic hydrocarbons, (b) Amide group of DOX in DMSO- carried out using 400MHz NMR at 25 °C .....	134
Figure 4-19: Chemical structure of coupling DOX-LA.....	134
Figure 4-20: Mass spectra of coupling DOX-LA.....	135
Figure 5-1: Chemical structure of MTT.....	141

Figure 5-2: Calibration curve of doxorubicin at R.T .....	144
Figure 5-3: Drug release of PAA-Ox5-HNPs-DOX-SP at 20 ° C over 24 h(n=3)(SD±) ....	148
Figure 5-4: Drug release of PAA-Ox5-HNPs-DOX-SP at 37 ° C over 24 h (n=3) (SD±)...	149
Figure 5-5: Drug release of PAA-Ox5-HNPs-DOX-SP at 44 o C for 24 h (n=3)(SD±) .....	150
Figure 5-6: Drug release profile of PAA-Ox5-HNPs-DOX-LA at 20°C over 24 h (n=3)(SD±) .....	151
Figure 5-7: Drug release profile of PAA-Ox5-HNPs-DOX-LA at 20°C over 24 h (n=3) (SD±) .....	151
Figure 5-8: Drug release profile of PAA-Ox5-HNPs-DOX-LA at 20°C over 24 h (n=3)(SD±) .....	152
Figure 5-9: MTT assay graph show the effect of various concentrations of doxorubicin, PAA-Ox5-HNPs ,PAA-Ox5-HNPs-DOX-SP and PAA-Ox5-HNPs-DOX- on BxPC-3 cells in 37 ° C at 24 h time points (n=3) (±23%) .....	154
Figure 5-10: MTT assay graph show the effect of various concentrations of doxorubicin, PAA-Ox5-HNPs ,PAA-Ox5-HNPs-DOX-SP and PAA-Ox5-HNPs-DOX- on BxPC-3 cells in 44 ° C at 24 h time points (n=3) (±23%) .....	155
Figure 5-11: Explain interaction of positive amine groups of doxorubicin with the gold coating .....	156
Figure 5-12: Theoretical imagination of doxorubicin –spermine and -lipoic acid coupling to the surface of the hybrid iron oxide core gold shell nanoparticles.....	157
Figure 5-13: Drug release of PAA-Ox5-HNPs-DOX-SP in deferent temperature (n=3) (SD±) .....	158
Figure 5-14: Drug release of PAA-Ox5-HNPs-DOX-LA in deferent temperature (n=3) (SD±) .....	159

## List of tables

Table 2-1 Materials which is used to synthesize the PAA amphiphiles. ....	43
Table 2-2 Polymer solutions of $1\text{mgmL}^{-1}$ , $3\text{mgmL}^{-1}$ and $6\text{mgmL}^{-1}$ were organized in deionized water .....	48
Table 2-3 show the percentages of yield of PAA for different molecular weight. ....	51
Table 2-4 Show the PAA surface tension with water at $21^{\circ}\text{C}$ (n=3) .....	65
Table 2-5 Drug loading of propofol in 0.25 % with Poly (allylamine) PAA (15 kDa) at RT. ....	66
Table 2-6 drug loading of propofol in 0.25 % with Poly(allylamine) PAA (17.5 kDa)at RT .....	67
Table 2-7 Drug loading of propofol in 0.25 % with Poly (allylamine) PAA (120 kDa) at RT.....	68
Table 2-8 Zeta potential and size of Polymer (15 kDa with propofol) at R .T (n=3, $\pm\text{SD}$ ) .....	70
Table 2-9 Zeta potential and size of polymer (17.5 kDa with propofol) at RT(n=3, $\pm\text{SD}$ ) .....	71
Table 2-10 Zeta potential and size of Polymer (120,000)+ propofol at R .T (n=3, $\pm\text{SD}$ ). .....	72
Table 2-11 Zeta potential and size of Polymer (900.000)+ propofol at R .T (n=3, $\pm\text{SD}$ )	73
Table 2-12 Drug loading of griseofulvin in 0.25 % with Poly (allylamine) PAA (15 kDa) at RT.....	75
Table 2-13 Drug loading of griseofulvin in 0.25 % with Poly (allylamine) PAA (17.5 kDa) at RT.....	76

Table 2-14 Drug loading of griseofulvin in 0.25 % with Poly (allylamine) PAA (120 kDa) at RT.....	76
Table 2-15 Zeta potential and size of Polymer (15000)+ griseofulvin at R .T, (n=3, ±SD) .....	78
Table 2-16 Zeta and size potential of Polymer (17.500)+ griseofulvin at R .T. (n=3, ±SD). .....	79
Table 2-17 Zeta and size potential of Polymer (120,000)+ griseofulvin at R .T (n=3, ±SD).....	80
Table 3-1 Explain the materials which is used in synthesis and description of hybrid iron oxide core gold shell nanoparticles.....	95
Table 3-2 Zeta potential and PDI ,Hydrodynamic radius of nanoparticle solution of hybrid nanoparticle synthesis at different steps .....	107
Table 4-1 Materials used in drug analogue synthesis.....	119
Table 4-2 Summary of functional of DOX-SP. ....	127
Table 4-3 Summary of functional of DOX-LA. ....	132
Table 5-1 Materials used in corporation of analogues into polymeric and biological investigations. ....	143
Table 5-2 Preparation of Excipient Solutions for MTT assay .....	146

### List of equations

Equation 2-1 Rate of release of the drug. ....	50
Equation 4-1 Retardation factor .....	124

## Abbreviation

<b>PAA</b> .....	Polyallilamin
<b>DCC</b> .....	N,N'-Dicyclohexylcarbodiimide
<b>DCM</b> .....	Dichloromethane
<b>DMSO</b> .....	Dimethyl Sulfoxide
<b>Etoh</b> .....	Ethanol
<b>HNPS</b> .....	Hybrid Iron Oxide Core Gold Shell Nanoparticles
<b>HPLC</b> .....	High Performance Liquid Chromatography
<b>h</b> .....	Hour
<b>IR</b> .....	Infrared
<b>MeoH</b> .....	Methanol
<b>Min</b> .....	Minute
<b>ML</b> .....	Millilitres
<b>RBF</b> .....	Round bottom flask
<b>mmol</b> .....	Millimoles
<b>Ms</b> .....	Mass Spectrum
<b>NHS</b> .....	N-Hydroxysuccinimide
<b>NMR</b> .....	Nuclear Magnetic Resonance
<b>RT</b> .....	Room Temperature
<b>SP</b> .....	Spermine
<b>R</b> .....	Retention factor

**DOX-SP**..... Doxorubicin-Spermine

**LA** .....Lipoic acid

**DOX-LA**..... Doxorubicin-lipoic acid

**TAA**..... Triethylamine

**μm** ..... Micromole

**TEM** ..... Transmission Electron Microscope

**TLC** ..... Thin Layer Chromatography

**t** ..... Triplet

**UV** ..... Ultraviolet

**NPs**..... Nanoparticles

**PCS**..... Photon correlation spectroscopy

**PDI**.....Polydispersity index

**PEI**.....Polyethyleneimine

**Mp**.....Melting Point

**m**.....Multiplet

**S**.....Singlet

**PBS**.....Phosphate Buffered Saline

**RPMI-1640**.....Roswell Park Memorial Institute 1640 Medium

**IC50**.....Inhibitory Concentration

**SPR**.....Surface Plasmon Resonance

# CHAPTER ONE

## GENERAL INTRODUCTION

## **1.1 General Introduction**

### **1.1.1 Cancer**

Cancer is the uncontrolled proliferation of cells. A cell is the basic functional unit of all organisms. In normal physiology, dead cells are replaced with new cells to sustain growth and development. This process is controlled by genes, and mutation of the genes can lead to cancer. Cancer appears due to an accretion of mutations in the DNA over numerous cell divisions. Some of these mutations such as a mutation of the ( k-ras) gene might cause uninterrupted cell division leading to the formation of tumours (Reckamp *et al.* 2016; Almoguera *et al.* 1988). Many reasons have been stated for the emergence of cancer. According to Doctor Jeff Yancey at the University of Utah Cancer Learning Centre, some factors responsible for cancer include unhealthy diet, smoking, exposure to toxic chemicals and UV (Surh 2003; Yancik 2005; Moiseeva & Manson 2009; Cancer Research 2016).

#### **1.1.1.1 Pancreatic cancer**

The pancreas Figure 1-1 is one of the most important organs of the body. It is linked to the small intestine, behind the stomach and in front of the backbone. The pancreas contains enzymes that are critical for the digestion of fat, starch, proteins and carbohydrates. These juices produced by the pancreas pass through a special channel to the first part and then to the second part of the small intestine (Bardeesy & DePinho 2002).

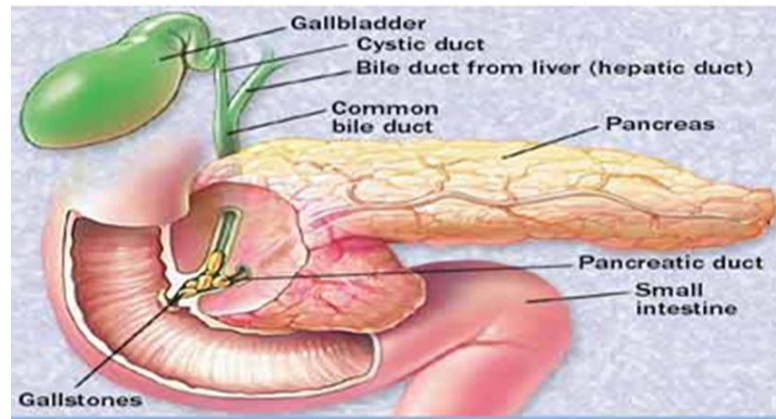


Figure 1-1: The pancreas location inside the body (Mayo foundation for medical education and research)

Pancreatic secretion consists of mineral salts and water to stimulate digestion and balance of acid in the stomach (Bardeesy & DePinho 2002).

Pancreatic cancer occurs as a result of genetic mutations that transform healthy cells into tumour cells. The increased death rates in pancreatic cancer are due to the rapid proliferation of the cancerous cell to other surrounding tissues. Pancreatic cancer is very difficult to diagnose due to lack of specificity of symptoms. Hence often patients are unaware until the late stages where treatment options are limited (Bardeesy *et al* 2014) & (Mayo foundation for medical education and research).

Pancreatic cancer Figure 1-2 has been shown to be resistant to most of the known anticancer agents. The treatment of pancreatic cancer requires an efficient drug delivery system that will target the tumour site instead of the normal tissues (Dimou *et al* 2012). In order to develop more efficient and efficacious therapies for pancreatic cancer, there are two main considerations; these are tumour-specific molecular targets and advanced drug-delivery systems. These improvements would enable drugs

to be delivered specifically to tumour cells thus preventing the widespread systemic toxicity experienced with existing chemotherapies. Additionally, sustaining drugs within the therapeutic window over longer durations should lead to more effective treatments (Duncan 2006).

It is argued that the ability of low-molecular-weight drug molecules to stop tumour cell progression devoid of causing harm has been problematic in reality, most especially in cases of gastrointestinal, breast, lung and prostate cancers. The cause of this challenge is recognised to be as a result of ineffective pre-clinical models, non-existence of a specific drug in the clinical situation and the acquired difficulty of drug resistance. However, over the past decade or so increased knowledge base and interdisciplinary studies have led to developments within cancer therapy in the form of nano-based drug-delivery systems (Duncan 2006). This project hopes to design and fabricate novel drug delivery systems for pancreatic cancer therapy.

Generally, the foremost chemotherapeutic agents used for the therapy of pancreatic cancer are gemcitabine, 5-fluorouracil and the nucleotide analogues. Despite therapeutic interventions by researchers, the condition continues to resurface thus propelling the design of novel therapeutics for the treatment of cancer (David *et al* 2015).

Yang reported that liposomal gemcitabine is established as the recognized therapy for advanced pancreatic cancer which related to clinical advantages (Yang *et al* 2011). Graeser and colleagues designed a newly established liposomal formulation of gemcitabine GemLip, 36 nm; 47% entrapment in order to preserve the drug and to ensure passive tumour targeting. This GemLip was established in order to improve the

pharmacodynamics and pharmacokinetics compared with traditional gemcitabine, and demonstrated superior anti-tumoral action in orthotropic mouse models at much lower concentrations than free gemcitabine, and is powerfully active regarding metastases. The improved *in vivo* effectiveness of GemLip is associated with its sustained release and passive tumour targeting. Other liposomal formulations in preclinical stages as delivery systems for pancreatic cancer consist of clinically used chemotherapeutic elements such as adriamycin, 5-fluorouracil (5-FU) and irinotecan. The similar success could be achieved utilising integrin-binding peptide conjugated liposomes. The use of integrin is more active on the angiogenic endothelial cells. 5-FU and doxorubicin loaded in PEGylated cationic liposomes, which demonstrated an importantly better relation with human endothelial versus cells of pancreatic cancer, is designed. (Khan *et al* 2015) *In vitro* studies demonstrated improved development of 5-FU and inhibitory properties of doxorubicin. The propensity of PEGylated cationic liposomes to gather alongside vessels in pancreatic tumour in disparity to the tumour interstitial shows that liposomes could be utilized to transmit chemotherapeutic elements to tumour vasculature.

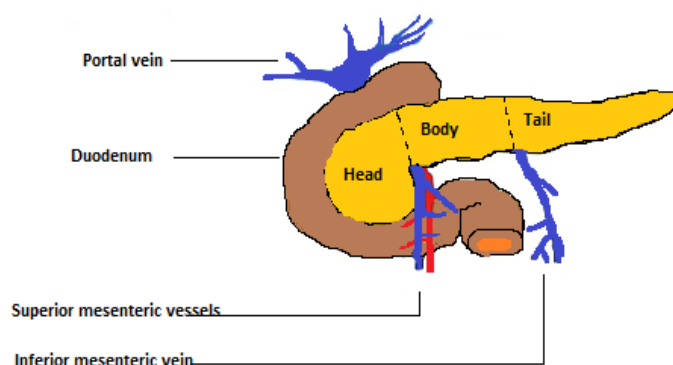


Figure 1-2: Pancreatic cancer and its development

### **1.1.1.2 Types of pancreatic cancer**

There are several factors causing pancreatic cancer, these include genetic syndromes, where the incidence of pancreatic cancer is 2% in adults and 10% in people aged 70 years or above (Bardeesy *et al.* 2014). There are many types of pancreatic cancer depending on the position of the pancreatic tumour. Therefore, pancreatic cancers are arranged based on the origin of the tumour into exocrine pancreatic tumour that ledge for approximately 95% of all pancreatic cancers where the tumour strikes the exocrine part of the pancreas and the endocrine pancreatic tumour which is inculpated in the endocrine part of the organ. Moreover, a range of rare pancreatic malignancies are examined, like; adenosquamous carcinoma and mucinous non-cystic carcinoma (Heining *et al* 2018).

#### **1.1.1.2.1 Adenosquamous carcinoma**

This is a carcinoma of the pancreas is a rare form of ductal adenocarcinoma that shows glandular and squamous differentiation Figure 1-3. Even though squamous characteristics in some cases predominate, careful examination almost always reveals a glandular component. These carcinomas often occur in patients who have received radiation or chemotherapy and This squamous component comprise at least 30% of the neoplasm. Due to relatively poor prognosis associated with this rare tumour, recognition is important (Weidner, 2009).

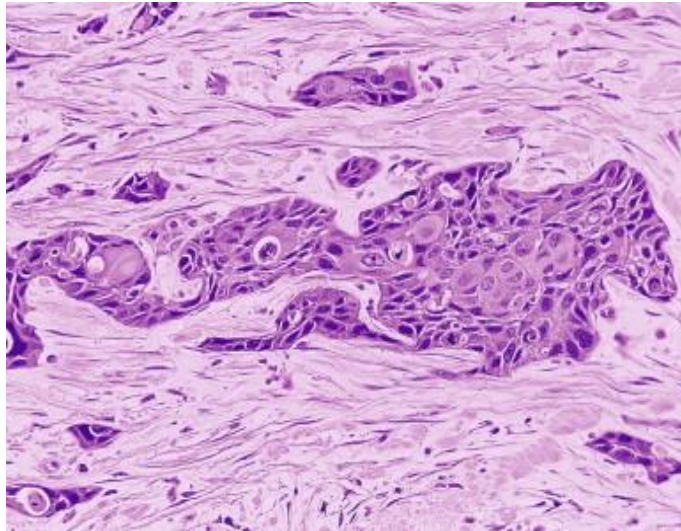


Figure 1-3: H&E staining with the typical trabecular pattern of a well-differentiated pNEN (Hruban & Wilentz. 2009)

The pancreas consists of three parts, the head, the body and the tail. The most common type is the one formed at the start of the head of the pancreas which is called pancreatic ductal adenocarcinoma (PDAC) (Hruban & Wilentz. 2009). Pancreatic cancer can be classified into four stages depending on the size of the tumour (Cancer research UK,2016).

#### **1.1.1.3 Clinical presentation**

Clinical display depends on the position of tumour and disease phase. Obstructive jaundice and weight loss are the most familiar presenting features of tumours in the head of the pancreas. Abdominal pain and weight loss are the most familiar presenting features of tumours emergent in the body and tail. Affliction is an essential clinical symptom stated as a deep, dull and aching pain originating from the upper abdomen and scattering to the back. Pancreatic cancer can cause alternative signs and symptoms such as asthenia, anorexia, hyperglycemia, abnormal liver function,

panniculitis and superficial venous thrombosis. Locally progressed tumours can cause gastric outlet obstruction, duodenal obstruction and rarely gastrointestinal bleeding (Hidalgo, 2010).

#### **1.1.1.4 Treatment of pancreatic cancer**

Pancreatic cancer can be classified as endocrine and exocrine neoplasm. Exocrine tumours constitute more than 95 % of all tumours diagnosed. The percentage of the endocrine type is very low at about 9 %.

Pancreaticoduodenectomy is the most effective form of treatment for pancreatic cancer in the early stage of the disease (where the disease has not spread to other parts of the pancreas) (Ferrone *et al.* 2012 & Shrikhande *et al.* 2007). Radiotherapy can also be used in the treatment of cancerous cells. Radiotherapy is a form of a curative treatment that uses high energy x-rays to target and destroy tumours and cancerous cells. Radiotherapy works along with chemotherapy which has side effect by targeting normal cells too, but usually, cancerous cells cannot repair themselves, unlike some normal cells. It is the less suggested and used cure than a surgery or even chemotherapy in treating pancreatic cancer.

The Radiotherapy can be given either:

- Before surgery to ease the fact to remove the tumour or the Neo-Adjuvant after shrinking it.

- After surgery, to make the tumour or the Neo-adjuvant small with less to no chance of coming back.

However, the fact that the Neo-adjuvant and adjuvant radiotherapy are still subject to experimental treatment, and aligning with chemotherapy to withdraw the cancer and make it under control is called chemo radiation (Shrikhande *et al.* 2007).

In addition to that, the radiotherapy has side effects and the common known ones are tiredness and bone pain. To minimize these effects, the treatment is split into twenty fractions given four times a week for example, the dosage of the radiotherapy given shorten the treatment sequences as well as relieving the symptoms of bone pain (Ferrone *et al.* 2012).

Targeting the cancerous cells or tumours by the radiotherapy requires a complex computer model, so the focus of targeting the tumour can be successful and improved. Moreover, Stereotactic radiotherapy which is a nonsurgical radiation therapy method used to target tumours with a high dosage although, it has the same side effects but in a shorter time.

Also, Cyberknife is another example of this type of therapy but with big potentials, lesser side effects even though there is no proof that it is more effective than the traditional treatment. IGRT which stand for “image guided radiotherapy” is for all types of radiotherapy for pancreatic cancer, and it requires taking images before and sometimes during treatments to help the delivery of an accurate delivery of the pancreatic cancer action (Oxford University Press. 2015).

Chemotherapy is another treatment option which involves using chemical substances to prevent growth of cancer cells (Avenida *et al.* 2015). Chemotherapy of cancerous tissues or tumours is used to curtail or shrink their size/volume.

#### **1.1.1.5 Metastasis of evolution pancreatic cancer**

Depending on the site of tumour, pancreatic cancer cells are classified into four stages

A. Stage 1: The damage is found only in the pancreas.

B. Stage 2: The disease develops to other parts closed to the pancreas such as the lymph nodes.

C. Stage 3: The disease spread to others parts, such as the spleen, abdomen, or large intestine.

D. Stage 4: This is an advanced stage of the disease. The disease spread to other parts of the body such as the lungs, the liver or stomach lining (Cancer research. 2017).

As expected, the chance of patient survival is highly dependant on stage at diagnosis. With those patients diagnosed with Stage 4 pancreatic cancer having a very slim chance of survival.

#### **1.1.2 Nanomedicine**

The use of nanomedicine is at the cutting edge of modern healthcare and represents a promising approach for targeted drug delivery and improved therapeutic efficacy (Miragol *et al.* 2018) Nanoparticles (NPs) is very small particulates in the  $1 \times 10^{-9}$  m range. NPs have the ability to inter relate with biological molecules both inside the cells and on the surface due to their size. This can help transform cancer diagnosis and treatment (Malekigorji, Curtis & Hoskins 2014, Soppimath *et al.* 2001 and Mccarroll *et al.* 2014). NPs possess multiple advantages over traditional delivery systems. These include decreased dosage requirements due to more effective absorption/penetration arising from increased solubility / bioavailability. Additionally, NPs result in reduced

side-effects, protection of drugs against premature metabolism or degradation hence improving drug stability. Furthermore, in cancer treatment the nanoparticles can undergo passive diffusion by an effect referred to as the Enhanced Permeability and Retention effect (EPR). EPR is experienced when the vasculature of cancerous tissue is mal-formed due to its rapid proliferation and nano-sized molecules possess the ability to permeate through tiny pores in the capillaries resulting in localised tumour accumulation. The poor lymphatic drainage of tumour tissues means the nanoparticles cannot escape and this results in effect targeting. (Liu, Miyosh , Nakamura. 2007 & Mccarroll *et al.* 2014).

Another main advantage of nanotechnologies specifically polymeric nanoparticles is their ease of functionalization Figure 1-4 (Srinivasan *et al.* 2015) . Their large surface area to volume ratio, dense surface and functional groups results in multiple sites for modification or addition of actively targeting moieties or proteins. Biocompatible and biodegradable monomers are used in polymers to ensure only non-harmful molecules like nitrogen, hydrogen and water is excreted from the body after the release of the encapsulated drug (Wissing *et al.* 2004 in Parveen & Sahoo (2008); Torchilin 2005 in Parveen & Sahoo. 2008).

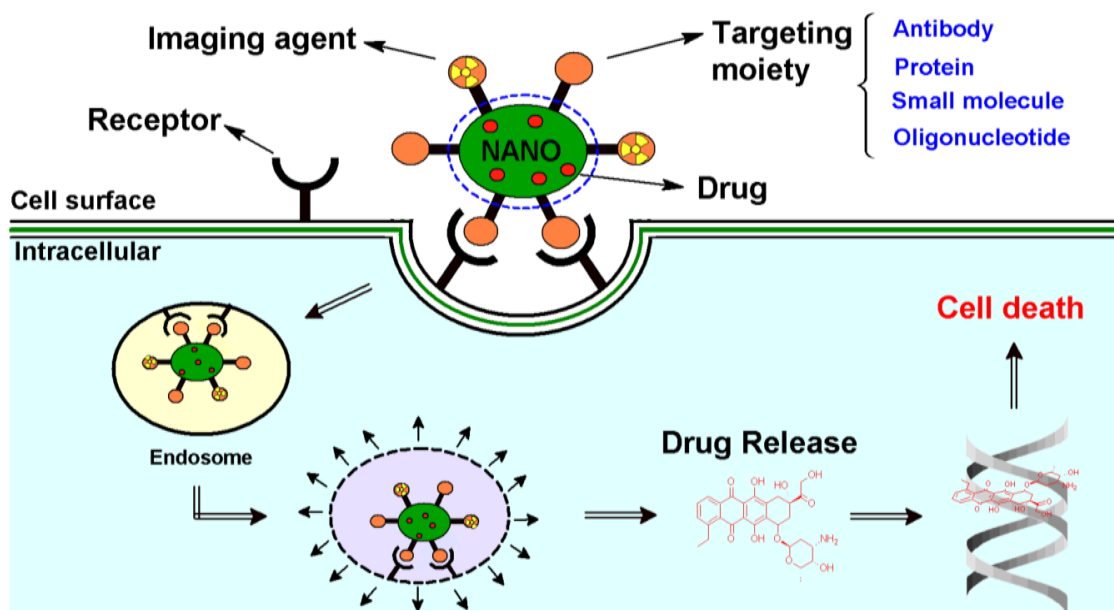


Figure 1-4: Schematic diagram representing the mode of action of targeted multifunctional nanoparticle (NP) (Srinivasan *et al.* 2015)

The use of nanoparticles in cancer therapy has been consistently shown to be more effective in preclinical studies compared to conventional therapies. Additionally, new advances have shown inclusion of imaging agents into the intrinsic structure of the nanoparticles enabling dual diagnosis and treatment in one platform (Liu, Miyosh & Nakamur. 2007). This suggests that nanoparticles have the ability to act as cellular probes for both diagnostic (imaging) and novel intravascular and therapeutic purposes (drug/gene delivery) and this is critical in modern medicine (Liu, Miyosh & Nakamura. 2007). In the aforementioned study, they reported the successful preparation of hollow mesoporous silica nanocapsules involving very tiny shells in the range of 3–10 nm. This ensured more than 70% ratio of the hollow core to nanocapsules, was encapsulated to achieve high drug concentrations. They used fluorescein isothiocyanate (FITC) as a model drug and looked at the loading and release *in vitro*.

The data showed that FITC in silica Nano capsules is released at a very slow space than free FITC. The FITC release went up at 1.5 h ( Miyosh & Nakamura. 2007).

Predominantly NPs are characterized by high solubility in water, so it can be used as a means of transport for insoluble drugs thus avoiding toxic solvents – although this is not possible on the metallic nanoparticles which require polymeric stabilisation themselves (Srinivasan *et al.* 2015). Nanoparticles have the ability to penetrate minor capillaries and can be taken up by cells, which ensures drugs effectively accumulate at targeting locations. A continued and controlled discharge of drugs at target locations over a period of time is conceivable. Several nanosystems developed in this regard including micelles, liposomes polymeric nanoparticles of poly(D,L-lactide-coglycolide) (PLGA), silica nanoparticles and dendrimers, ( Miyosh & Nakamura .2007).

However, little is known to this date on the overall toxicity of nanoparticulates over long time periods when administered to the body. This is due to the relatively novel nature of the technology and the lack of little or no regulation. It is important to consider some downsides of this technology. Studies have shown that there is lack of enzymes which are capable of degrading the polymeric materials *in vivo*, hence, accumulation inside patients over long therapeutic regimes may result in localised or systemic toxicity (Lee *et al.* 2015). It is also noted that the high cost of production for some of the nanotechnologies especially liposomes is a serious issue for consideration in addition to the fact that it not appropriate for room temperature storage which might allow drug leakage owing to the unpredictability of phospholipids. Moreover, it permits reasonably small drug loading, drug leaking throughout storage and great water content of dispersions (70–99.9%) are said to characterise solid lipid

nanoparticles. It is important to note that the word nanotechnology relates to any particulate on the nanoscale which includes metals, biological molecules, polymers and other organic and inorganic substances. In the case of polymers, as long as the appropriate toxicological studies are performed in pre-clinical testing the systems should be valid for clinical application. It is clear from the above discussion the advantages far outweigh the disadvantage in the cancer therapy therefore the need for utilisation of the nanoparticle.

A study by Maskos and Stauber (2011) showed that there is a difference in the individual properties of the particles between the aggregates and agglomerates. Such as ionic strength, particle surface studying, solubility in water, size and shape, as well as the ability to consequent cellular interaction. In the aggregates, there are heterogeneous molecules and the different ingredients cannot be easily separated while in agglomerates, the forces that bind the molecules are the Van der Waals (VDW) forces and the surface tension in addition to the electrostatic forces. Key aspects previously neglected are aggregation conduct of nanoparticles in the biological environment (Maskos & Stauber.2011). Aggregation is a status that can be happen in protein-rich and electrolyte environments. Often a protein corona can form between the nanoparticle surface and the surrounding proteins – the extent of which is largely dependant on nanoparticle surface charge (Casals *et al.* 2012).

### **1.1.3 Drug Solubility**

Solubility is the ability of solid, liquid or gaseous compounds to dissolve in a suitable solvent. The solubility of compounds depends on the temperature, pressure and the solvent used. Some compounds completely dissolve, like methanol in water while

others materials have a poor solubility. Insoluble is a term referring to extremely poorly soluble compounds (Gajjar *et al.* 2012). Also the size and shape of the drug molecule affects the solubility of the drug.

Chemotherapies are often practically insoluble which hinders their clinical translation. Therefore, formulation strategies are required in order or allow these drugs to be administered in aqueous media and improve their chances in clinical trials.

#### **1.1.4 Polymers for drug delivery**

Polymers are large molecules (macromolecules) generated from smaller molecular units. These may exist in different architectures such as linear, randomly branched or highly branched in generations. The building blocks of polymers are referred to as 'monomers' (Nicholson 2012, Campbell 2000 and de Ilarduya & Gonzalez-Aseguinolaza, 2012).

The idea of using polymers in the development of therapeutic agents has been the focus of many studies in the past decade (Larson & Ghandehari, 2012). The interdisciplinary research relating to biomedical sciences and polymer chemistry led to the development of polymer-based nanomedicines enabling the diagnosis, management and treatment of cancer (Vicent & Duncan 2006). Cancer is said to be the third principal source of death in developed countries (after heart disease and stroke) and/or modern societies and second (after heart disease) in United State of America (Malekigorji, Curtis & Hoskins 2014, de Ilarduya 2012 & Liu, Miyosh & Nakamura

2007). It is fast growing to the deadliest disease in the world (Shroff & Vidyasgar 2013 & Lee, Loo, Traini and Young, 2015).

For polymers to be clinically relevant, the key aspects are that the polymer is water-soluble, non-immunogenic, non-toxic and safe at all stages of the delivery process including safe excretion (Schmaljohann 2006 & Yan, Zhuo & Zheng 2007). The term of polymer therapeutics is adopted to include different families of polymer-drug conjugates, polymer pro-drugs with polymer-associated delivery systems (Vicent and Duncan 2006 & Yan, Zhuo & Zheng 2001). Polymers are employed to convey 'the drug to targeted site in controlled manner, achieving the high-therapeutic efficacy' (Paramjot *et al.* 2015).

#### **1.1.5 Types of polymeric constructs**

Polymer constructs have shown great potential in cancer therapy. This can be through drug encapsulation, site-specific targeting or stimuli-responsive release of compounds. The family of 'Polymer therapeutic' has been described to include all the constructs utilizing 'water-soluble polymers' as constituents in the process of the design. These include polymer drug-conjugates, polymeric drugs, polymer-protein conjugates and polymeric micelles (Duncan *et al* 2006) & (Prabhu *et al.* 2015).

Platforms for polymeric nanoparticle are considered by their physicochemical composition, including polymeric micelle, nanoshell, polyerosome, solid polymeric nanoparticle, polymer-drug conjugates and dendrimer (Alexis *et al.* 2008:506).

##### **1.1.5.1 Polymer-drug conjugates**

Polymer-drug conjugates are systems where drug molecules are chemically conjugated onto long chain polymers *via* covalent linkages. At the moment there are more than 14

polymer-drug conjugates that have made it through the rigorous clinical evaluation, these are based on poly(glutamic acid) (PGA)-paclitaxel conjugates (CT-2303, OPAXIO®, initially known as Xyotax®) (Greco & Vicent 2009). Polymer-drug conjugates hold the potential to protect the drug from early degradation, an inhibit drug from prematurely releasing with the biological setting and improve the absorption of the drugs into the tissues (by means of improved permeability and retaining effected or active targeting). Drugs molecules possess the ability to be conjugated to water-soluble polymers or amphiphilic block copolymers through biodegradable ester or amide bonds. This increases water solubility, decrease removal from the reticulum endoplasmic system (RES), offer an extended circulation time, enhance pharmacokinetics and stimulate tumour targeting through improved permeability and retaining capability. In comparison, with polymeric nanoparticles, polymer–drug conjugates have the benefits of increased drug loading, improved stability and enhanced control over the drug release kinetics. Additionally, it is possible to conjugate the drugs onto the polymer structure *via* ‘smart’ or stimuli responsive linkers enabling drug release on demand (Paramjot *et al.* 2015 & Vicent 2007).

#### **1.1.5.2 Amphiphilic polymers**

Amphiphilic polymers consist of both hydrophilic and hydrophobic moieties (Hoskins,2010). Amphiphilic polymers over huge improvements over the low molecular weight surfactants in the process of drug solubilisation (Zhang & Kim 2015 & Santos *et al.* 2016). These surfactants are significant in recent drug delivery as they help in ‘the control of drug uptake and release rate and minimization of drug degradation and toxicity’ (Santos *et al.* 2016). The main parameters for amphiphilic polymer optimisation

in drug delivery are the type of hydrophilic/hydrophobic subunits and their relative sizes; as well as the ratio of hydrophilicity to hydrophobicity (Leser & Garli 2001).

Once inside an aqueous environment these systems spontaneously aggregate into core-shell structures due to a reduction in Gibbs free energy. The hydrophobic core of the nano aggregates has been exploited in numerous studies for the incorporation and hence solubilisation of poorly soluble drugs. Micelles forming colloidal dispersions from amphiphilic molecules can be in the range of ~20 nm-200 nm in diameter. The small size still results in increased circulation time, as well as tumour tissue penetration after extravasation when compared to larger macromolecular systems such as liposomes (Blanco *et al.* 2009 cited in Khan 2010). Degim and Celebi (2007 cited Khan 2010:60) state that 'the hydrophobic core found within micelles allows for the encapsulation and delivery of hydrophobic drugs which many can be used for chemotherapy. The solubilisation of hydrophobic drugs further eases the danger of drug aggregation in the process of intravenous administration and possible embolism formation' (Degim & Celebi, 2007 cited Khan 2010:60). Aliabadi indicated that the 'polymeric micelles are nanoscopic core/shell structures formed through self-assembly of amphiphilic block copolymers' (Aliabadi *et al.* 2008:619).

Larson and Ghandehari (2012) also indicate that micelles are colloidal particles which have a size of nearly 5-150 nm comprising self-assembled collections of amphiphilic molecules or surfactants. Lower concentrations of amphiphiles in aqueous media, occur as unimers in solution but as the concentration was improved, thermodynamic processes allows the formation of aggregates, which sequester hydrophobic drives into corelike structures enclosed by a hydrophilic corona or shell. The level of

concentration the aggregate occurs is usually known as the critical aggregation concentration (CAC). Amphiphilic molecules (in the form of unimers or micelles) have the potential to increase drug permeability through physiologic obstacles, defend the drug from cases of inactivation by its biologic backgrounds, reduce its toxicity, decrease the occurrence and robust of side effects, and reverse MDR (Garrec, Ranger & Leroux 2004).

Amphiphilic polymer can exist in several architectures. The most popular in drug solubilisation being the block copolymers and graft polymers.

### 1.1.5.3 Block copolymer

Block copolymers systems consisting of a hydrophobic segment attached to a hydrophilic segment in a linear fashion as show in Figure 1-5. These can be composed of two, three, four or multiple segments.

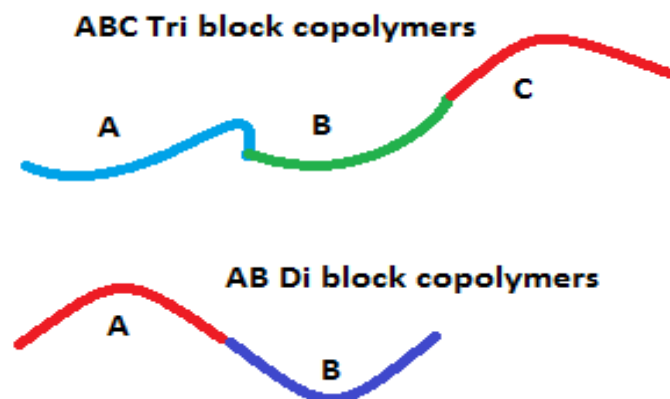


Figure 1-5: Schematic representation of the varied architectures of block copolymers

It has been demonstrated these nano-containers have the capability to encapsulate poorly soluble drugs, within their lipophilic core, via hydrophobic-hydrophobic

interactions. On their *in vivo* journey, the nano-carriers protect the drug payload from enzymatic degradation, leading to an efficient delivery to the target site. The most of the self-assembling polymers comprise of block copolymers are shaped largely through copolymerisation of hydrophobic and hydrophilic monomers (Hoskins *et al.* 2010).

Drugs loading is achieved by encapsulation of the drugs into the hydrophobic core when in the aqueous phase, additionally more sophisticated methods of encapsulation include adjusting surface elements of NPs, trapping drugs through chemical cross-linking, etc. A significant amount of polymeric NPs is in the preclinical stage for the transmission of cancer therapeutics to the unlimited likelihood for targeted delivery. Most especially in recent times the interest of engaging synthetic polymers like poly(ethylene glycol) (PEG), poly(lactide) (PLA), and poly(D,L-lactide-co-glycolide) (PLGA) is growing (Shroff & Vidyasagar (2013).

Numerous drugs have experienced great challenge in the ability to target their specific site of therapeutic need as a result of blood–brain barrier in the instance of central nervous system cancers. Drug-loaded NPs are capable of overcoming this barrier and have demonstrated to significantly improve therapeutic required that the concentrations of anticancer drugs in brain tumours (Koziara *et al.* 2004 in Parveen & Sahoo (2008); Steiniger *et al.* 2004 in Parveen & Sahoo (2008). Significantly, P-glycoprotein (P-gp)-associated multi-drug resistance is an added challenge that leads to the resistance of tumours to anticancer agents. The small size of NPs and suitable surface coating might have the capability to resolve the challenge of drug resistance (Feng &Chien 2003 in Parveen & Sahoo 2008).

Pluronics were the first commercially available amphiphilic polymers for universal drug solubilisation. Pluronics are block copolymers comprised of poly(ethyleneoxide) and poly(propylene oxide). Pluronics have been shown to enhance the oral bioavailability of the numerous drugs because of their capability to prevent the efflux carriers found on intestinal epithelial cells (Aliabadi 2008). Johnson *et al.* (2002 cited in Aliabadi, 2008) in their study made use of the intestinal uptake of digoxin and verapamil from rat jejunal tissue using Pluronic® P85. and it revealed that Pluronic® P85 inhibited both drug efflux and drug metabolism. This kind of inhibition was made possible as a result of 'reduced substrate uptake, direct inhibition of the cytochrome P450 3A4 enzyme or P-gp, or an indirect effect on the normal function and the permeability of cells' (Aliabadi 2008:622). Earlier studies discovered an upsurge 'in the oral bioavailability of amikacin and tobramycin antimicrobials that are P-gp substrates, in the presence of Pluronic® CRL-1605 in mice' (Aliabadi, 2008:622).

#### **1.1.5.4 Graft polymers**

Graft polymers are composed of a water soluble homopolymer backbone with hydrophobic groups randomly grafted on Figure 1-6 (Nicholson, 2012). In aqueous environments the hydrophobic groups shield themselves forming core-shell structures which like block copolymers are capable of solubilising poorly soluble drugs.

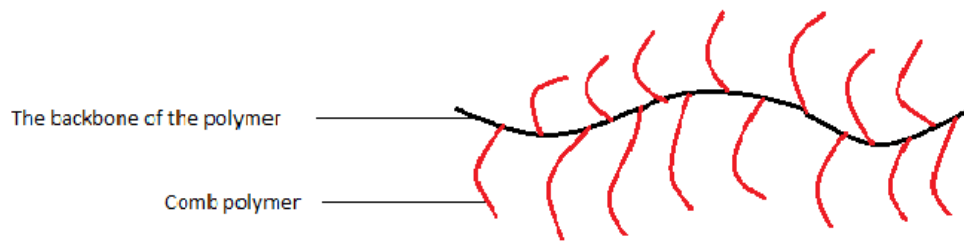


Figure 1-6: Schematic representation of a graft polymer

Usually, poly(allylamine), poly(ethylenimine) and chitosan backbones have been utilized in the formation of these amphiphiles. Studies have shown the potential of poly(allylamine) (PAA) grafted with cholesteryl and dansyl moieties to perform as universal hydrophobic drug solubilizers. Typical drugs in this instance include  $11\beta$ -11,17,21-trihydroxypregna-1, 2,6-diisopropylphenol (propofol), 4-diene-3, 20-dione (prednisolone) and (2S,6'R)-7-chloro-2',4,6-trimethoxy-6'-methyl-3H,4'H-spiro[1-benzofuran-2,1'-cyclohex[2]ene]-3,4'-dione (griseofulvin) (Barnet *et al.* 2014).

The major advantage of graft polymers over block copolymers is their ability not only to aggregate through intermolecular aggregation but also through intramolecular aggregation. This results in much lower CAC values which infers increased stability upon dilution and lower excipient: drug ratios making the overall system more efficient and cost effective.

In structural suitability relating to drug polymer interfaces (Gu *et al.* 2011) demonstrated that the chemical structure of the hydrophobic pendant group of the

amphiphilic graft copolymers has considerable impact of the solubilisation of poorly water-soluble drugs. Gu *et al.* 2011 indicated that 'the pendant group of graft copolymers could be the only hydrophobic moiety that will form the hydrophobic micro domains and contribute to the major interaction with the hydrophobic drug molecules'. Gu *et al.* Indicated that studies have shown that the supramolecular structures shaped through amphiphilic graft copolymers can change from polymeric micelle to solid nanoparticle resulting in an increase of hydrophobicity (Wang *et al.* 2004; Qu *et al.* 2008)& (Gu *et al.* 2011).

Hoskins *et al.* showed the potential of an aqueous polymer-drug formulation comprising of poly(allylamine)-cholesterol as drug carriers for pancreatic cancer therapy. The aggregates formed possessed a mean hydrodynamic size of 138 nm (Hoskins *et al.* 2010).

They formulated novel anticancer drug Bisnaphthalimidopropyldiaminooctane. The drug aqueous solubility was increased from negligible concentration to  $0.3 \text{ mgmL}^{-1}$ . The new polymer- drug formulation exhibited effectiveness *in vitro* and *in vivo* anticancer activity, whilst CH5-PAA polymer only could not show cytotoxicity, therefore the *in vivo* results showed that the CH5-PAA in isolation did not possess any anti-proliferate effect . However, the formulation showed related tumour reduction efficacy as gemcitabine does, therefore this formulation has the potential to function effectively in pancreatic cancer therapy (Hoskins *et al.*2010:1). A vital method in drug delivery strategy is related drugs can be targeted to precise organs, tissues or cells. In this process, the toxic side effects of the drugs in question is inhibited and the

circulation of drugs are altered after injection, to enhance the usefulness toward malignant cells, and decrease the drug dose (Yan *et al*, 2007).

#### 1.1.5.5 Star shaped polymers

Star shaped polymers have been reported for drug delivery for over a decade now because of their solution and solid-state properties as in Figure 1-7. The key characteristics of star-shaped polymers include its solid structure (for example radius of gyration and hydrodynamic volume) and a considerable concentration of functional terminal groups, giving them high solubility in common solvents, melt viscosities and lower solution, and modified thermal properties.

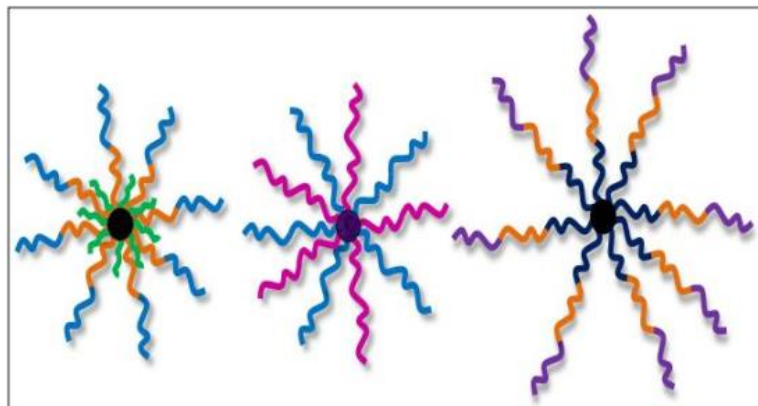


Figure 1-7: Schematic representation of star shaped polymers (Iatridi & T. Sitsilianis, 2011)

Rozga-Wijas successfully prepared two novel silsesquioxane based initiators for ring opening polymerization of L,L-dilactide. They were synthesized by thiol-ene addition of 6-mercapto-1-hexanol to mono- and octavinylsilsesquioxanes (Rozga-Wijas, 2015:4420). The mono- and multihydroxy silsesquioxane initiators could be

effective used for the synthesis of tailor-made biodegradable inorgano-organic star shape and linear polymers. The structure both of initiators and the respective polymer composites was proven by mass spectrometric analysis and systematic  $^1\text{H}$ ,  $^{13}\text{C}$  and  $^{29}\text{Si}$  NMR. Also, (Hart *et al.* 2014:8-9) In this work reported that 'both the comb and star copolymers exhibited significant degree of inter-lamellar bridging, as exemplified for this systems at the weight fraction 0.49 and  $\chi\text{N} = 175\text{x}'$ . (Fonseca *et al.* 2015) reportedly synthesized a star-shaped PCL which was again prolonged with a terminal block of poly(ethyl ethylene phosphate) (PEEP) to achieve a PCL-PEEP star-shaped copolymer. The copolymer demonstrated an effective capability to form micelles in aqueous solutions and was utilized to encapsulate DOX as show in Figure 1-8. The release *in vitro* examination demonstrated that DOX was delivered in a pH-dependent way, which was faster at pH = 5.4 than at physiological pH. The DOX-loaded micelles showed an improved cytotoxicity for both drug resistant human breast cancer cell positions (MCF-7) and drug-sensitive. The examination of the cellular absorption of the DOX-loaded micelles was ensured by the ways of confocal microscopy. An efficient fluorescence in the cytoplasm involving the cells demonstrates that the micelles were adopted via endocytosis. Significantly, the drug-resistant cells demonstrated greater cellular absorption than their drug-sensitive colleagues (Fonseca *et al.* 2015).

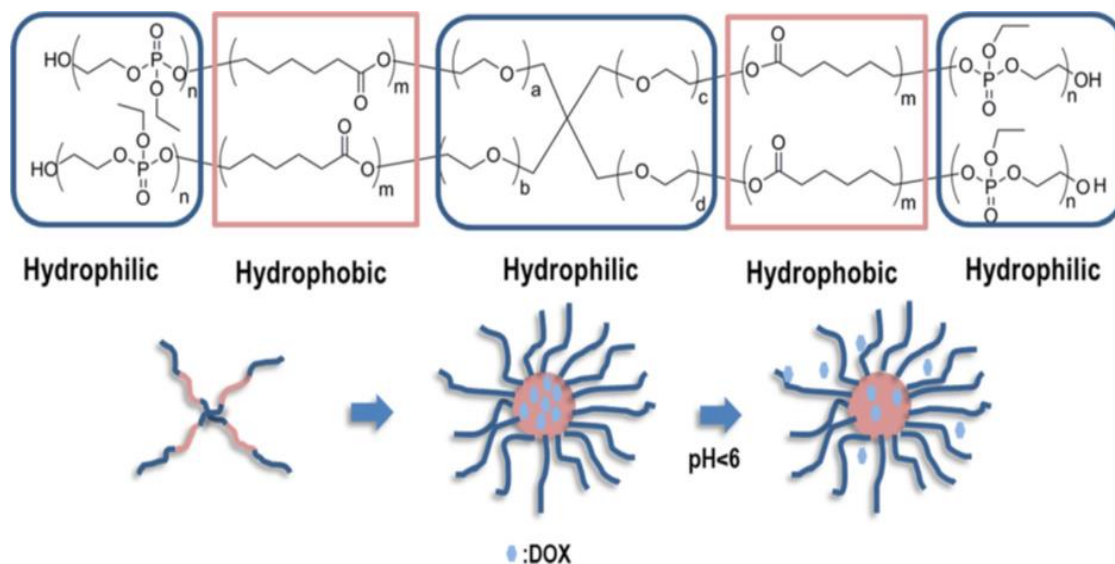


Figure 1-8: Structure of the PCL-PEEP star-shaped copolymer and micelles' development (Fonseca (2015 :11))

Boyer *et al.* reported that they developed and made cationic biodegradable star polymers utilizing DMAEMA (N,N-dimethyl aminoethyl methacrylate) as the monomer and reversible addition-fragmentation chain transfer RAFT polymerization to achieve an organised star polymers which are stable in water and soluble (Boyer *et al.* 2013). The polymers consisted advance amino collections alongside the polymer arms, which permitted for quick and effective self-assembly with siRNA. In this instance the star polymer–siRNA complexes were smaller and same in size and were nontoxic in both lung cancer cells and pancreatic. Also, the star polymer capably delivered siRNA to quiet target genes in both cancer cell types. Moreover, the star polymer was capable of transmitting good siRNA and silences its target gene in an *in vivo* mouse tumour ideal.

### **1.1.5.6 Dendrimers**

Nicolson stated that dendrimers are macromolecules consisting of many branches developed from one main point or centre Figure 1-9 (Nicolson ,2012). They are said to greatly mono disperse (characteristically polydispersities in the order of 1.02-1.04, it is however in some cases lower than 1.001). (De Ilarduya & Gonzalez-Aseguinolaza .2012) also describes dendrimers as branches macromolecules with tree shapes but variety of dendrimers can emerge during polymerisation process depending on its core structure. The branches emanating from the core of the molecule are nearly identical length thereby developing a globular morphology. Different dendrimers molecules consist of three different zones; they are the core, the branches and the end-groups (Nicolson, 2012).

Dendrimers have unique properties that include the capability to capture minor molecules in their central region and very little intrinsic viscosities in solution. These properties need molecules to have attained a specific size but not all molecules branching from central point are adequately huge to advance these distinctive properties of real dendrimers. Those branched molecules below this vital size are referred to as dendrons and are the comparable in dendrimer chemistry oligomers in polymer chemistry (Nicolson, 2012).

According to (Nicolson, 2012) dendrimers are often created by one of the two synthetic methods. The methods are the following;

- I. Growing resurgent from the central point, referred to as the divergent method. In this approach the potential dendrimer central point is made

first and the subsequent branches developed out of it by use of suitable methods of synthesis.

- II. Growing from the end-groups inward, referred to as the convergent method. In this approach the potential periphery of the molecule is developed first, subsequently the synthesis continues inwards in appropriate manner till the central point is finished.

In talking about the shapes and confirmation of dendrimer as demonstrated in (Nicolson,2012) states that they can either folded be in or at the external part of the dendrimer globule, which is referred to as the periphery. The shape or form it takes is influenced by the degree of strictness in the branching process. True dendrimers tend to be a globular structure and fairly rigid in nature whilst the interior appears to empty enabling it to accommodate guest molecules and sometimes nanoparticles (Nicolson, 2012).

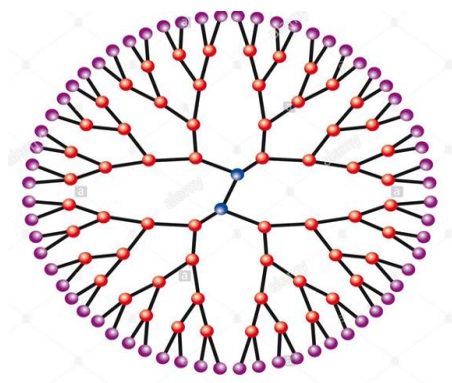


Figure 1-9: Schematic representation of dendrimer structure (Science Photo Library / Alamy Stock Photo,2016)

Dendrimers solubilise drugs in a different manner to the other polymeric systems. The drug molecules can be trapped in the inner hydrophobic core in polymeric micelles, whereas the surface shell is hydrophilic and soluble in aqueous media.

The family of dendrimers examined the most by researchers for drug delivery are the poly(amidoamine) (PAMAM) dendrimers. These PAMAM dendrimers are biocompatible, water-soluble, non-immunogenic and possess terminal-modifiable amine functional groups for holding various targeting or guest molecules together.

Pancreatic cancer researchers who are in search of treatment have demonstrated that drug delivery and tumour specific targeting which has the potential to prevent side effects is essential. Dendrimers show the potential for the delivery of platinum compounds in this process, making it a significant polymer in the treatment of pancreatic cancer (Yang *et al.* 2011 & Kesharwani *et al.* 2015). Current improvements in polymer and dendrimer chemistry have given a different class of molecules referred to as dendronized polymers, these are linear polymers that accept dendrons at each repeat unit. The attitude of these polymers differs from that of linear polymers and permit drug delivery benefits as a result of their improved circulation time. Additional method has been to synthesize the drug to the dendrimers in order to allow incorporating of a degradable relation that can further be used to control the release of the drug (Singh & Lillard Jr, 2012).

Lee *et al.* 2006 reported the careful design of size and molecular architecture was done which ensured that DOX was conjugated to a biodegradable dendrimer with enhanced blood circulation time. In this instance, the DOX-dendrimer controlled drug-loading using several attachment sites, solubility through PEGylation, and drug release

through the utilization of pH-sensitive hydrazone dendrimer linkages as in Figure 1-10 (Lee *et al.* 2006 cited in Singh & Lillard Jr, 2012). At the same instance in culture, 'DOX-dendrimers were >10 times less toxic than free DOX toward colon carcinoma cells'. Upon intravenous administration to tumour possessing mice, tumour absorption of DOX-dendrimers were nine-fold greater than intravenous free DOX and permitted comprehensive tumour recession and 100% existence of the mice afterwards 60 days.

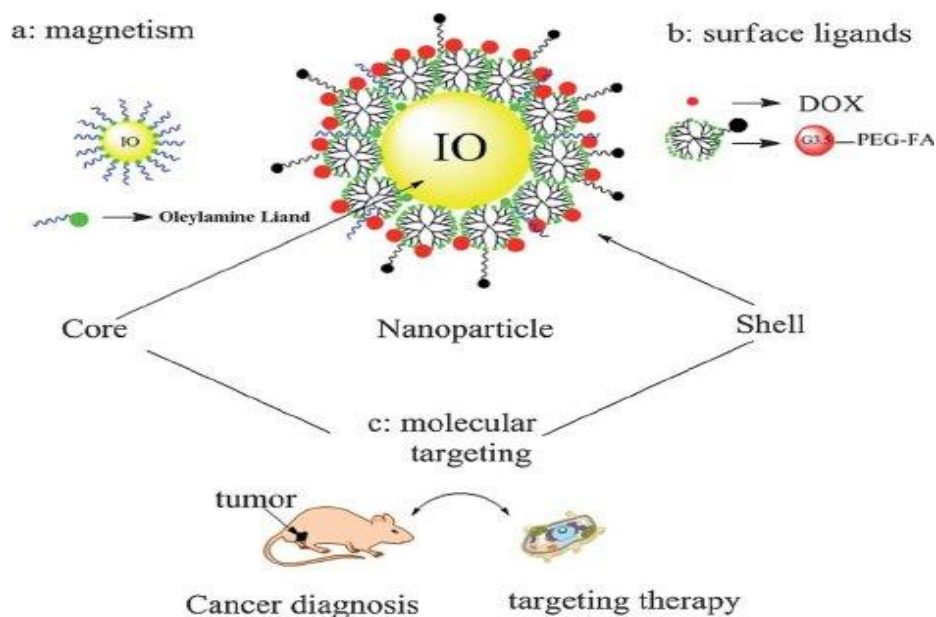


Figure 1-10: The conjugate of Dox to a biodegradable dendrimer (Wang *et al.* 2012)

Also, (Kesharwani *et al.* 2015) in their study used dendrimer related drug-delivery approach utilizing HA as targeting ligands to provide 3, 4-difluorobenzylidene curcumin (CDF) precisely to cells affected by pancreatic cancer. Also, a reduction of the cationic surface charge of the noble PAMAM was achieved thereby improving the possibility of its transformation at the clinical level.

### 1.1.5.7 Stimuli response polymers (smart polymers)

Stimuli responsive or 'smart' polymers Figure 1-11 possess unique properties whereby they undergo change (either chemical or physical) upon external or internal stimuli (Schmaljohann 2006). These properties can be exploited in drug delivery as a triggered release mechanism. These types of polymers can again be categorized depending on the stimuli they react to as: temperature, pH, ionic strength, light, electric and magnetic field sensitive. Some polymers react to a mixture of two or more stimuli (Meng & Li, 2013). (Gil & Hudson, 2004) Whilst categorizing the diverse stimuli use to moderate the response of polymer systems into two physical (such as cross-linked hydrogels, reversible hydrogels, modified interfaces, micelles and so on) or chemical stimuli (such as pH, ionic factors, chemical agents and so on), they state further that several names like intelligent, stimuli responsive, smart or environmental sensitive polymers have used to describe polymers stimuli response.

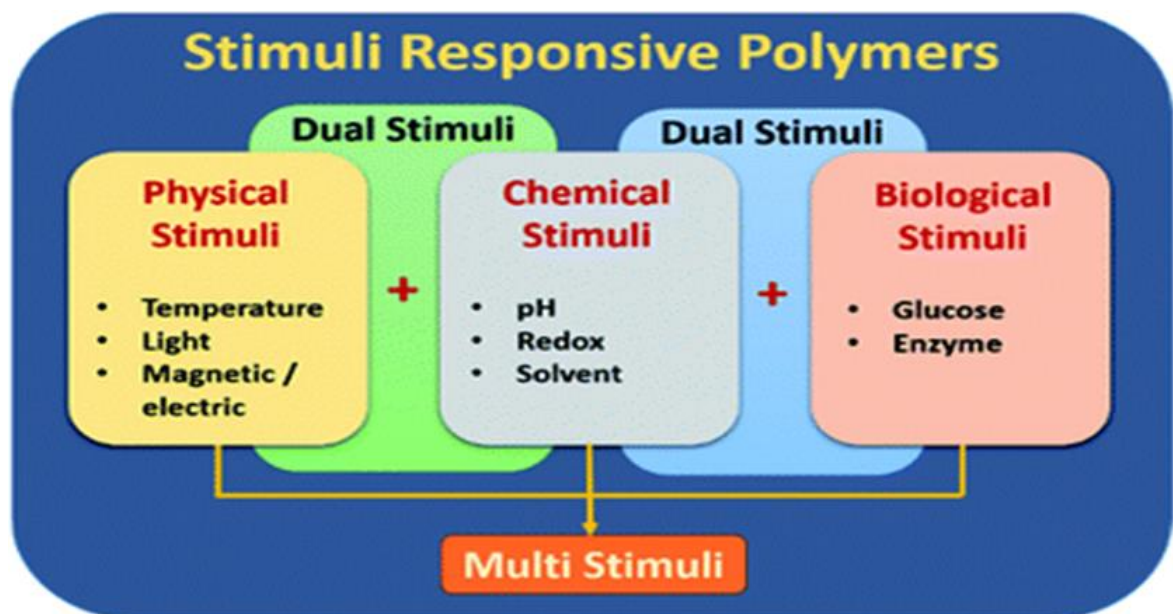


Figure 1-11: Cataloguing of stimuli responsive polymers. (Ganesh,2014)

Smart polymers have been designed to contain varieties of properties, including the its potential to react to changes occurring in the environmental stimuli for instance pH, ionic strength, temperature magnetic including electric fields or sound. This type of polymers react through conformational and/or electronic changes is the potential to be explored to aid a certain function (for example drug release and so on.) Those carriers that react to disparities in pH and temperature have created flexibility in drug delivery (Larson & Ghandehari, 2012).

In the application of stimuli response polymers in drug delivery it is observed that hyalouronic acid hydrogel that experiences photosensitized degradation in the existence of methylene blue permits the likely application of observable light-responsive hydrogels for temporal drug delivery can be largely grounded on the reaction of cross. Additional activation mechanism can be used of infrared light which elicits a response in hydrogels in the absence of chromophores. The key advantage of this method is the high infrared light absorbency of water which is key in this process. When hydrogels without chromophores are irradiated by CO<sub>2</sub> infrared laser the volume phase transition along with gel bending towards the laser beam is observed, while the relaxation of the gel to its original form after irradiation was terminated is followed (James, John, Alex & Anoop 2014).

### **1.1.6 Magnetomicelles**

Magnetomicelles are a new class of macromolecules comprising of amphiphilic polymers with magnetic iron oxide nanoparticles impregnated into their structure. The combination of the amphiphilic polymers with Inorganic metallic nanoparticles results

in a multifunctional platform image-guided drug delivery. Barnett *et al.* Reported of a poly(allylamine)-oxadiazole amphiphilic graft polymer with a gold coated iron oxide nanoparticle incorporated into the polymer structure (PAA-Ox5-HNP). The results show that once conjugation of metallic HNPs onto the polymer amphiphile structure, the drug loading is improved with an associated reduction in the *in vitro* drug release (Barnett *et al.* 2013).

Magnetic particles have exclusive characteristics it possible for different medical use. The most vital aspect of the magnetic particles is their response to a magnetic force, and this characteristic is used in cases of drug targeting and bio-separation as well as cell sorting. In recent times magnetic nanoparticles have gained attention as result of their ability as contrast agents for magnetic resonance imaging (MRI) and heating mediators for cancer treatment (hyperthermia) (Ito *et al.* 2005).

(Kim *et al.* 2008) reported that for the first time running, separately well-dispersed thermo-sensitive magnetomicelles with a size of around 18 nm, involving a functionalized Fe<sub>3</sub>O<sub>4</sub>-OA magnetic core and a thermo-sensitive amphiphilic P(OA-co-NIPAAm) surface layer, were developed and constructed. The ready designed Fe<sub>3</sub>O<sub>4</sub>-OA-*g*-P(OA-co-NIPAAm) magnetomicelles demonstrated temperature sensitivity with a LCST at 30.9 °C, as well as good magnetic character Figure 1-12.

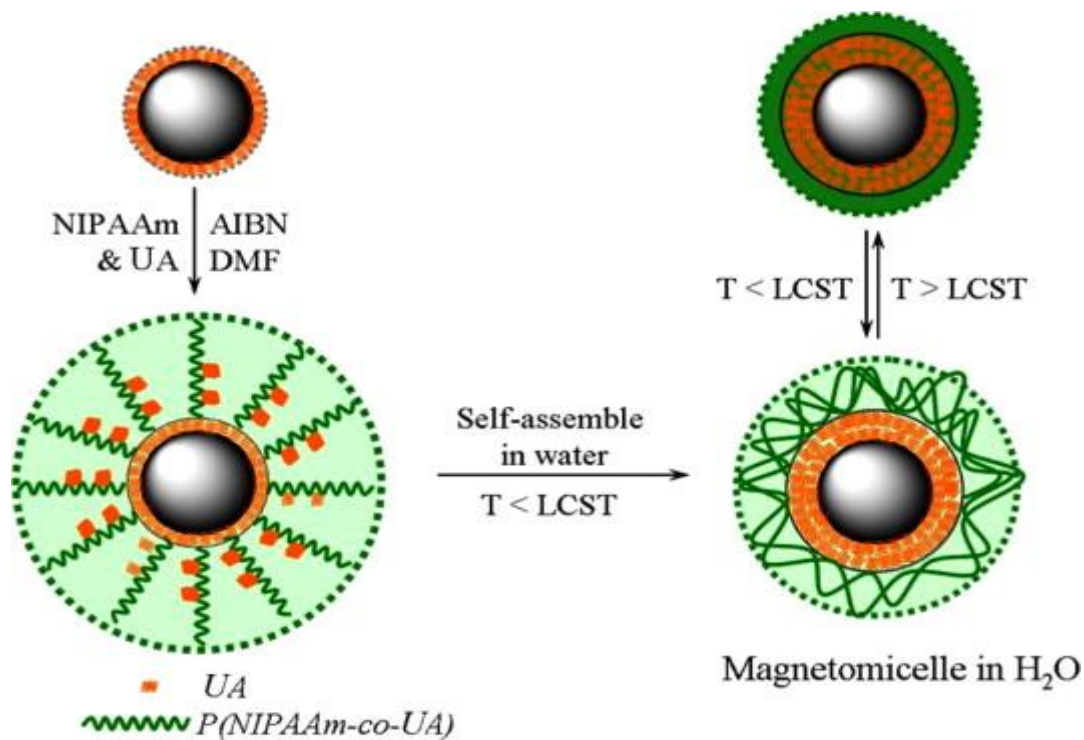


Figure 1-12: Schematic explanation of the nano-sized thermo-sensitive magnetic micelle for drug delivery

Controlled drug-release data showed that the  $\text{Fe}_3\text{O}_4\text{-OA-g-P(OA-co-NIPAAm)}$  magnetomicelles have the greatest possibility as thermo-sensitive drug carriers. Also, (Kim *et al.* 2005) reported that TEM images of the magnetomicelles showed that the number of encapsulated particles could be organized rationally by synthetic conditions. The magnetic elements of the particles were characterized by superconducting quantum interference device SQUID magnetometry and followed the overall Langevin magnetic model for superparamagnetic materials. The micellar shells of these particles were functionalized using covalent chemistry that would not usually be possible on the magnetic particle surface. The outcome of this has been that, this non-covalent method offers a new way to technological usage of

hydrophobic magnetic nanomaterials that lack appropriate conjugate surface chemistry.

### **1.1.7 Research Aim**

The aim of this work is to develop a thermally releasing magnetomicelle preparation for pancreatic cancer therapy.

To fulfil this aim, a novel PAA-oxadiazole graft polymer will be created into which a hybrid nanoparticle will be incorporated via dative covalent binding between the thiol of the oxadiazole pendant and the gold surface. The polymer will be chemically characterized using nuclear magnetic resonance (NMR) and fourier transform infrared (FTIR) spectroscopy. Ability of the polymers to aggregate in aqueous environments will be determined using photon correlation spectroscopy and surface tension measurement. Ability of the amphiphile to encapsulate hydrophobic drugs will be determined using model drugs propofol and griseofulvin and measured using high performance liquid chromatography (HPLC). Optimal PAA molecular weight for use as a drug delivery vehicle will be identified.

The organic synthesis will be carried out using established protocols from the literature. Structural analysis of the compounds will be carried out using nuclear magnetic resonance, Fourier transforms infrared spectroscopy and thin-layer chromatography.

Hybrid nanoparticle will form the basis for drug incorporation. Two novel doxorubicin analogues will be developed as in Figure 1-13. The organic synthesis will be carried out using established protocols from the literature. Structural analysis of the

compounds will be carried out using nuclear magnetic resonance, Fourier transforms infrared spectroscopy,  $^{13}\text{C}$  NMR spectrum and thin-layer chromatography. These will be capable of electrostatic attachment onto the hybrid nanoparticle within the micelle core of the nano-aggregate formed. It is hypothesised that upon laser irradiation, that the thermal energy required to break the electrostatic binding will be achieved resulting in localised drug release. This will be tested *in vitro*. Finally, *in vitro* evaluation of the system will be carried out in order to determine whether the novel heat triggered drug delivery will result in improved treatment in pancreatic cancer cell lines.

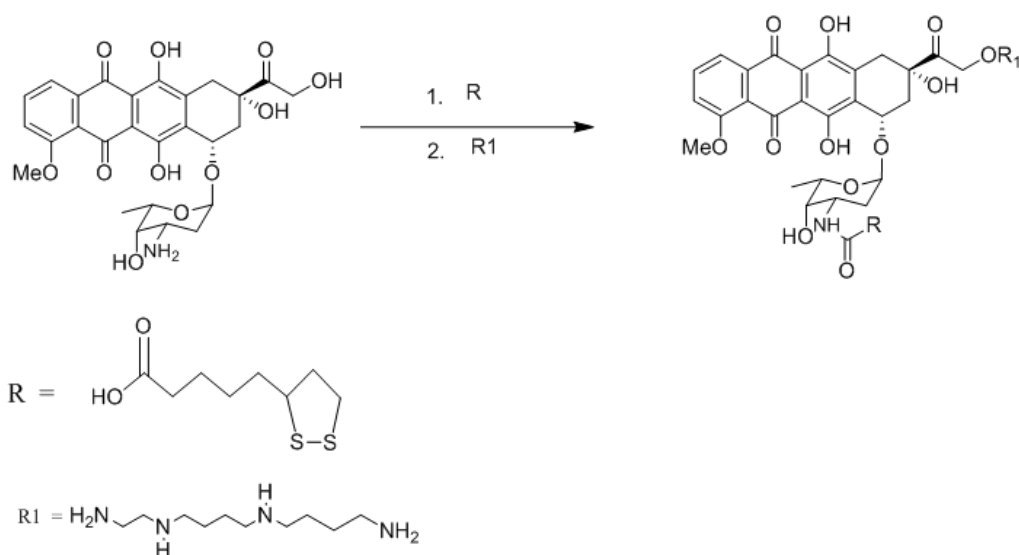


Figure 1-13: Fabrication of novel doxorubicin analogues for enhanced pancreatic cancer therapy

CHAPTER TWO

SYNTHESIS,  
CHARACTERISATION AND  
OPTIMISATION OF POLYMERIC  
AMPHIPHILES FOR DRUG  
DELIVERY

## 2.1 Introduction

Amphiphilic polymers have played a key role in the development of drug delivery technology by controlling long-term release of therapeutic factors hence stabilising doses. Polymeric nano-aggregate can be organised from different variety of architectures but of interest to this project are graft polymers and polymeric micelles. Graft polymers are composed of a water soluble homopolymer backbone with hydrophobic groups randomly grafted on (Nicholson 2012 & Barnett *et al.* 2013).

In the process of delivery of drugs to their target site and particularly for a number of anticancer drugs polymer micelles have been generally utilised as nano-sized vehicles for solubilizing several poorly soluble drugs. In this instance, the solubilization of poorly soluble drugs is largely reliant on hydrophobic relations between the drug and the micelle core (Kim *et al.* 2011).

Amphiphilic polymers consist of a hydrophilic and hydrophobic domain and have been generally explored in recent times. The amphiphilic molecules associate through weak non-covalent hydrophobic-hydrophobic interactions in aqueous environments whereas, the hydrophilic moiety will remain in connection with the aqueous phase whilst the hydrophobic moiety will 'shield' themselves, thereby forming a polymeric micelle. Amphiphilic polymers form a wide range of structures in aqueous environments including vesicles, polymeric micelles, and nanoparticles (Hoskins, 2010).

Amphiphilic polymers have the ability to encapsulate hydrophobic anticancer drugs inside their polymeric aggregates which spontaneously form in aqueous environments. Here, the inner core consists of the hydrophobic pendants surrounded by the

hydrophilic outer shell. Furthermore, the hydrophilic corona which forms *in vivo* can increase the polymeric aggregate stability in blood plasma allowing for increased circulation time and reduced opsonisation and capture by reticulo-endothelial system. Polymeric aggregates are well-known to possess lower critical micelle concentration (CAC) compared with the surfactant micelles, recording as low as  $10^{-6}$  M. All these points make polymeric aggregates a model carrier for anticancer drugs and tumour targeting as in Figure 2-1 (Neha *et al* 2013).

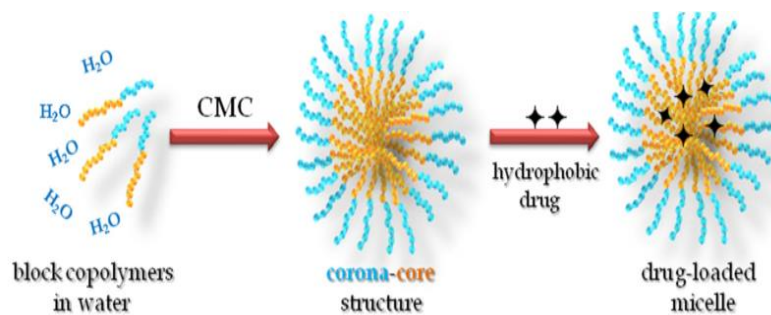


Figure 2-1: Schematic explaining the micellization of copolymers and drug encapsulation inside polymeric micelle ( Hussein & Youssry, 2018)

Poly(allylamine) has previously been investigated for its use as a drug delivery vehicle (Barnett *et al.* 2013). Poly(allylamine) (PAA) is a positively charged polymer that is to some extent non-toxic, making it an excellent model biomaterial to be explored in drug delivery. The cross-linked PAA is available clinically as an oral phosphate cover. Therefore, modification of PAA to form amphiphilic polymers has been explored for biomedical application (Hoskins, 2010). PAA can undergo chemical adjustment via its primary amine functional groups enabling grafting of a multitude hydrophobic moieties by a simple nucleophilic replacement reaction. Thompson and colleagues have reported that varying the hydrophobic groups on the PAA backbone had an

important impact on the polymer properties and the self-assemblies formed in the aqueous environment.

However, the effect on aggregation ability and solubilisation potential of varying its molecular weight have not been studied. Hence, in this work, we will develop a series of amphiphilic PAA polymers modified with hydrophobic pendant group oxadiazole. We will vary the molecular weight of the homopolymer backbone whilst maintaining 5% molar pendant substitution. Oxadiazole has been identified as a promising hydrophobic pendant group due to this thiol functionality which can be used to bind gold nanoparticulates – a quality which will be required further into this thesis.

In this work two model hydrophobic drugs will be investigated in order to estimate whether the amphiphiles created can be used for drug delivery. These are propofol and griseofulvin.

Propofol (6-diisopropylphenol) Figure 2-2 is used as an intravenous sedative. It was discovered in 1977 and approved for use in humans by the food and drug administration FDA in 1989. Propofol has not yet been earmarked as a controlled drug anywhere in the world except in Korea even though there is the possibility to obtain and abuse it (Kim *et al.* 2015). The chemical formula of propofol is  $C_{12}H_{18}O$  with molar mass is 178.271 g/mol (Muzi *et al.*1997). It is a small hydrophobic molecule with is currently administered in an oil based formulation. This is problematic because it causes pain on injection, hence an aqueous based formulation would be much more desirable.

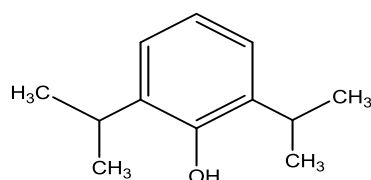


Figure 2-2: Chemical structure of propofol, 2,6-diisopropylphenol (C<sub>12</sub>H<sub>18</sub>O) M.W (178.27 g/mol)

Griseofulvin Figure 2-3 was discovered in 1939 (Stanton ,2001). It is insoluble in water but sparingly soluble in acids such as acetic acid, and in low molecular weight alcohols such as methanol and ethanol. Griseofulvin is used in the treatment of many dermatological diseases such as delicate skin and nails as well as scalp and the systematic treatment of inflamed lesions. The solubility of griseofulvin in water is very low (15 pg. /ml at 37 ° C) and this explains the incomplete absorption of the drug after oral administration. Several factors affect the absorption of the drug within the body such as fat intake, structure, particle size and the rate of dissolution (Lin & Symchowicz, 1975). The solubility of griseofulvin is extremely significant for its efficacy. Hydrophobicity of drugs is a major problem in clinical applications, thus the main focus is to enhance the solubility of the drug by reducing the particle size (Jambhrunkar, 2014).

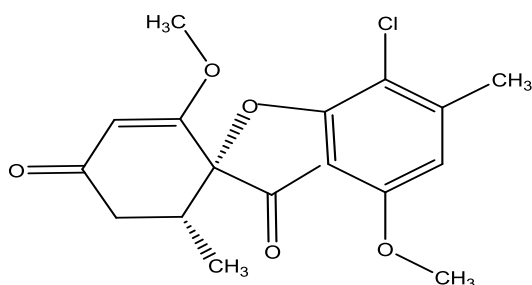


Figure 2-3: Chemical structural of 7-Chloro-2',4,6-trimethoxy-6'B-methylspiro[ benzo furan -2( 3H)J '[ 21 cyclohexene ] -3,4'-dione(griseofulvin)

## **2.2 Aims and Objectives**

The aim of this chapter was to fabricate a PAA based amphiphilic polymer capable of aggregate formation and hydrophobic drug solubilisation. The polymer will be synthesized and chemically characterized using nuclear magnetic resonance (NMR) and fourier transform infrared (FTIR) spectroscopy. Ability of the polymers to aggregate in aqueous environments will be determined using photon correlation spectroscopy and surface tension measurement. Ability of the amphiphile to encapsulate hydrophobic drugs will be determined using model drugs propofol and griseofulvin and measured using high performance liquid chromatography (HPLC). Optimal PAA molecular weight for use as a drug delivery vehicle will be identified.

## 2.3 Materials and method

### 2.3.1 Materials

The following materials in Table 2-1 were acquired for purposes of the project.

Poly(allylamine) (PAA) and 5-(4-chlorophenyl)-1,3,4-oxadiazole -2-thiol.

Table 2-1 Materials which is used to synthesize the PAA amphiphiles.

Item No	Materials	Supplier
1	Poly(allylamine) Hydrochloride ave.Mw 15 kDa, 17.5 kDa, 120 kDa, and 900 kDa.	Sigma-Aldrich Co., UK
2	5-(4-chlorophenyl)-1,3,4-oxadiazole-2- thiol (Oxadiazole)	Sigma-Aldrich Co., UK
3	Griseofulvin	Alfa Aesar
4	Propofol	Sigma-Aldrich Co.
5	Triethylamine.	Sigma-Aldrich Co., UK
6	Sodium hydroxide	Fisher Scientific, UK
7	Dialysis tubing membranes	Medical International Ltd, UK
8	Deuterated Methanol	Cambridge Isotope Laboratories Inc., USA
9	Methyl orange	Sigma-Aldrich Co., UK
10	Sodium Tetraborate	Sigma-Aldrich Co., UK
11	0.45µm GDX PVDF filters	Whatman, UK

### 2.3.2 Method

#### 2.3.2.1 PAA-Ox5 Synthesis

PAA was responded in 1:0.05 molar feed with 5-(4-chlorophenyl)-1,3,4-oxadiazole-2-thiol (Oxadiazole, Ox) (monomer: pendant) Figure 2.4. In short, the PAA dissolution

was achieved in 1:1 (v/v) (methanol 25 mL: chloroform 25 mL) with stirring for 10 min, subsequently Trimethylamine (2 mL) was added. The reaction that emanated was stirred at room temperature for 0.5 h. The dissolution of 5-(4-chlorophenyl)-1,3,4-oxadiazole-2-thiol was recorded in 1:1 (v/v) methanol(10 mL): chloroform(10 mL) and an additional drop wise to the polymer solution over 0.5 h. The response was stirred at 37 °C for 18 h. The using a rotary evaporator an evaporation of the solvent was done on a reduced pressure, the washing of polymer residue was done three times with (10 mL) diethyl ether and dried effectively. The dissolution of the residue was done in deionised water and thoroughly dialysed utilizing visking membrane 12-14 kDa against deionised water for 24 h.

### **2.3.2.2 Nuclear magnetic resonance spectroscopy (NMR)**

<sup>1</sup>H NMR was executed on all modified polymers in deuterated (D<sub>2</sub>O) (15 mg mL<sup>-1</sup>) at 25 °C, utilizing a Bruker 400 MHz Ultra shield NMR spectrometer (Bruker BioSpin, Germany). Sonication of models utilizing a Soniprep 150 (MSE Ltd, UK) was undertaken for 10 mins to ensure that the polymers were completely dissolved in the deuterated methanol earlier than the examinations.

### **2.3.2.3 Fourier transform infrared spectroscopy (FTIR)**

Fourier Transform Infrared Spectroscopy (FTIR) is a system which has been widely used by chemists to identify the presence of certain functional groups in a sample that can be in solids, liquids or gaseous state. FTIR spectroscopy offers qualitative and quantitative analysis for organic and inorganic compounds, polymers and polymer blends (Shaikh and Agrawal, 2014). In this chapter FTIR examinations of all the polymers was committed with a Perkin Elmer (Spectrum BX, UK), fitted with a

diamond powder tip. The polymers (5 mg) were placed under the diamond tip and 20 scans were run following a background correction.

#### **2.3.2.4 Photon correlation spectroscopy and zeta potential measurement (PCS,ZS)**

Particle size of the nano aggregates was measured using photon correlation spectroscopy and transmission electron spectroscopy. One of the important methods used to measure the surface charge of nanoparticles where the stability of these particles is determined by measuring the zeta potential.

Hydrodynamic diameters and zeta potential Density were completed using a photon correlation spectrometer (PCS, Zetasizer Nano-ZS, Malvern Instruments, UK). Models were Thinned in deionised water to make  $1 \text{ mgmL}^{-1}$  of polymer and sonicated for 30 s before calculating the size and surface charge of the polymer at 25 °C. 1 mL of sample was localized in screw-top glass vials and hydrodynamic radius, PDI and zeta potential of models were calculated during the synthesis process (Hoskins *et al.* 2012b).

#### **2.3.2.5 Critical aggregation concentration (CAC) as a function of PAA molecular weight**

##### **2.3.2.5.1 Critical aggregation concentration using methyl orange hydrophobic probe**

This approach was a reworking of Uchegbu's approach (Uchegbu & Schätzlein, 2006). A stock solution of methyl orange ( $25 \mu\text{M}$ ) was arranged with sodium tetraborate buffer (0.02 M, pH 9.4) in deionised water. The solution was settled in a sonic bath for 3h. Twenty two concentrations of altered polymers ( $0.0195 \text{ mgmL}^{-1}$  -  $5 \text{ mgmL}^{-1}$ ) were created using the methyl orange solution as the diluent. Each modal was probe sonicated for 10 min and allowed to cool for 5 min to room temperature. The polymer

solutions were examined in a UV-2600 UV-VIS(NIR) spectrometer (Shimadzu, Germany) and their maximum absorbance was reported (350 nm - 600 nm). The methyl orange stock solution was used as the control. The existence of hypochromic shift was resulted by contrasting the polymer solution wavelength maxima with the  $\lambda_{\max}$  of methyl orange stock solution (465 nm).

#### **2.3.2.5.2 Surface tension**

The measuring of surface tension of the polymer is method used to identify the CAC which made up in aqueous solution ( 0.0195 mgmL<sup>-1</sup> – 5 mgmL<sup>-1</sup>) were prepared and sonicated for 10 min for the PAA 15kDa , 17.5 kDa, 20 min for 120kDa and 30 min for 900kDa before cooling to room temperature. The surface tension of polymer solutions was measured at 25 °C using a torsion balance (OS, White Electrical Instrument Co, London). The platinum ring was cleaned with ethanol and distilled water prior to analysis of each sample. The measurement was recorded in triplicate for each polymer solution to get an average value.

#### **2.3.2.6 Drug loading**

Polymer dissolved in deionised water (1 mgmL<sup>-1</sup>, 3 mgmL<sup>-1</sup> and 6 mgmL<sup>-1</sup> ) with probe sonicated for 10 min. Propofol was added at 1:1, 5:1 and 10:1 initial drug: polymer weight ratios and the drug-polymer solutions were probe sonicated for a further 10 min. After cooling to room temperature, the solution was filtered using 0.45 µm syringe filters (with pre-filters) to remove any excess drugs.

### 2.3.2.6.1 Quantification of Propofol

The drug loading capacity of the self-assemblies was determined using high performance liquid chromatography (HPLC) (Shimadzu prominence UFLC, UK), as previously reported by Qu and . A RP Zorbax ODS 250 mm x 46 mm x 5  $\mu\text{m}$  HPLC column (Hichrom, UK) was used with flow rate of 1  $\text{mLmin}^{-1}$  (80:20 v/v methanol :water) in an isocratic mode. The samples were diluted with mobile phase and 20  $\mu\text{L}$  was injected onto the column. The amount of propofol present in the samples was determined by comparing to a standard calibration carried out previously with propofol dissolved in methanol (4  $\mu\text{gmL}^{-1}$  – 250  $\mu\text{gmL}^{-1}$ ),  $R^2 = 0.9857$  Figure 2-4.

Polymer solutions of 1  $\text{mgmL}^{-1}$ , 3  $\text{mgmL}^{-1}$  and 6  $\text{mgmL}^{-1}$  were organized in 4 mL aliquots utilizing deionized water as the diluting. Every sample was sonicated for 10 mins to permit maximum solubilisation and allowing aggregation to happen. Subsequently suitable amount of propofol was put together in 1:1, 5:1, and 10:1 drug: polymer ratios. The solution of drug-polymer were sonication for 10 min. Next, solution were filtered through 0.45  $\mu\text{m}$  to gathered of any excess undissolved drug, all analyses was done by using HPLC see Figure 2-4 and Table 2-2.

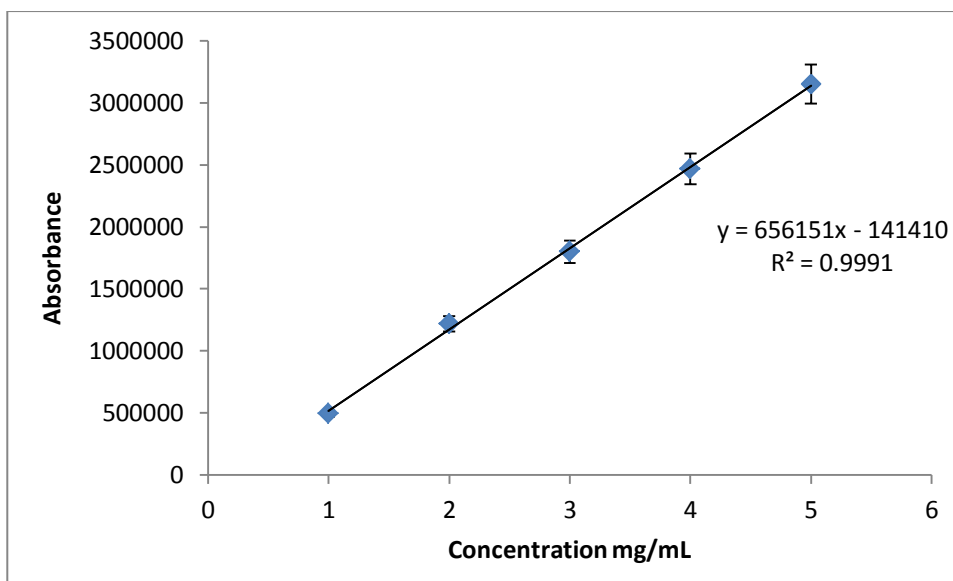


Figure 2-4: Calibration curve of propofol at 229 nm

Table 2-2 Polymer solutions of 1mgmL<sup>-1</sup>, 3mgmL<sup>-1</sup> and 6mgmL<sup>-1</sup> were organized in deionized water

Polymer	Propofol amount (mg)		
	1:1	5:1	10:1
1 mgmL <sup>-1</sup>	1 mg	5 mg	10 mg
3 mgmL <sup>-1</sup>	3 mg	15 mg	30 mg
6 mgmL <sup>-1</sup>	6 mg	30 mg	60 mg

### 2.3.2.6.2 Quantification of griseofulvin

This method was an adaptation of Trimaille's method (Trimaille & Möller, 2006). The samples were passed through a RP Phenomenex C18 250 mm x 46 mm x 5 µm HPLC column and detected at 293 nm (Shimadzu prominence UFLC, UK). The mobile phase

(45:55 v/v) acetonitrile: 45 mM potassium dihydrogen phosphate made up in water and pH adjusted to pH 3 with orthophosphoric acid) ran at a rate of 1 mLmin<sup>-1</sup>. The samples were diluted with mobile phase and 20 µL was injected onto the column, the resultant peak at 9.5 min was analysed. The quantification of griseofulvin present in the samples was determined from a standard calibration of griseofulvin in mobile phase (0.6 µg mL<sup>-1</sup> – 10 µg mL<sup>-1</sup>), R<sup>2</sup> = 0.9987 Figure 2-5.

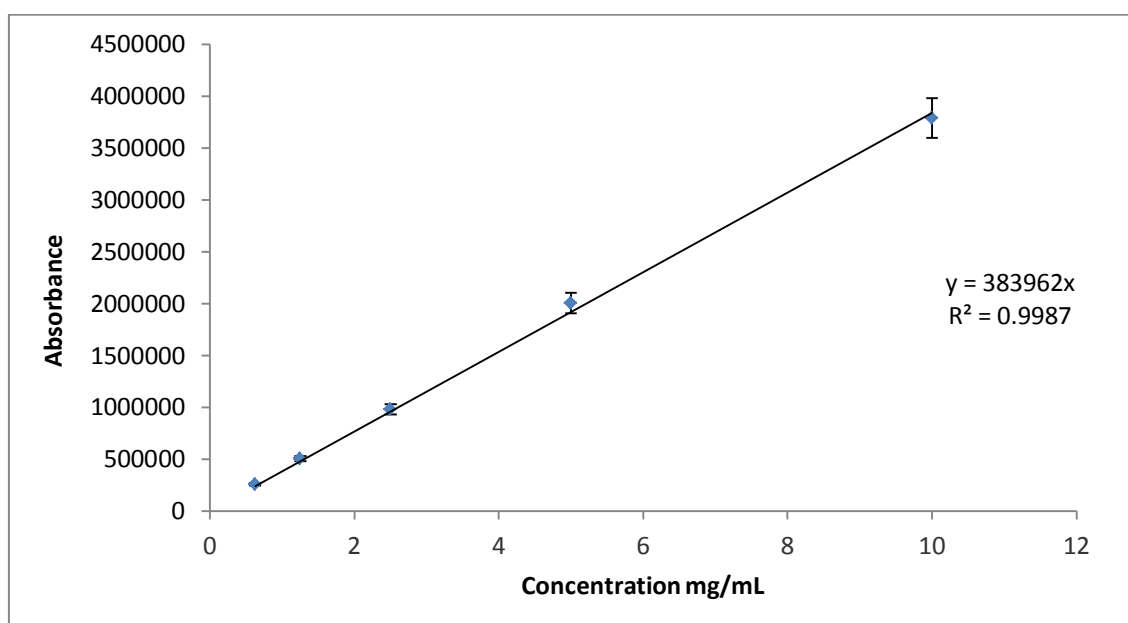


Figure 2-5: Standard curve of griseofulvin

### 2.3.2.7 *In vitro* drug release from nano-aggregates

Dynamic dialysis procedure has been used to determine the rates of drug release from polymers formula. Briefly, drug loading was carried out at 1:10 polymer:drug ratio and polymer concentration at 6 mg mL<sup>-1</sup> polymer concentration 2 mL of each sample was transferred into a dialysis tube (MW cut off = 12000-14000 Da). Subsequently, the polymer containing dialysis tube was dialyzed against 200 mL deionised water for 24 h with stirring at different temperatures. 1 mL of the external deionised water was

periodically sucked up and replaced with 1 mL of fresh deionised water. The amount of the released drug was determined by using HPLC. Equation 2-1 describes the rate of release of the drug from optimum formula.

Equation 2-1 Rate of release of the drug.

$$\% \text{ Drug release} = \frac{\text{Amount of drug released}}{\text{The initial amount of drug in optimum}} \times 100$$

## 2.4 Results

### 2.4.1 Synthesis and Characterisation of PAA-Ox5

PAA-Ox5 polymers were fabricated through an easy substitution reaction onto the primary amines in the parent PAA structure and the chloride functionality of the oxadiazole compound Figure 2-6.

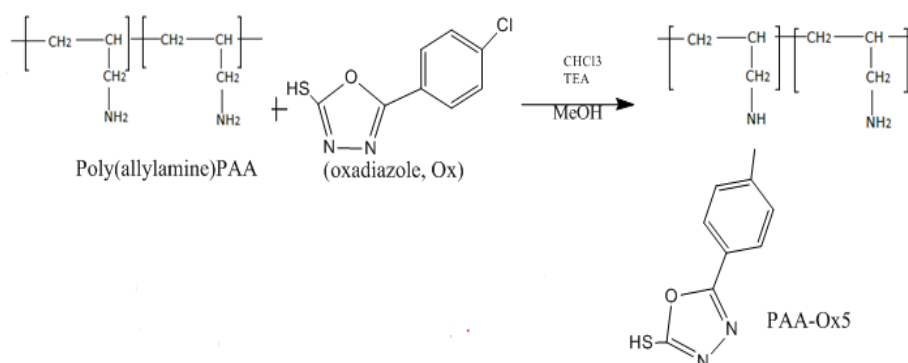


Figure 2-6: Chemical synthesis of PAA-Ox5

The percentages of yield of PAA Table 2-3 was calculated as next :- % Yield = (Product weight / Weight of reactants ) X 100 %

Table 2-3 show the percentages of yield of PAA for different molecular weight.

Molecular weight of PAA		Weight of product	% yield
a	PAA 15 kDa	1.806 g	80
b	PAA 17,5 kDa	1.99 g	84
c	PAA 120 kDa	2.083 g	87.82
d	PAA 900 kDa	1.7 g	74.2

The polymer structure was confirmed using NMR. The NMR spectra for the different molecular weight amphiphiles compared to the parent PAA are shown in . The spectra observed et all molecular weights was comparable after oxadiazole attachment had been carried out. Peaks were observed at 0.75 ppm, 2.50 ppm, 3.00 ppm, 1.40 ppm and 1.50 ppm which is attributable to the respective CH<sub>2</sub> and CH groups in the homo polymer backbone. Also, peaks were observed between at 7.25-7.75 ppm are ascribed to the aromatic CH sets located in the oxadiazole pendant collection, see Figure 2-7 (A1)(PAA 15 kDa) and (A2) PAA-Ox5 15 kDa), Figure 2-8 (B1)(PAA 17.5 kDa)and (B2) (PAA-Ox5 17.5 kDa), Figure 2-9 (C1) (PAA 120 kDa) and (C2)( PAA-Ox5 120 kDa), Figure 2-10 (D1) (PAA 900 kDa) and (D2)(PAA-Ox5 900 kDa),. An observation of the proton on the –SH set of the oxadiazole pendant was not made on this field, possibly as a result of quick exchange involving the thiol and D<sub>2</sub>O solvent.

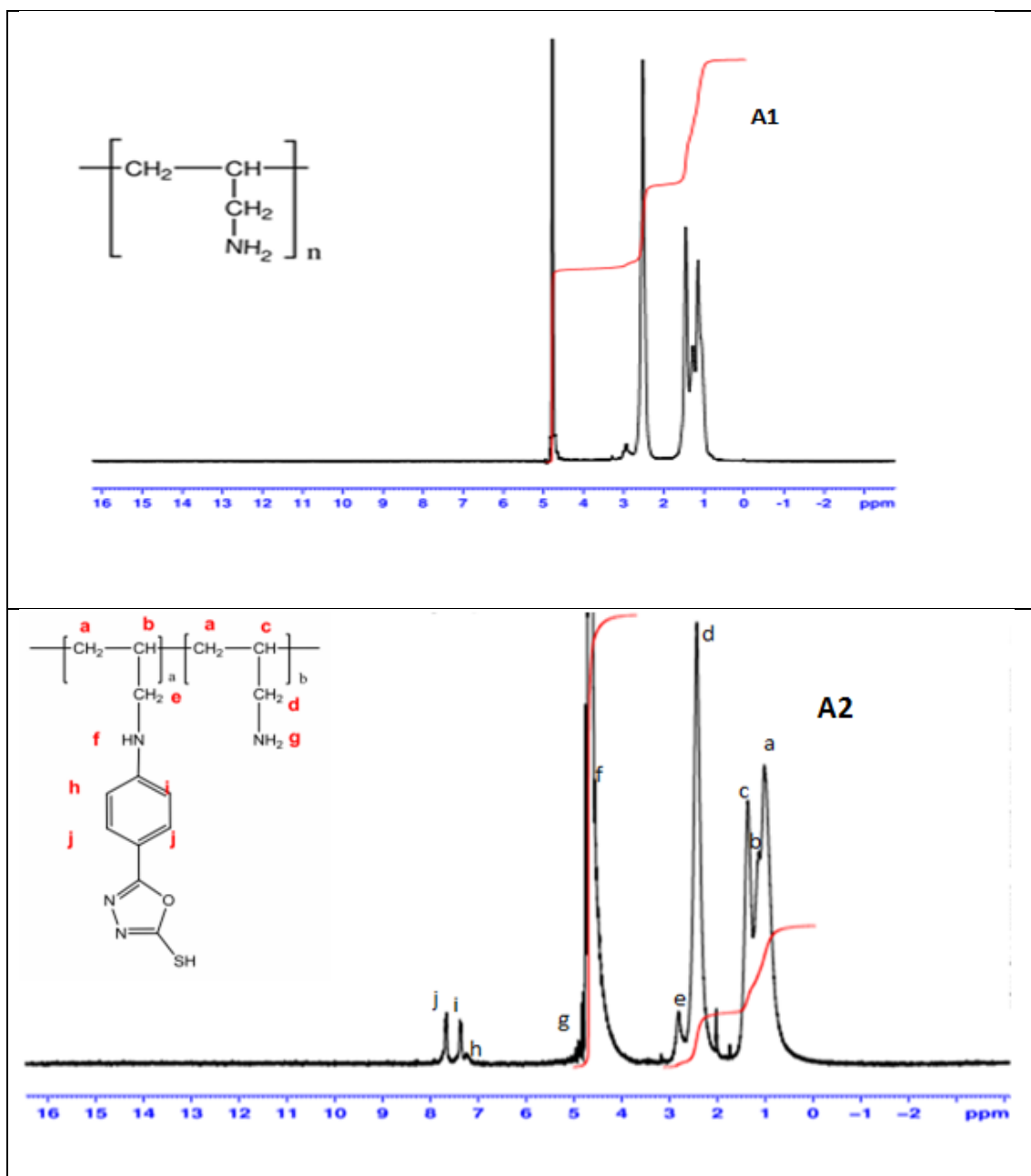


Figure 2-7: The spectra of  $^1\text{H}$  NMR spectroscopy of (A1) PAA 15kDa , (A2) PAA-Ox5 15 kDa carried out on 400MHz NMR at 25 °C

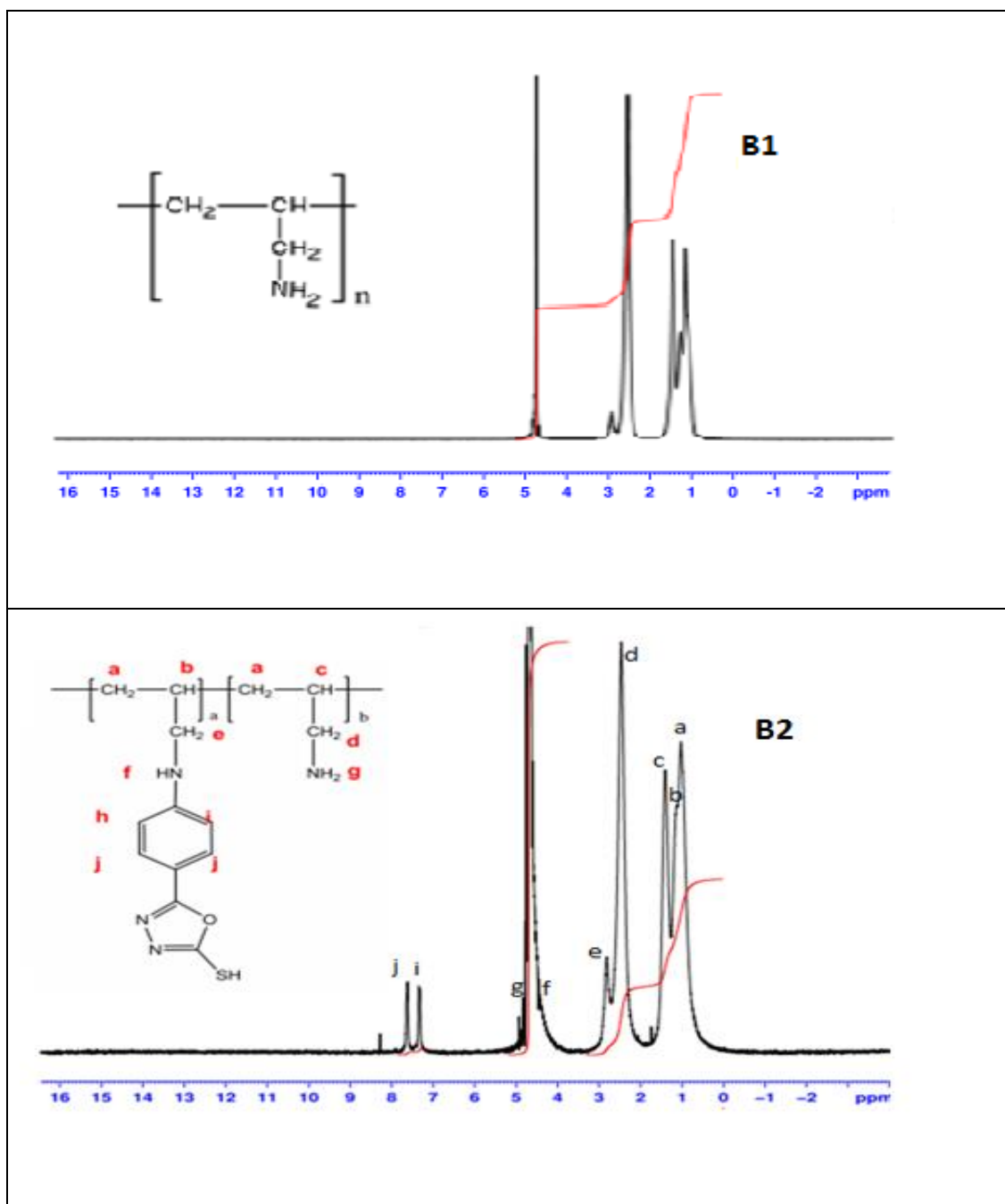


Figure 2-8: The spectra of 1H NMR spectroscopy of (B1) PAA 17.5 kDa, (B2)PAA-Ox5 17.5 kDa carried out on 400MHz NMR at 25 °C

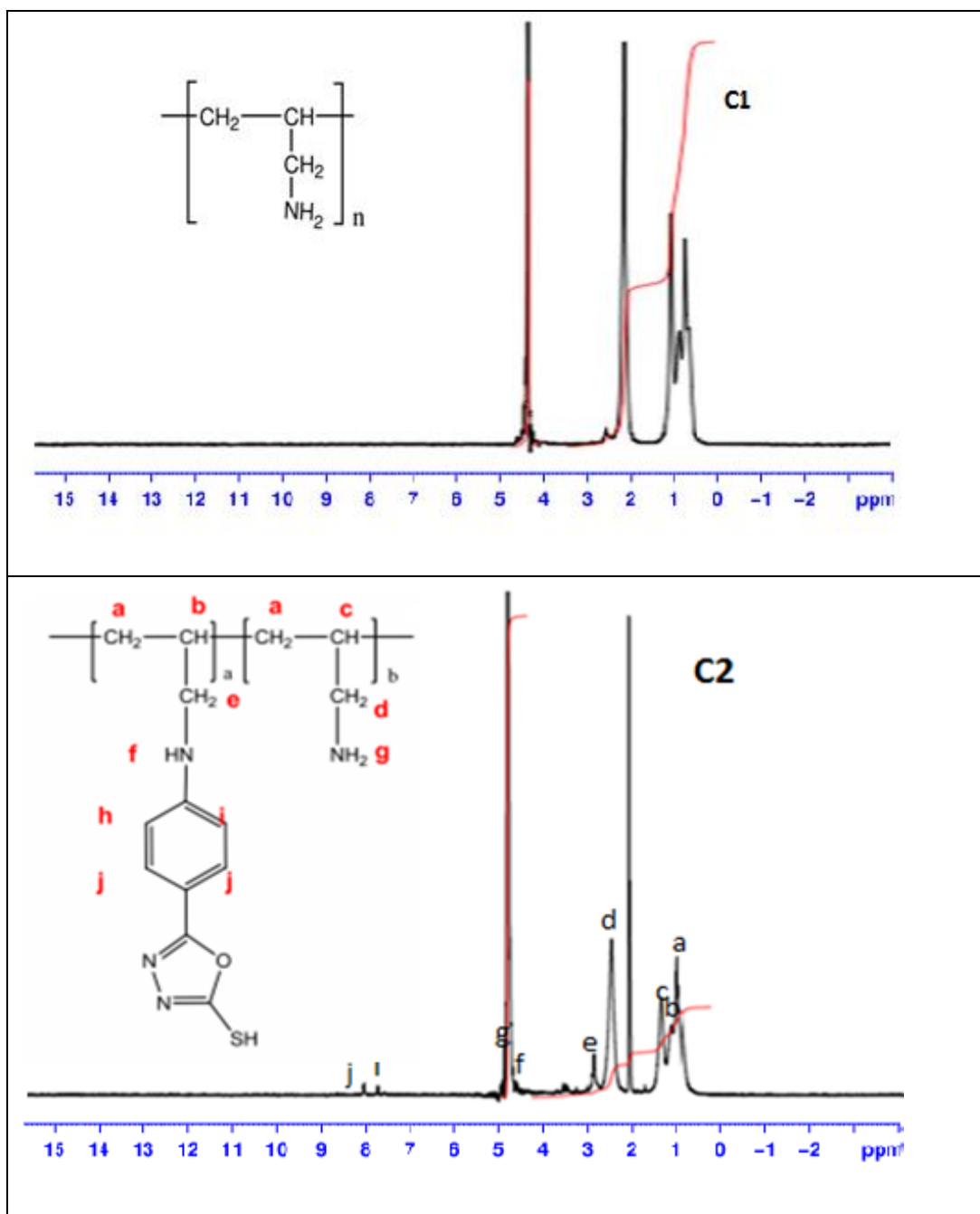


Figure 2-9: The spectra of <sup>1</sup>H NMR spectroscopy of (C1) PAA 120 kDa, (C2)PAA-Ox5 120 kDa carried out on 400MHz NMR at 25 °C

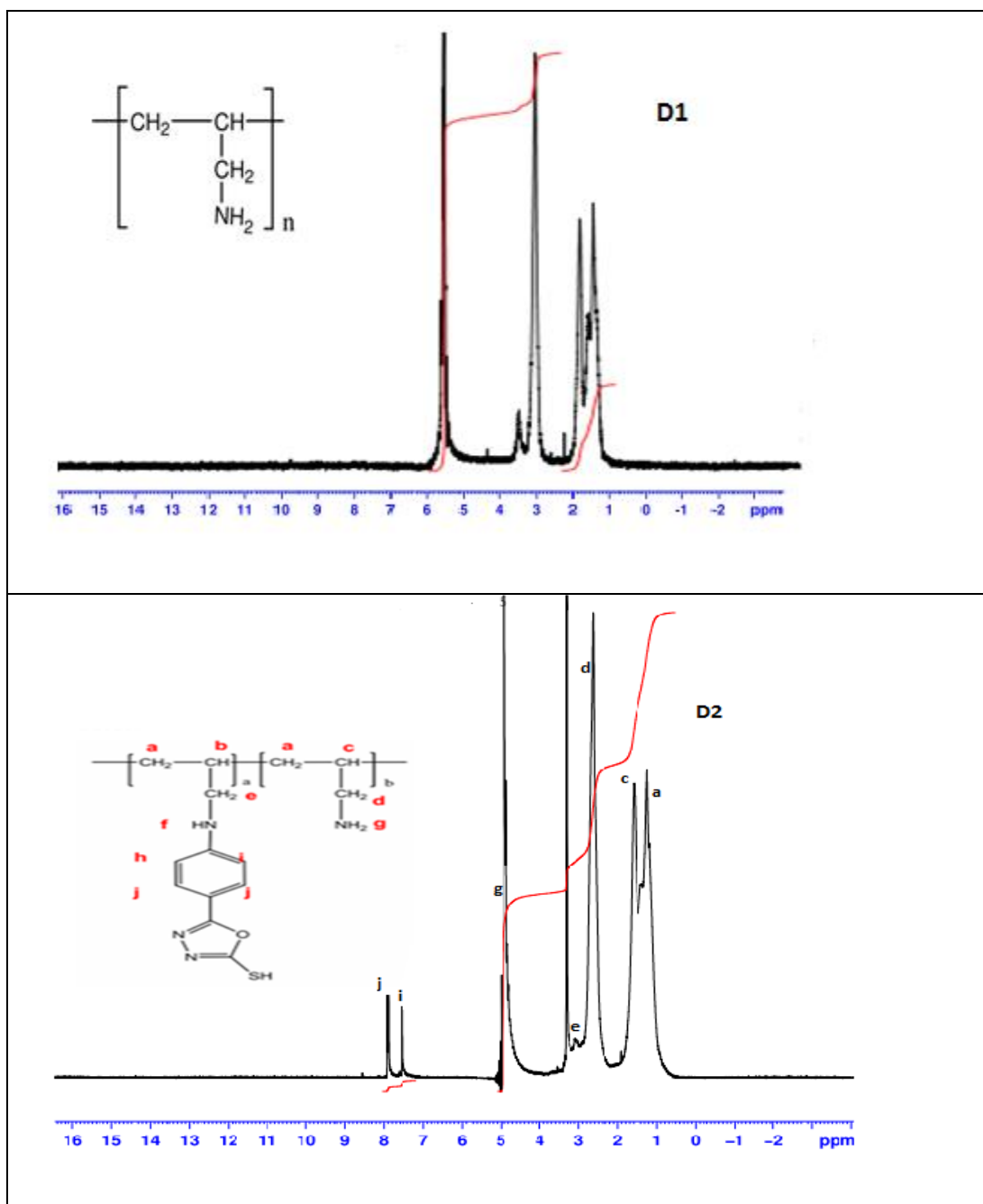


Figure 2-10: The spectra of  $^1\text{H}$  NMR spectroscopy of (D1) PAA 900 kDa, (D2)PAA-Ox5 900 kDa carried out on 400MHz NMR at 25 °C

In order to identify the functional groups present within the polymer structure, FTIR analysis was carried out between  $4000\text{ cm}^{-1}$  –  $650\text{ cm}^{-1}$  to detect the specific functional groups existing. See Figure 2-12, Figure 2-13 ,2-13 and Figure 2-14.

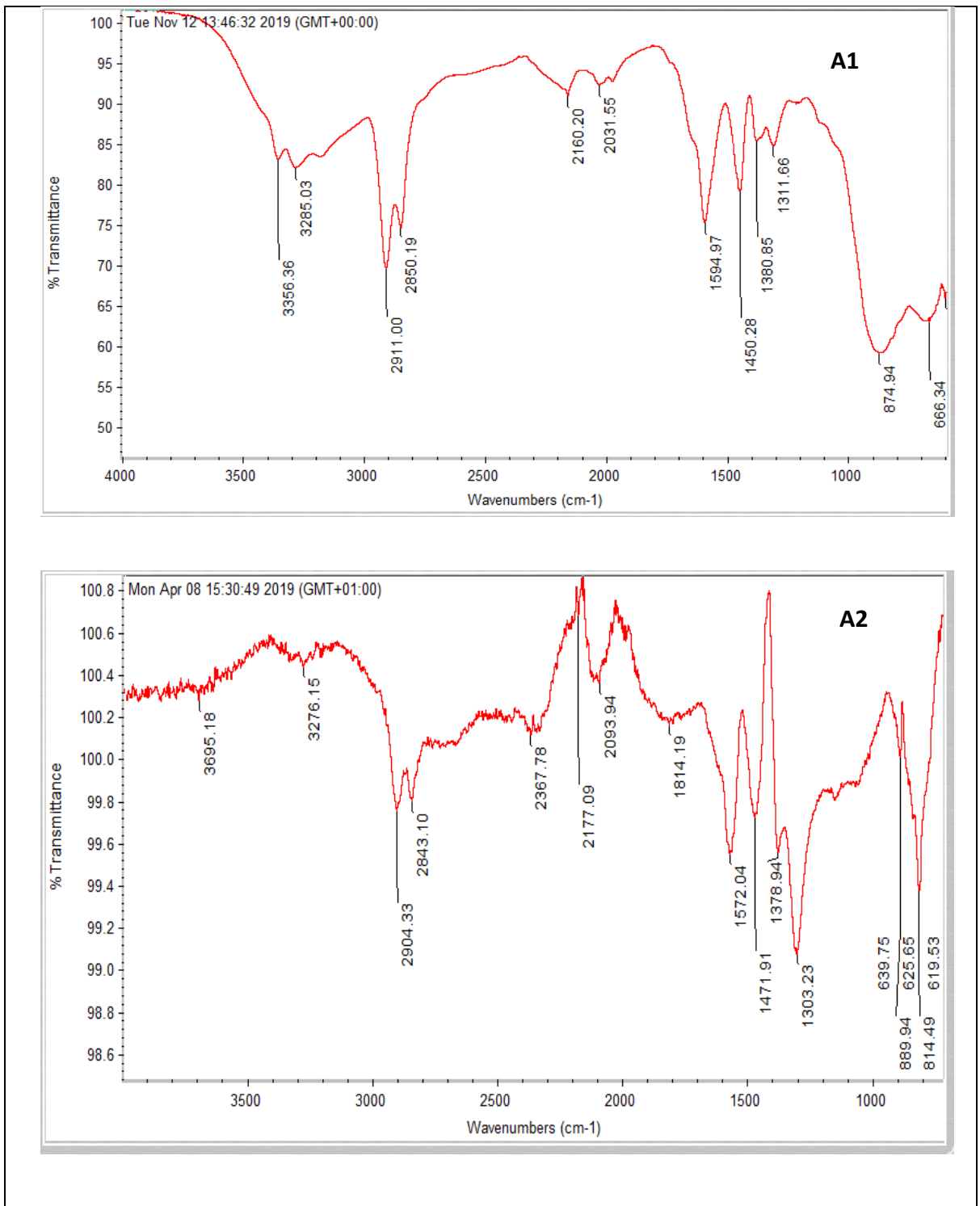


Figure 2-11: The spectra of (A1) PAA 15kDa and (A2) PAA-Ox5 15kDa polymer structure using diamond tripped ATR-FTIR (64scan)

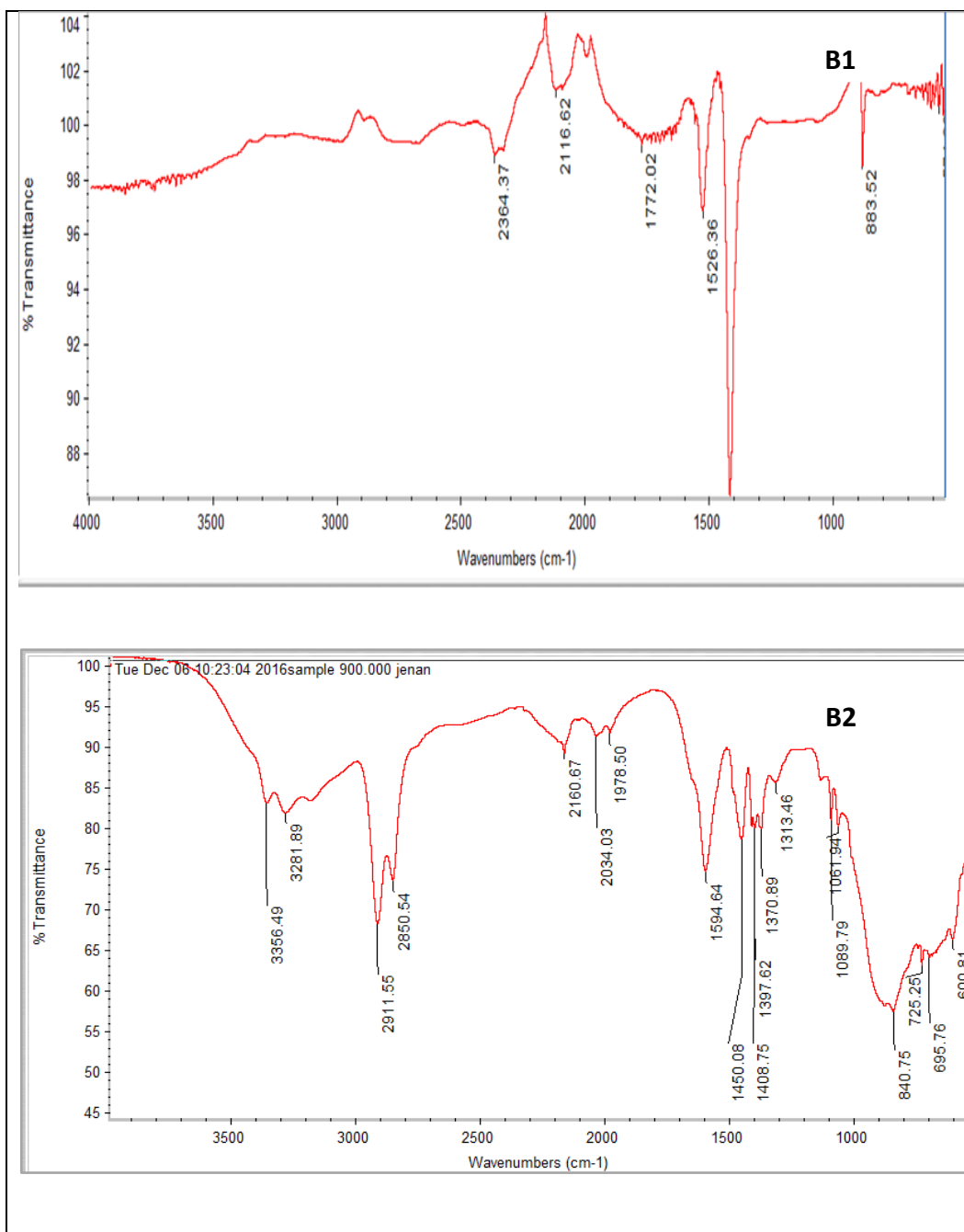


Figure 2-12: The spectra of (B1) PAA 17.5 kDa and (B2) PAA-Ox5 17.5 kDa polymer structure using diamond tripped ATR-FTIR (64scan)

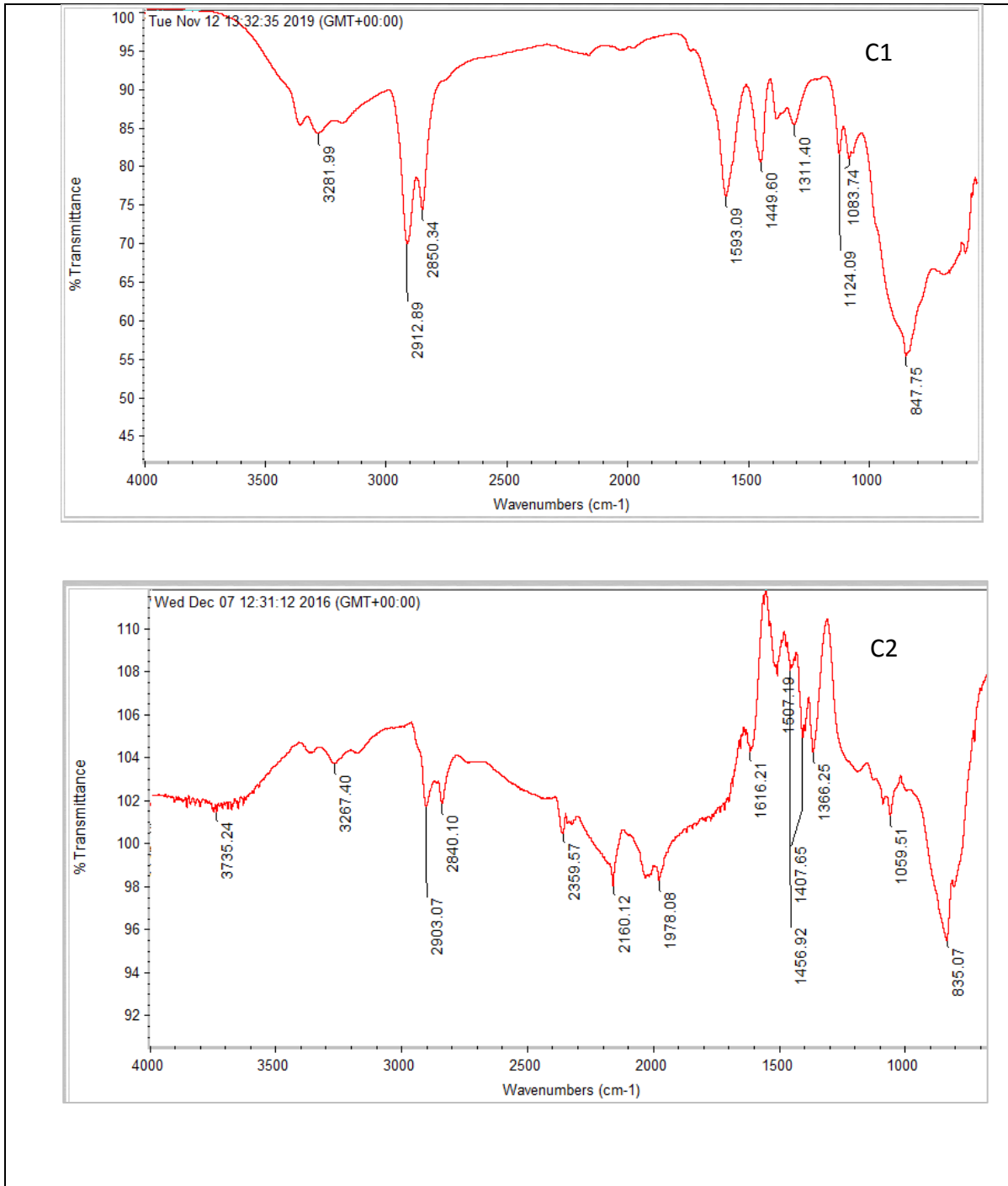


Figure 2-13: The spectra of (C1) PAA 120 kDa and (C2)PAA-Ox5 120 kDa polymer structure using diamond tripped ATR-FTIR (64scan)

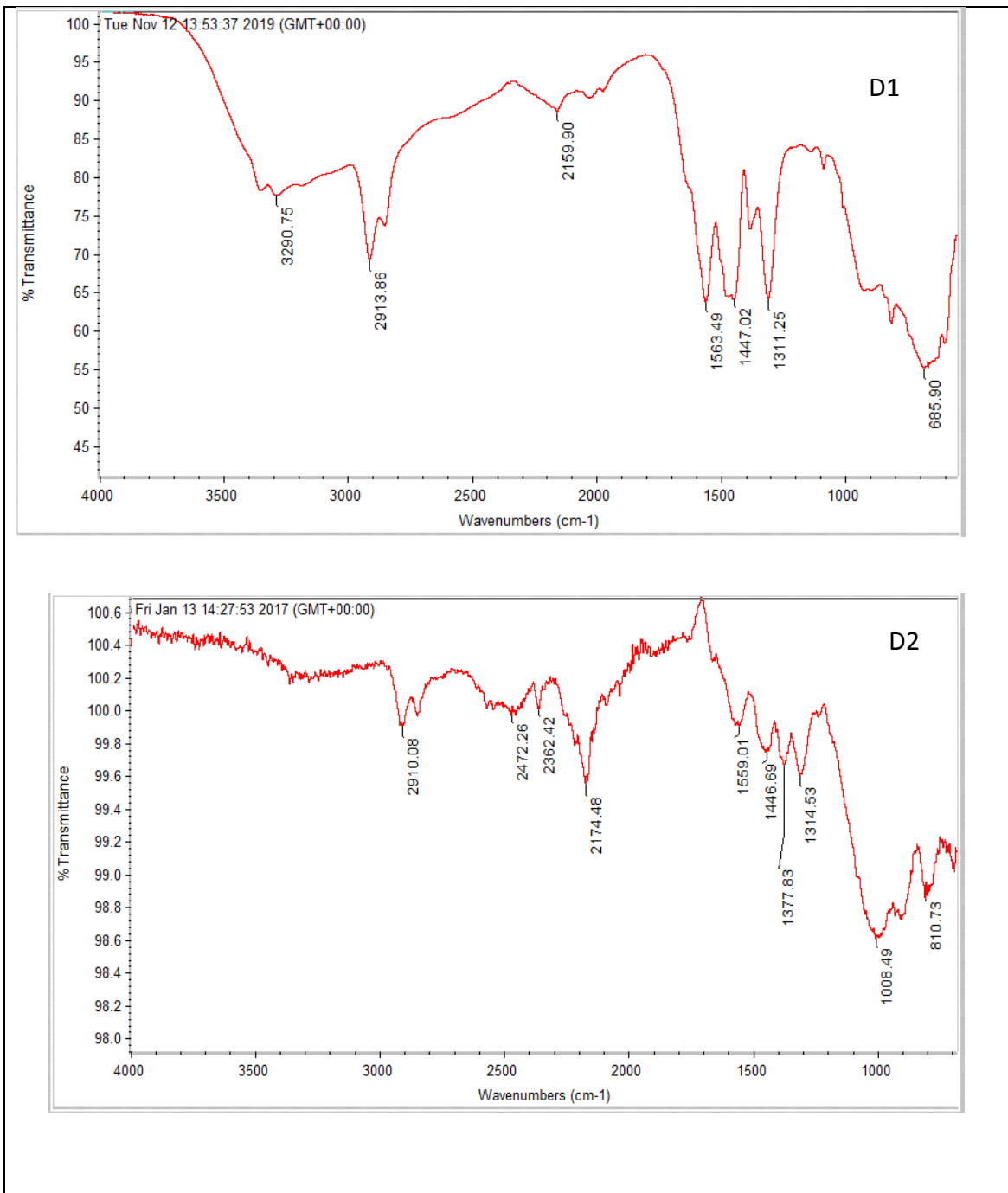


Figure 2-14: The spectra of (D1) PAA 900 kDa and (D2) PAA-Ox5 900 kDa polymer structure using diamond tripped ATR-FTIR (64scan)

Here, characterisation distinguishing feature peaks were observed at 3279 cm<sup>-1</sup> and 2849 cm<sup>-1</sup> arising from the respective N-H stretching and C-H stretching in the PAA backbone. Also, peaks determined at 1580 cm<sup>-1</sup> and showed that hydrophobic pendant collection involvement had been attained as a result these peaks being

associated to the bending and stretching vibrations of the aromatic ring C=C located in the oxadiazole structure.

## **2.4.2 Critical aggregation concentration (CAC)**

Critical aggregation concentration (CAC) has the equivalent value of amphiphilic polymers. Hydrophobic-hydrophobic interactions and non-polar between the aqueous media and amphiphilic polymer are the force behind the aggregate forming. Investigation of the capability of the nano-aggregates to encapsulate of hydrophobic drug molecules has been done by using many types of technical (Gaucher *et al.* 2005).

### **2.4.2.1 Methyl orange**

The ability of the polymeric amphiphiles to form aggregates in aqueous solutions was investigated using a hydrophobic methyl orange probe. Literature has shown that incorporation of methyl orange into polymeric aggregates results in a hypochromic shift which can be observed on the UV spectra and is indicative of the critical aggregation concentration.

The lambda max wavelength for methyl orange mixed with PAA 15 kDa, PAA 17,5 kDa, 120 kDa and 900 kDa are shown in Figure 2-15. As observed this particular method did not result in a shift – the increase in wavelength at high polymer concentration is merely due to the turbidity of the solutions. Hence, it was decided to use a different method for CAC measurement – surface tension.

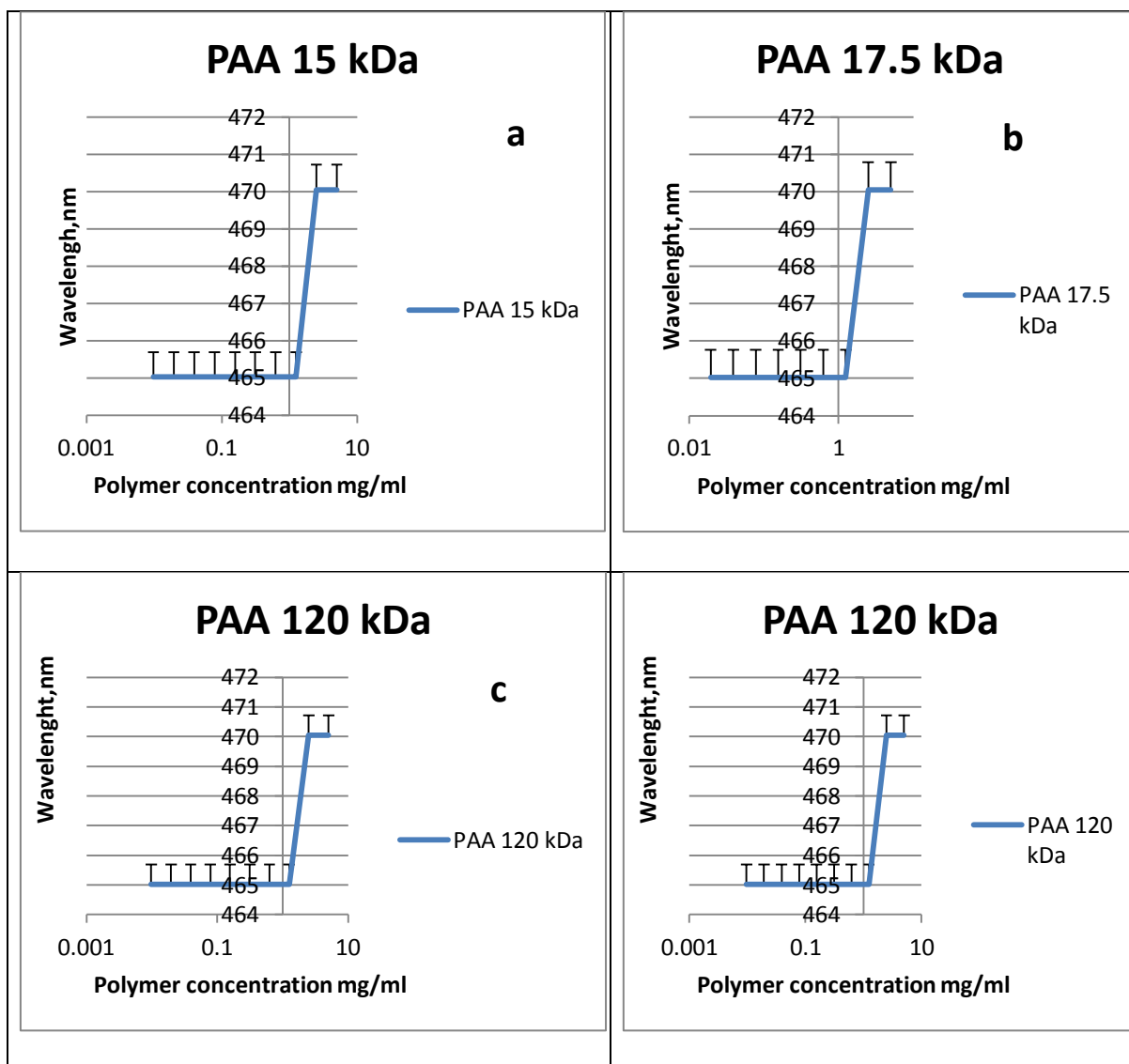


Figure 2-15: Effect of PAA-Ox5 (15 kDa, 17.5 kDa ,120 kDa and 900 kDa) on the peak absorbance of methyl orange at 465 nm (n=3, ave ± SD)

#### 2.4.2.2 Surface tension

Surface tension is the attraction between particles that make the surface layer of any liquid, resulting in a minimal surface area. Other molecules in the medium move in all directions. However, this does not apply at the liquid air interface. Liquid surface molecules are less surrounded with molecules and so, cohesive forces can only be established with those molecules while they are adjacent or below. Surface tension occurs at the interface while inward force is experienced by the molecules

resulting in a free energy state. Increasing temperature and pressure lead to decreases in surface tension, and at higher pressure the temperature dependence of surface tension is less evident (Park *et al.* 2007).

In order to increase the surface tension, there is need for an increase in free energy. Surface tension change in the aqueous environment, with increased in polymers concentration were observed (Churchill 1998).

The hydrophobic chains form the core of the micelle and are shielded from the aqueous environment by the surrounding shell composed of the hydrophilic groups that serve to maintain solubility in water.

For a micellar system at normal temperatures the entropy term is by far the most important in determining the free energy changes. The explanation most generally accepted for the entropy change is concerned with the structure of water. Water possesses a relatively high degree of structure owing to hydrogen bonding between adjacent molecules. If an ionic or strongly polar solute is added to water it will disrupt this structure, but the solute molecules can form hydrogen bonds with the water molecules that more than compensate for the disruption or distortion of the bonds existing in pure water. Ionic and polar materials thus tend to be easily soluble in water. No such compensation occurs with non-polar groups and their solution in water is accordingly resisted, the water molecules forming extra structured clusters around the non-polar region. This increase in structure of the water molecules around the hydrophobic groups leads to a large negative entropy change. To counteract this and achieve a state of minimum free energy, the hydrophobic groups tend to withdraw from the aqueous phase either by orientating themselves

at the interface with the hydrocarbon chain away from the aqueous phase or by self-association into micelles (Aulton,2002).

This tendency for hydrophobic materials to be removed from water as a result of the strong attraction of water molecules for each other and not for the hydrophobic solute, has been termed hydrophobic bonding. However, because there is, in fact, no actual bonding between the hydrophobic groups the phenomenon is best described as the hydrophobic effect. When the non-polar groups approach each other until they are in contact, there will be a decrease in the total number of water molecules in contact with the non-polar groups. The formation of the hydrophobic bond in this way is thus equivalent to the partial removal of hydrocarbon from an aqueous environment and a consequent loss of the ice-like structuring that always surrounds the hydrophobic molecules. The increase in entropy and decrease in free energy that accompany the loss of structuring make the formation of the hydrophobic bond an energetically favourable process (Aulton,2002).

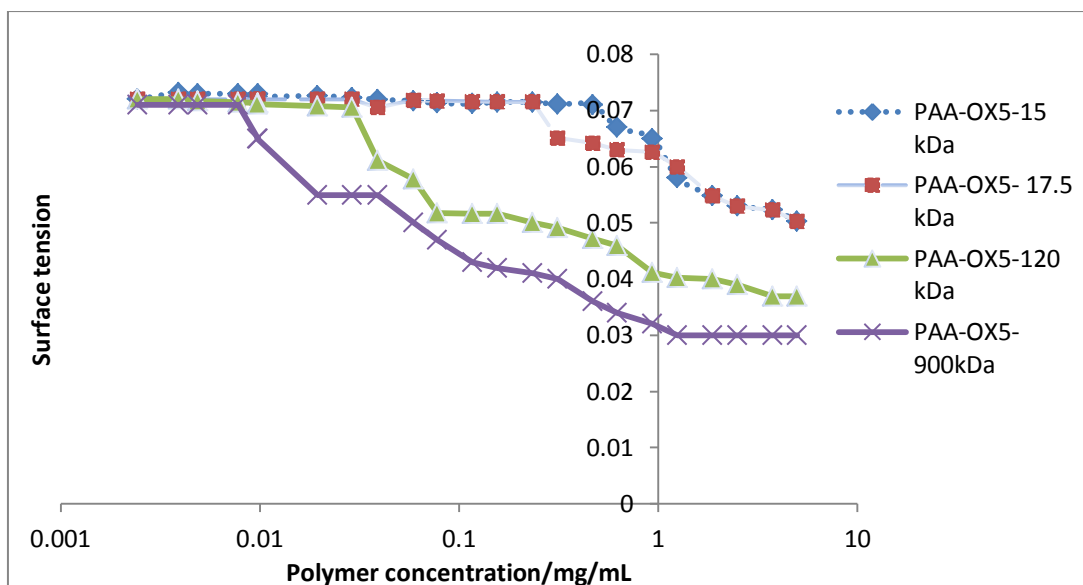


Figure 2-16: Surface Tension results for  $\blacklozenge$  PAA 15 kDa ,  $\blacksquare$  PAA 17.5 kDa,  $\blacktriangle$  PAA 120 kDa and  $\times$  900 kDa at 25 °C, (n=3, ave  $\pm$  SD)

The surface tension of water is 0.072 N/m. The critical aggregation concentration is measured as the point of inflexion in the surface tension as in Table 2-4. Here it is observed that increasing molecular weight of the polymer (at fixed molar ratio modification with oxadiazole) resulted in a decrease in CAC value. This is probably because there is a shift in the hydrophilic-lipophilic balance and thus there is less tendency to spontaneously aggregate at the higher molecular weight. This data indicates that the most stable aggregates are formed at the lower molecular weight. The surface tension of a surfactant solution decreases progressively with the increase of concentration as more surfactant molecules enter the surface or interfacial layer. However, at a certain concentration, this layer becomes saturated and an alternative means of shielding the hydrophobic group of the surfactant from the aqueous environment occurs through the formation of aggregates of colloidal dimensions, called micelles. Figure 2-16 shows the surface tension varied the molecular weight of PAA-Ox5. Many properties of polymers are known to be

molecular weight dependent. The increases in molecular weight led to a decrease in surface tension due to an increase in entropy (Moreira & Demarquette,2001).

Table 2-4 Show the PAA surface tension with water at 21<sup>0</sup> C (n=3).

Molecular weight of PAA Ox5 mgmL <sup>-1</sup>		Value of surface tension N/m	Appearance in solution above CAC
a	15 kDa	0.625 mgmL <sup>-1</sup> , (0.067)	Colourless clear solution
b	17.5 kDa	0.3125 mgmL <sup>-1</sup> , (0.0651)	Colourless clear solution
c	120 kDa	0.0390 mgmL <sup>-1</sup> , (0.0611)	Yellow clear solution
d	900 kDa	0.0195mgmL <sup>-1</sup> , (0.055)	Colourless clear solution

### 2.4.3 Drug loading

#### 2.4.3.1 Propofol

After the nano-aggregates were loaded with Propofol, the resultant peak at 5 min Figure 2-17 was observed at 229 nm (Shimadzu prominence UFLC, UK).

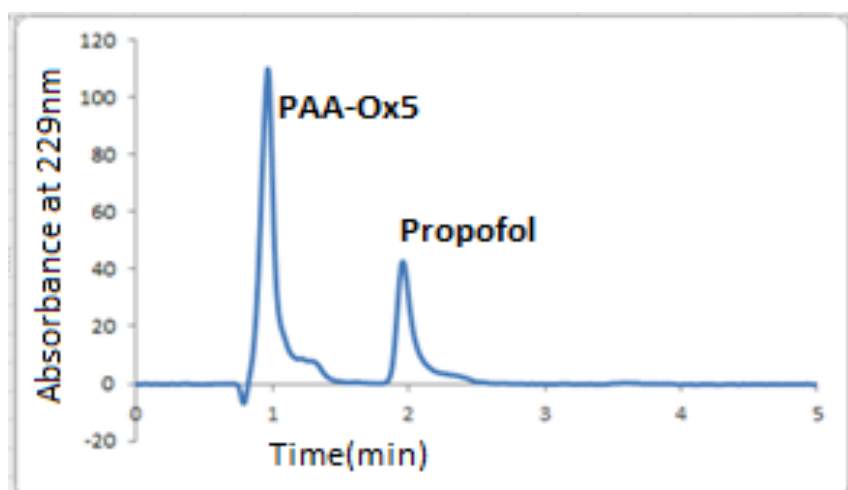


Figure 2-17: Drug loading of propofol representative spectra using HPLC

The polymer concentration has effect on drug loading, in Figure 2-18 the highest percentage of drug loading was 12,169 mgmL<sup>-1</sup> at (6 mgmL<sup>-1</sup> polymer : 60 mg/ml initial drug feed) for the PAAOx5 15 kDa / polymer and propofol respectively. While, the lower loading (0.592 mgmL<sup>-1</sup>) was recorded at 1 mgmL<sup>-1</sup>:1 mgmL<sup>-1</sup> polymer,propofol respectively, Table 2-5.

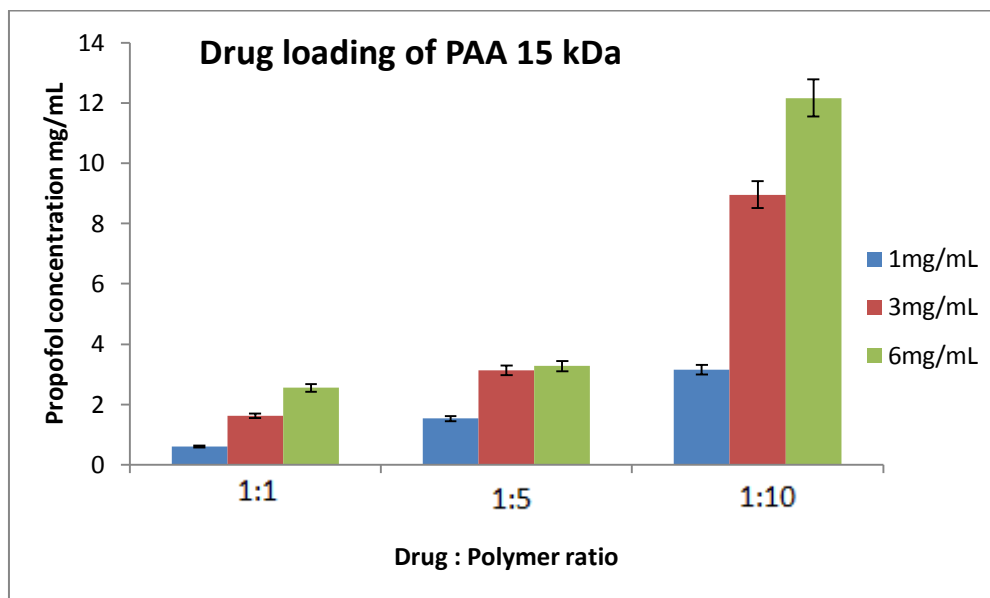


Figure 2-18: Drug loading of propofol in 0.25 % with Poly (allylamine) PAA (15 kDa) at RT (n=3)

Table 2-5 Drug loading of propofol in 0.25 % with Poly (allylamine) PAA (15 kDa) at RT.

Drug:polymer ratio	1 mgmL <sup>-1</sup>	3 mgmL <sup>-1</sup>	6 mgmL <sup>-1</sup>
1:1	0.592	1.62	2.545
1:5	1.526	3.13	3.269
1:10	3.155	8.953	12.169

Figure 2-19 shows the percentages of drug loading of PAA-OX5-17.5 kDa to propofol was ( $18.7 \text{ mgmL}^{-1}$ ) at  $6 \text{ mgmL}^{-1}$  polymer:  $60 \text{ mgmL}^{-1}$  initial drug feed), while only  $1.7 \text{ mgmL}^{-1}$  was solubilised at lower polymer concentrations. This result indicated the drug loading is depending on molecular weight of polymer. This result is due to the increase in length chain of hydrophilic of polymer Table 2-6.

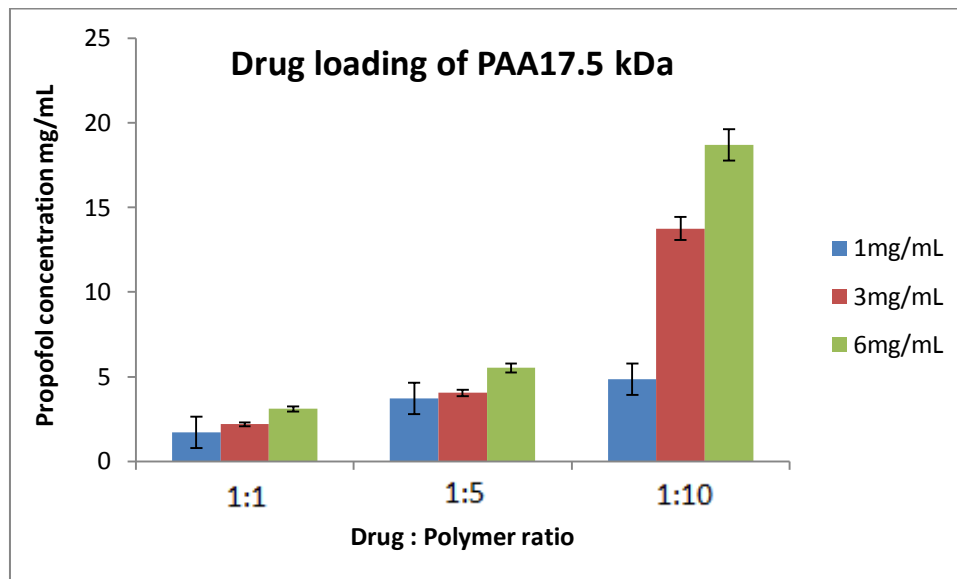


Figure 2-19: Drug loading of propofol in 0.25 % with Poly (allylamine) PAA (17.5 kDa) at RT (n=3)

Table 2-6 drug loading of propofol in 0.25 % with Poly(allylamine) PAA (17.5 kDa) at RT

Drug:polymer ratio	1 $\text{mgmL}^{-1}$	3 $\text{mgmL}^{-1}$	6 $\text{mgmL}^{-1}$
1:1	1.7	3.72	4.848
1:5	2.2	4.04	13.758
1:10	3.1	5.52	18.7

Figure 2-20 shows the maximum concentration of propofol drug loading in polymer concentration of PAA-OX5- 120 kDa. Comparing the drug loading values is observed

the loading of propofol in  $6 \text{ mgmL}^{-1}$  and feed ratio 10:1 was  $25.74 \text{ mgmL}^{-1}$ , while, at lower concentration  $1 \text{ mgmL}^{-1}$  and feed ratio 1:1 was  $2.3 \text{ mgmL}^{-1}$ , due to the increase in chain length see Table 2-7.

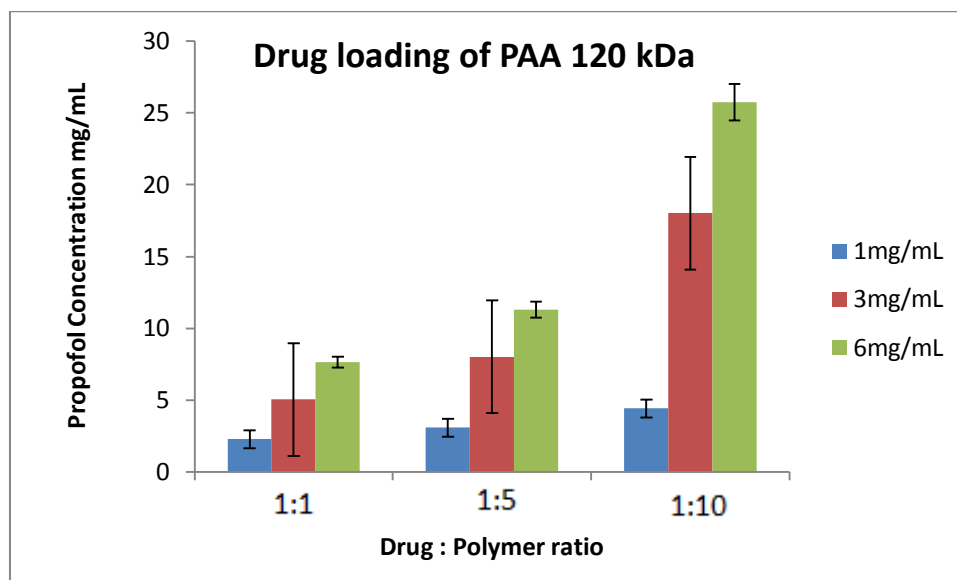


Figure 2-20: Drug loading of propofol in 0.25 % with Poly (allylamine) PAA (120kDa) at RT (n=3 )

Table 2-7 Drug loading of propofol in 0.25 % with Poly (allylamine) PAA (120 kDa) at RT.

Drug: polymer ratio	$1 \text{ mgmL}^{-1}$	$3 \text{ mgmL}^{-1}$	$6 \text{ mgmL}^{-1}$
1:1	2.3	5.06	7.66
1:5	3.1	8.02	11.31
1:10	4.43	18.02	25.74

The results revealed that THE increase in the molecular weight led to increase in drug loading, this was due to an increase in chain length of polymers (Wong *et al.* 2017).

Characterisation of drug loaded aggregates of propofol with PAA-OX5 was indicated by using size and zeta potential Figure 2-21.

Size of PAA-OX5 alone and PAA-OX5 loaded with propofol is shown in Table 2-8. The data show that size of PAA-OX5 alone was smaller than PAA-OX5 loaded with propofol. The effect of drug loading on the resulting PAA-OX5 size was clear with propofol formulations. Increasing the drug loading caused an increase in the mean diameter of the copolymer self- assemblies.

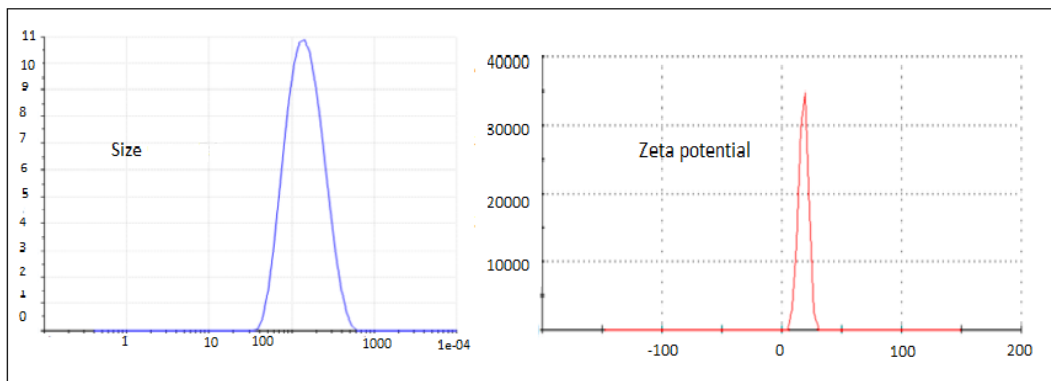


Figure 2-21: Zeta potential and size of PAA 17.5 kDa (n=3)

Table 2-8 Zeta potential and size of Polymer (15 kDa with propofol) at R .T (n=3,  $\pm$ SD)

Concentration of polymer	Drug: polymer ratio	Size PAA-OX5 ( $\pm$ SD)	PAA-OX5 with propofol				
			Size	S.D	pdl	S.D	Zeta( $\zeta$ ) Mv( $\pm$ SD)
1 mgmL <sup>-1</sup>	(1:1)	40.04	60.15	0.6718	0.202	0.0006	28.26
1 mgmL <sup>-1</sup>	(1:5)	51.55	95.434	0.5196	0.178	0.009	28.07
1 mgmL <sup>-1</sup>	(1:10)	70.76	117.5	0.6471	0.192	0.009	24.06
3 mgmL <sup>-1</sup>	(1:1)	44.6	87.72	0.7654	0.186	0.012	20.3
3 mgmL <sup>-1</sup>	(1:5)	86.04	101.4	1.323	0.145	0.002	17.86
3 mgmL <sup>-1</sup>	(1:10)	128.60	170.3	4.541	0.448	0.053	15.44
6 mgmL <sup>-1</sup>	(1:1)	74.18	131.8	1.709	0.412	0.052	17.66
6 mgmL <sup>-1</sup>	(1:5)	83.65	111.7	4.900	0.6512	0.053	16.71
6 mgmL <sup>-1</sup>	(1:10)	139.61	172.6	5.505	0.1281	0.083	16.1

Table 2-9 shows the size values of the PAA-OX5 17.5 kDa with propofol , which had the highest value (172.6 nm) for the concentration (6 mgmL<sup>-1</sup>) and feed ratio 1:10 and the lowest value was (60.15 nm) for the concentration of 1 mgmL<sup>-1</sup> and feed ratio 1:1.

The size of PAA-OX5 (without propofol was smaller than the size with propofol as explain in Table 2-8. The zeta potential values were record the highest value (28.26 mV) at low concentration while the lowest values (16.1 mV) were recorded for 6 mgmL<sup>-1</sup> concentration and feed ratio of 1:10.

Table 2-9 Zeta potential and size of polymer (17.5 kDa with propofol) at RT(n=3,  $\pm$ SD)

Concentration of polymer	Drug: polymer ratio	Size PAA-OX5 ( $\pm$ SD)	PAA-OX5-with propofol				
			Size nm	S.D	pdl	S.D	Zeta( $\zeta$ ) Mv( $\pm$ SD)
1 mgmL <sup>-1</sup>	1:1	59.38	68.35	1.146	0.167	0.018	26.0
1 mgmL <sup>-1</sup>	1:5	90.06	101.9	1.345	0.132	0.029	24.4
1 mgmL <sup>-1</sup>	1:10	101.00	121.2	29.06	0.424	0.026	28.76
3 mgmL <sup>-1</sup>	1:1	56.04	87.72	0.222	0.212	0.006	17.96
3 mgmL <sup>-1</sup>	1:5	83.61	101.4	1.970	0.291	0.007	17.06
3 mgmL <sup>-1</sup>	1:10	100.60	144.7	1.332	0.422	0.058	17.4
6 mgmL <sup>-1</sup>	1:1	88.07	117.01	4.799	0.340	0.069	19.56
6 mgmL <sup>-1</sup>	1:5	90.55	111.7	9.928	0.452	0.093	19.5
6 mgmL <sup>-1</sup>	1:10	116.76	172.6	57.71	0.052	0.087	20.6

Table 2-10 shows the change in the size values of the PAA 120 kDa with the concentration change. The highest values were (186.7 nm) at 6 mgmL<sup>-1</sup> and feed ratio 1:10, whereas the lowest values (35.22 nm) were at 1 mgmL<sup>-1</sup> and feed ratio (1: 1) for the drug.

The highest value of zeta potential was 28.6 mV for the 1 mgmL<sup>-1</sup> concentration and feed ratio 1: 10 for the drug, while the lowest values 14.3 nm were at 6 mgmL<sup>-1</sup> and feed ratio 1: 5 for the drug.

Table 2-10 Zeta potential and size of Polymer (120,000)+ propofol at R .T (n=3,  $\pm$ SD).

Concentration of polymer	Drug: polymer ratio	Size PAA-OX5 ( $\pm$ SD)	PAA-OX5-with propofol				
			Size nm	S.D	pdl	S.D	Zeta( $\zeta$ ) Mv( $\pm$ SD)
1 mgmL <sup>-1</sup>	1:1	27.33	35.22	0.5597	0.366	0.0005	28.6
1 mgmL <sup>-1</sup>	1:5	48.09	54.13	0.5004	0.27	0.0005	25.0
1 mgmL <sup>-1</sup>	1:10	55.7	57.55	0.5551	0.790	0.044	23.8
3 mgmL <sup>-1</sup>	1:1	112.00	144.4	22.44	0.72	0.166	26.1
3 mgmL <sup>-1</sup>	1:5	150.04	164.8	10.76	0.177	0.151	25.2
3 mgmL <sup>-1</sup>	1:10	167.21	175.7	6.09	0.581	0.028	22.3
6 mgmL <sup>-1</sup>	1:1	117.63	132.6	61.773	0.662	0.022	25.0
6 mgmL <sup>-1</sup>	1:5	130.05	151.66	97.2	0.803	0.101	21.1
6 mgmL <sup>-1</sup>	1:10	160.11	186.7	5.003	0.700	0.036	20.9

The poly disparity index of the PAA-Ox5 demonstrates the mono disparity of the nano-aggregation is not prevailing for long time. PAA-Ox5 zeta potential quoted and displayed (+26 mV), this elevated value is related to the existence of active amine accumulated in PAA backbone.

Table 2-11 showed the size values of the PAA-OX5 120 kDa with propofol , which had the highest value (186.11 nm) for the concentration (6 mgmL<sup>-1</sup>) and feed ratio of 1:5 and the lowest value was (27.33 nm) for the concentration of 1 mgmL<sup>-1</sup>and feed ratio of 1:1.

The zeta potential values were record the highest value (28.6 mV), while the lowest values (20.9 mV) were recorded for 6 mgmL<sup>-1</sup> concentration and feed ratio (1:1).

The next table show the values of size and zeta potential of PAA-OX5 which has high molecular weight 900 kDa, the size was recorded the same values as the low molecular weight this due to the aggregates formed were too large to filter and hence this molecular weight was disregarded.

Table 2-11 Zeta potential and size of Polymer (900.000)+ propofol at R .T (n=3, ±SD)

Concentration of Polymer	Drug: polymer ratio	Size PAA-OX5 (±SD)	PAA-OX5-with propofol				
			Size nm	S.D	pdl	S.D	Zeta mV(ζ) (±SD)
1 mgmL <sup>-1</sup>	1:1	44.91	69.94	0.4620	0.231	0.0.005	27.8
1 mgmL <sup>-1</sup>	1:5	46.73	62.01	0.6700	0.250	0.0005	27.4
1 mgmL <sup>-1</sup>	1:10	55.03	55.16	0.833	0.307	0.044	20.8
3 mgmL <sup>-1</sup>	1:1	141.4	162.9	40.67	0.479	0.166	25.1
3 mgmL <sup>-1</sup>	1:5	98.6	115.3	19.88	0.360	0.151	22.2
3 mgmL <sup>-1</sup>	1:10	90.0	108.8	5.910	0.318	0.028	23.1
6 mgmL <sup>-1</sup>	1:1	88.2	131.6	1.518	0.175	0.022	17.0
6 mgmL <sup>-1</sup>	1:5	95.6	117.85	197.2	0.215	0.101	19.1
6 mgmL <sup>-1</sup>	1:10	157.8	194.9	4.583	0.395	0.036	21.2

### 2.4.3.2 Griseofulvin

Drug loading for griseofulvin was achieved at the 1 mgmL<sup>-1</sup>, 3 mgmL<sup>-1</sup> and 6 mg mL<sup>-1</sup> polymer concentration and 1:1, 5:1 and 10:1 initial drug: polymer feed ratio.

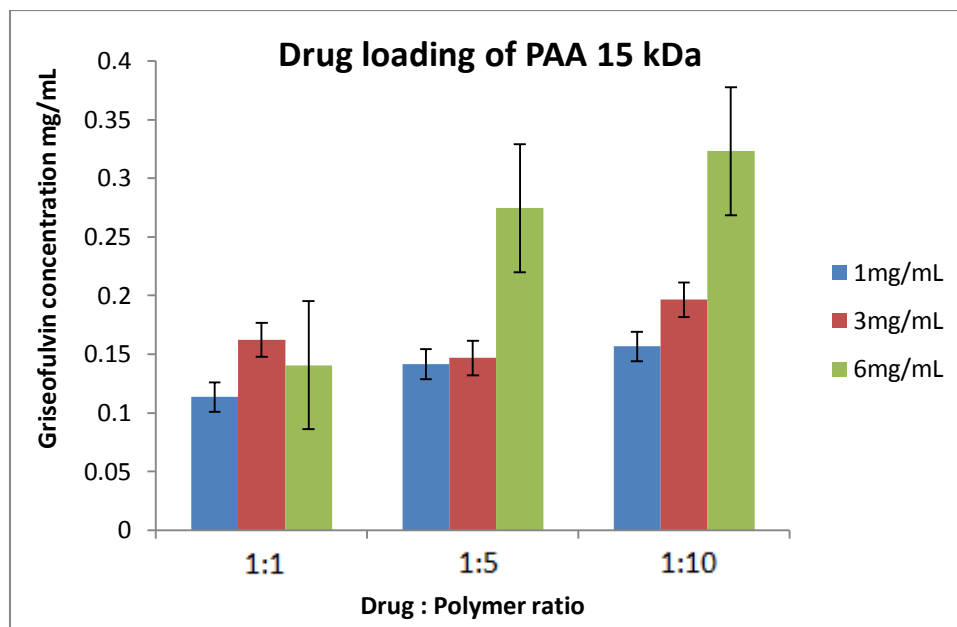


Figure 2-22: Drug loading of Griseofulvin in 0.25 % with Poly(allylamine) PAA (15kDa) at room temperature, (n=3)

Table 2-12 shows the concentration of griseofulvin in 0.25 % drug loading in polymer PAA 15kDa concentration of PAA-OX5- griseofulvin, Figure 2-22. Comparing the drug loading values is observed the loading of griseofulvin in 6 mgmL<sup>-1</sup> and feed ratio 10:1 was 5.1 mgmL<sup>-1</sup>, while, at lower concentration 1 mgmL<sup>-1</sup> and feed ratio 1:1 was 0.22 mgmL<sup>-1</sup>.

Table 2-12 Drug loading of griseofulvin in 0.25 % with Poly (allylamine) PAA (15 kDa) at RT.

Drug:polymer ratio	1 mgmL <sup>-1</sup>	3 mgmL <sup>-1</sup>	6 mgmL <sup>-1</sup>
1:1	0.11	0.14	0.16
1:5	0.16	0.15	0.20
1:10	0.14	0.27	0.32

The concentration of drug loading of polymer 17.5 kDa at 1, 3 and 6 mgmL<sup>-1</sup> ,its describe in Figure (2-17) and Table 2-13.

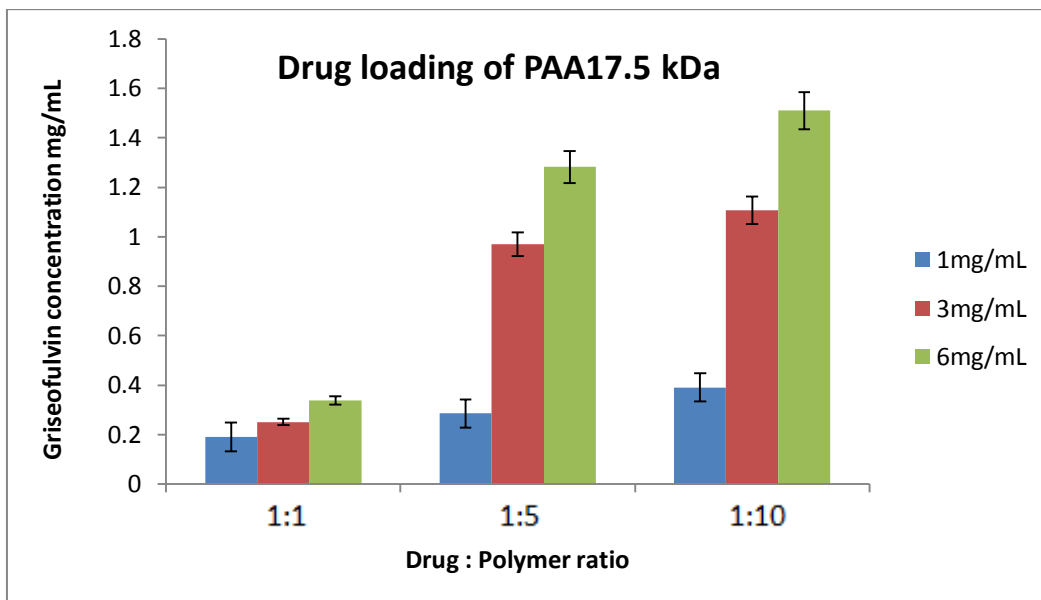


Figure 2-23: Drug loading of griseofulvin in 0.25 % with Poly (allylamine) PAA (17.5 kDa) at R. T, (n=3)

Table 2-13 Drug loading of griseofulvin in 0.25 % with Poly (allylamine) PAA (17.5 kDa) at RT.

Drug:polymer ratio	1 mgmL <sup>-1</sup>	3 mgmL <sup>-1</sup>	6 mgmL <sup>-1</sup>
1:1	0.19	0.25	0.34
1:5	0.28	0.96	1.28
1:10	0.39	1.11	1.51

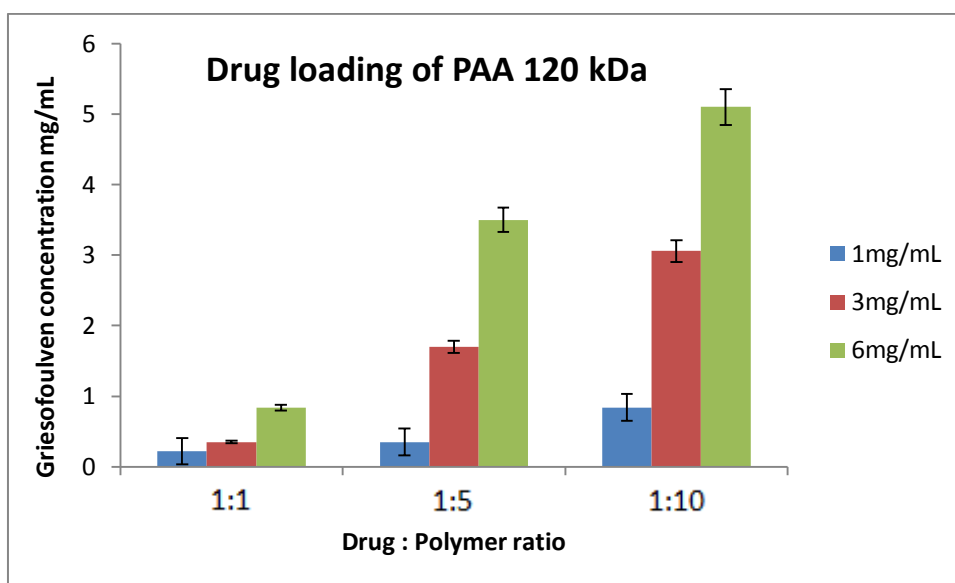


Figure 2-24: Drug loading of Griseofulvin in 0.25 % with Poly(allylamine) PAA (120kDa) at R. T, (n=3, ±SD)

Table 2-14 Drug loading of griseofulvin in 0.25 % with Poly (allylamine) PAA (120 kDa) at RT.

Drug:polymer ratio	1 mgmL <sup>-1</sup>	3 mgmL <sup>-1</sup>	6 mgmL <sup>-1</sup>
1:1	0.22	0.35	0.84
1:5	0.35	1.70	3.06
1:10	0.84	3.50	5.10

Table 2-14 shows the concentration of griseofulvin in 0.25 % drug loading in each polymer concentration of PAA-OX5- 120 kDa loading to griseofulvin. Comparing the drug loading values is observed the loading of griseofulvin in 6 mgmL<sup>-1</sup> and feed ratio 10:1 was 5.1 mgmL<sup>-1</sup>, while, at lower concentration 1 mgmL<sup>-1</sup> and feed ratio 1:1 was 0.22mgmL<sup>-1</sup>.

Size and zeta potential drug loaded aggregates was shown in Table 2-15. The change in the size values of the PAA 15kDa polymer with the concentration change appeared the highest values were (112.65 mV),(121.33 mV± 2.819) at 6 mgmL<sup>-1</sup> for PAA-OX5 and PAA-Ox-propofol, respectively and feed ratio 1:10, while the lowest values was (44.72 mV) and feed ratio 1:5 for the PAA-OX5 and (49.16 mV±0.501) for the PAA-Ox-propofol was at 1 mgmL<sup>-1</sup> and feed ratio (1: 1) for the drug.

The highest values of zeta potential were 29.7 mV for the 1 mgmL<sup>-1</sup> concentration and feed ratio 1:10 for the drug, while the lowest values of zeta potential was 15.8 mV were at 6 mgmL<sup>-1</sup> and feed ratio 1: 10 for the drug.

Table 2-15 Zeta potential and size of Polymer (15000)+ griseofulvin at R .T, (n=3,  $\pm$ SD)

Concentration of polymer	Drug: polymer ratio	Size potential PAA-OX5	Size potential PAA-OX5 propofol	PAA-OX5-with propofol			
				S.D	pdl	S.D	Zeta( $\zeta$ ) mV ( $\pm$ SD)
1 mgmL <sup>-1</sup>	1:1	47.66	49.16	0.501	0.25	0.01	28.0
1 mgmL <sup>-1</sup>	1:5	44.72	52.18	1.009	0.23	0.01	21.3
1 mgmL <sup>-1</sup>	1:10	65.88	73.09	0.598	0.49	0.01	29.7
3 mgmL <sup>-1</sup>	1:1	61.19	79.99	0.989	0.31	0.02	22.9
3 mgmL <sup>-1</sup>	1:5	80.01	104.11	0.862	0.27	0.01	26.0
3 mgmL <sup>-1</sup>	1:10	93.67	105.6	0.655	0.20	0.01	27.6
6 mgmL <sup>-1</sup>	1:1	86.08	111.11	0.702	0.21	0.01	17.9
6 mgmL <sup>-1</sup>	1:5	97.22	117.44	1.11	0.34	0.05	19.7
6 mgmL <sup>-1</sup>	1:10	112.65	121.33	2.819	0.281	0.014	15.8

Table 2-16 showed the size values of the PAA-OX5 17.5kDa with propofol, which had the highest value (130.3 nm) for the concentration (6 mgmL<sup>-1</sup>) and feed ratio (1:5) and the lowest value was (52.47 nm) for the concentration of 1 mgmL<sup>-1</sup> and feed ratio(1:1). The zeta potential values were record the highest value (33.1 mV), while the lowest values (16.5 mV) were recorded for 6 mgmL<sup>-1</sup> concentration and feed ratio (1:1).

Table 2-16 Zeta and size potential of Polymer (17.500)+ griseofulvin at R .T. (n=3,  $\pm$ SD).

Concentration of polymer	Drug: polymer ratio	Size PAA-OX5	Size potential PAA-OX5 propofol	PAA-OX5-with propofol			
				S.D	pdl	S.D	Zeta( $\zeta$ ) mV ( $\pm$ SD)
1 mgmL <sup>-1</sup>	1:1	48.15	52.47	0.32	0.26	0.01	31.4
1 mgmL <sup>-1</sup>	1:5	48.77	54.53	1.02	0.28	0.01	29.3
1 mgmL <sup>-1</sup>	1:10	67.17	71.80	0.77	0.16	0.02	33.1
3 mgmL <sup>-1</sup>	1:1	64.03	91.90	1.60	0.41	0.01	20.9
3 mgmL <sup>-1</sup>	1:5	88.83	109.7	1.25	0.32	0.01	23.2
3 mgmL <sup>-1</sup>	1:10	95.19	91.63	0.83	0.21	0.01	28.4
6 mgmL <sup>-1</sup>	1:1	89.11	103.2	0.93	0.45	0.02	16.5
6 mgmL <sup>-1</sup>	1:5	121.12	130.3	1.07	0.31	0.04	18.5
6 mgmL <sup>-1</sup>	1:10	117.16	123.1	4.96	0.24	0.02	20.8

Table 2-17 illustrates the change in the size values of the PAA 120kDa with propofol with the concentration change.

Table 2-17 Zeta and size potential of Polymer (120,000)+ griseofulvin at R.T (n=3,  $\pm$ SD).

Concentration of polymer	Drug: polymer ratio	Size PAA-OX5	Size PAA-OX5 propofol	PAA-OX5-with propofol			
				S.D	pdl	S.D	Zeta( $\zeta$ ) mV ( $\pm$ SD)
1 mgmL <sup>-1</sup>	1:1	51.03	59.37	0.55	0.38	0.01	28.8
1 mgmL <sup>-1</sup>	1:5	53.66	60.25	0.24	0.80	0.14	29.7
1 mgmL <sup>-1</sup>	1:10	63.17	79.97	2.49	0.32	0.04	29.9
3 mgmL <sup>-1</sup>	1:1	75.91	80.43	1.43	0.34	0.04	29.0
3 mgmL <sup>-1</sup>	1:5	83.07	97.41	0.99	0.22	0.01	24.0
3 mgmL <sup>-1</sup>	1:10	89.55	92.54	1.53	0.20	0.01	23.1
6 mgmL <sup>-1</sup>	1:1	86.52	91.46	0.70	0.20	0.01	23.4
6 mgmL <sup>-1</sup>	1:5	92.05	107.6	1.42	0.53	0.04	14.3
6 mgmL <sup>-1</sup>	1:10	123.31	196.6	3.790	0.44	0.035	17.7

The highest values were (196.6 nm) at 6 mgmL<sup>-1</sup> and feed ratio 1:10, whereas the lowest values (59.37 nm) were at 1 mgmL<sup>-1</sup> and feed ratio (1: 1).

The highest values of zeta potential were 29.7 nm for the 1 mgmL<sup>-1</sup> concentration and 1: 10 for the drug, this high value is related to the presence of active amine accumulated in PAA backbone, while the lowest values 14.3 nm were at 6 mgmL<sup>-1</sup> and feed ratio 1: 5 for the drug.

The conclusion from these obtained values can be that the size fits proportionately with the concentration while zeta values varied. Further conclusion of these values could be that Zeta potential was increased with increasing molecular weight of the same concentration at 1 mgL<sup>-1</sup> concentration and load ratio of 1:10.

## 2.4.4 Drug release

### 2.4.4.1 Drug release of Propofol and Griseofulvin

*In vitro*, drug release analyses were completed under ‘sink conditions’ for all of the exquisite formulations. Figure 2-25.

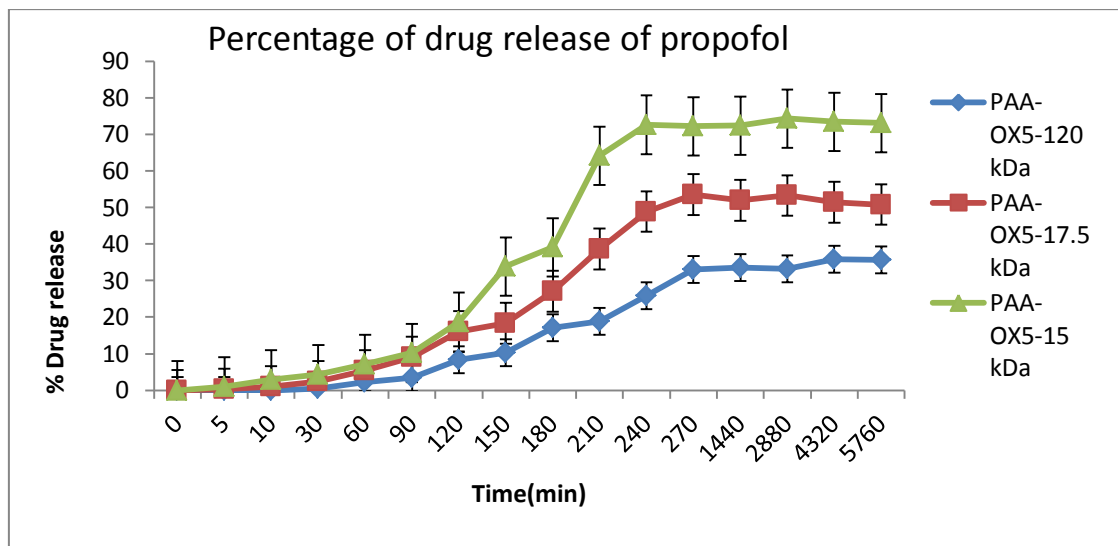


Figure 2-25: The percentages of drug release of PAA 15 kDa ,PAA 17.5 kDa and 120 kDa with propofol at R .T , (n=3, ±SD)

The analyses were completed in different duration and drug release at 48 h was (74.3%), 4 h was (53.54%) and 72 h was (35.84%) for PAA 15kDa, 17.5 kDa and 120 kDa respectively.

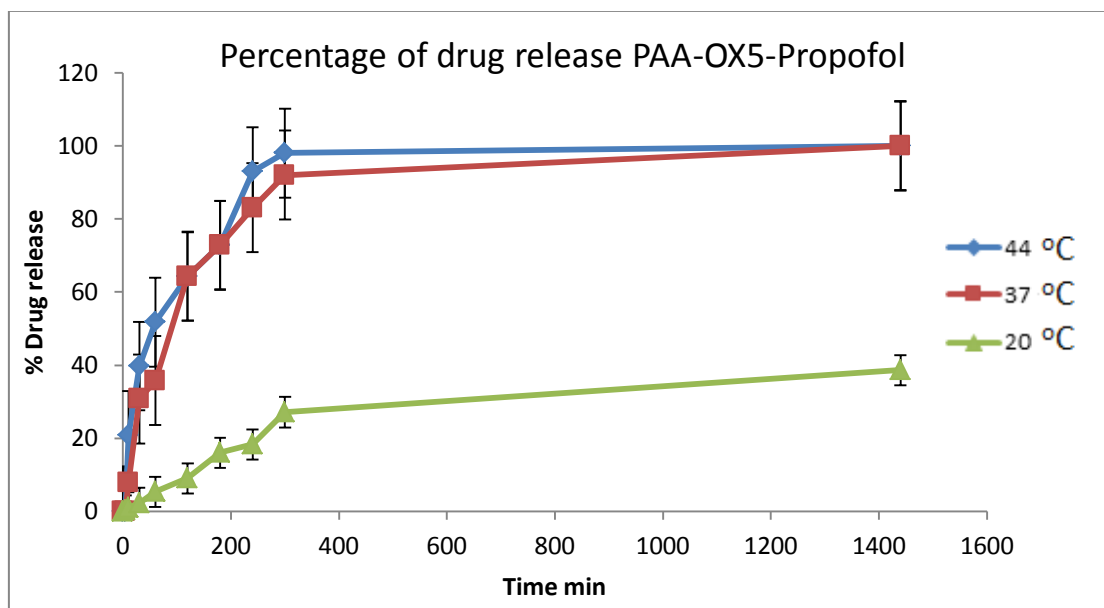


Figure 2-26: The percentages of drug release of PAA 17.5 kDa at different temperature with propofol, (n=3,  $\pm$ SD)

Griseofulvin release was indicated by using HPLC, release study was conducted in aqueous solution by placing PAA-OX5-griseofulvin formulation into a visking tubing (2 mL, 12-14 kDa) and dialysed against 200 mL of deionised water at (20 °C, 37 °C, 44 °C). The PAA-OX5 17.5 kDa was investigated as in Figure 2-27 and in Figure 2-28. The hydrophobic drug formulations showed an initial 'burst' release over the first 4 h period. Griseofulvin was released consistently throughout the study period until 0.3314 %.

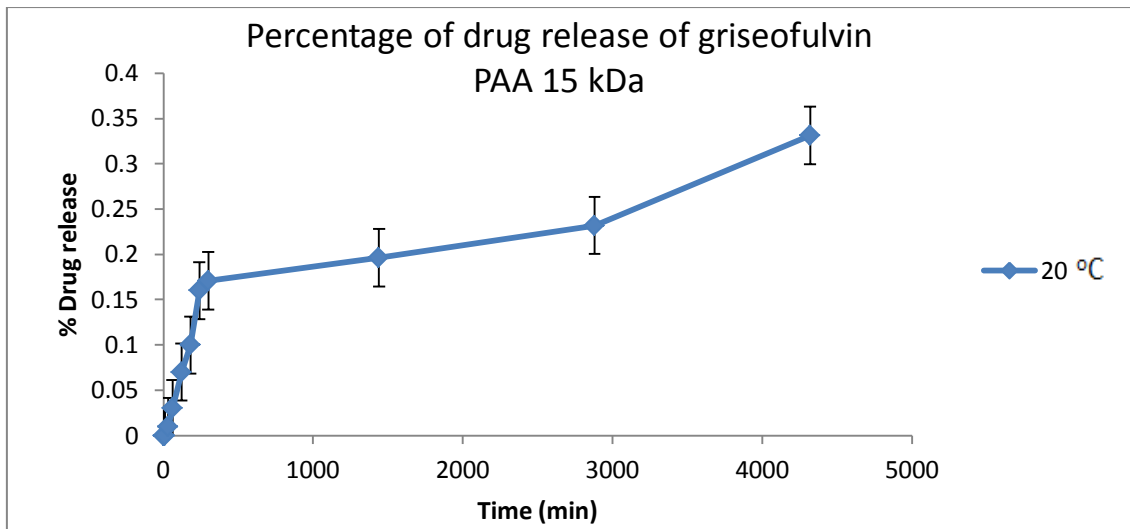


Figure 2-27: The percentages of drug release of PAA 15000 with griseofulvin at room temperature, (n=3)

Figure 2-28 shows the percentages of drug release of griseofulvin with PAA-OX5-17.5 kDa from formulation at different temperatures. The drug release was recorded 5.51 % at 37°C after 5 h, while at 44 °C the percentages was recorded 6.8 % after 5h. This results show the increasing in temperature led to increasing in drug release.

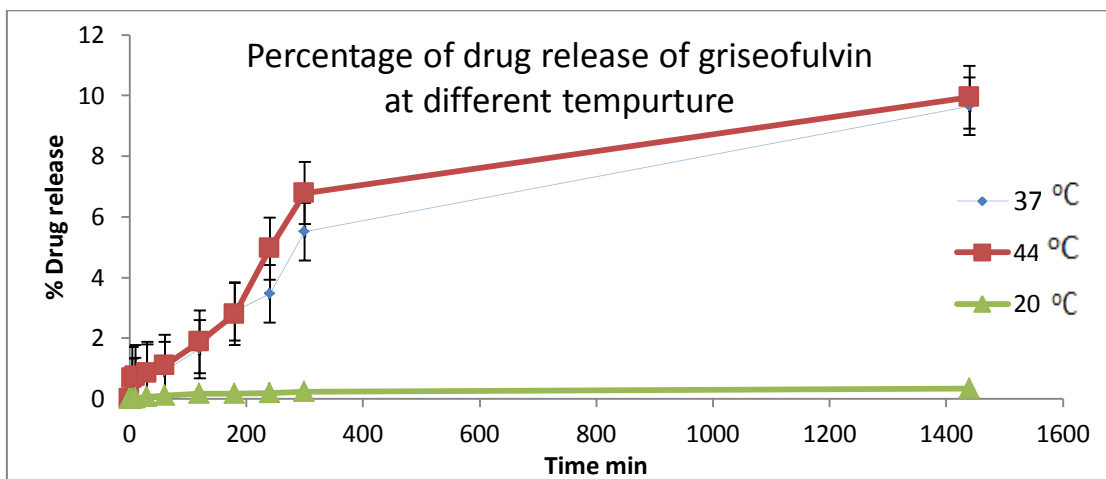


Figure 2-28: The percentages of drug release of griseofulvin with PAA-OX5-17.5 kDa from formulation at different temperatures(n=3)

## 2.5 Discussion

This study investigated the use of poly(allylamine) amphiphiles at varied molecular weight in the development of macromolecules. Four molecular weights were used: 15,000 Da, 17,500 Da, 120,000 Da and 900,000 Da. Poly(allylamine) (PAA) was grafted with 5-(4-chlorophenyl)-1,3,4-oxadiazole-2-thiol to act as universal hydrophobic drug solubilizers. In this project model drugs included propofol and griseofulvin. Figure 2-23

In this study successful synthesis of both PAA-OX5 amphiphile was achieved figure 2.19, confirmed by NMR and FTIR characterisation.

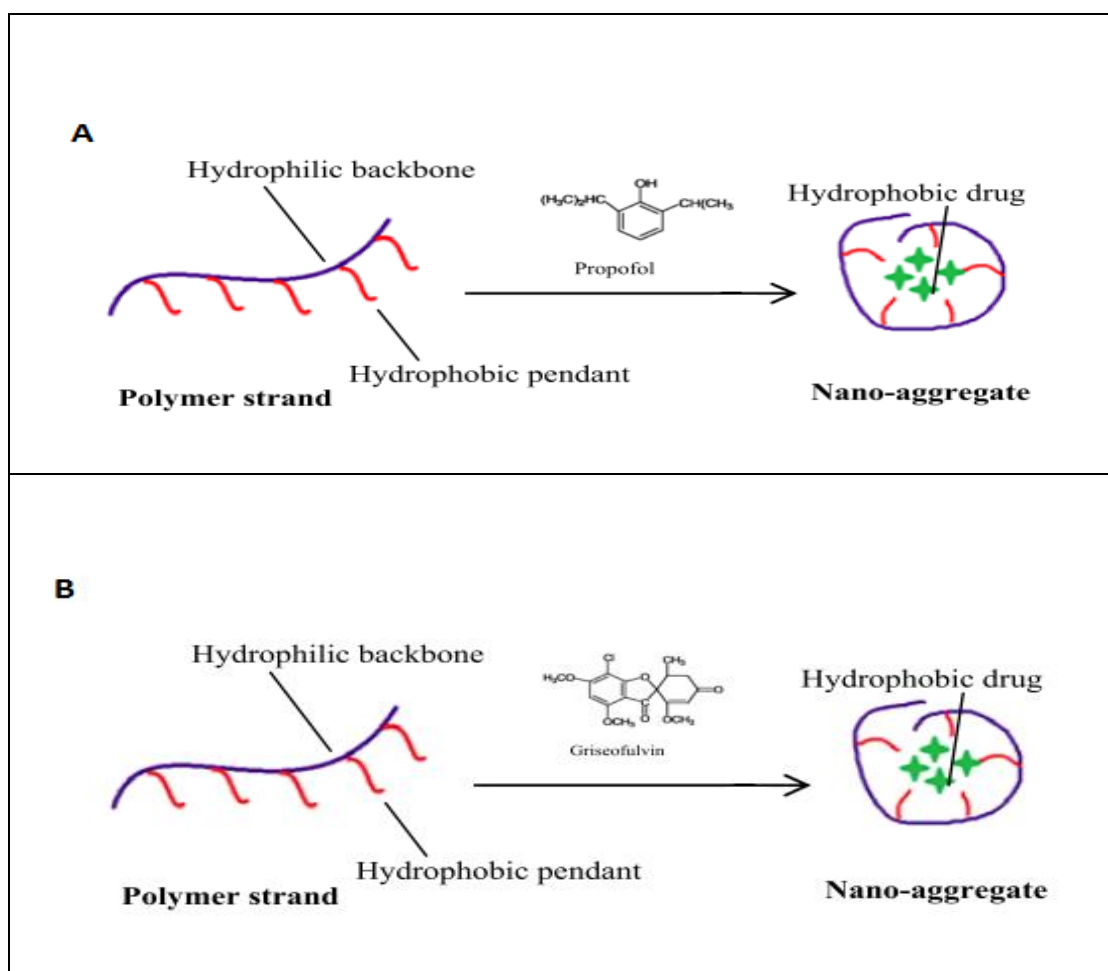


Figure 2-29: Mechanism of hydrophobic drug molecule encapsulation A) propofol and B) griseofulvin

It is of significant interest to design polymeric micelles that are capable of acting as universal delivery vehicles for various potent drugs, which are not in therapeutic formulations due to their water-insoluble, hydrophobic natures.

The concentration at which micelles first form in solution is termed the critical micelle concentration or CMC. This commencement of micelle formation can be noticed by a multitude of tested techniques. The CMC diminishes with a growth in the length of the hydrophobic chain.

The data clearly displays that size of polymers charged with multitude drugs model can be varied, changing in particle size allocation was reliant on the drug loading.

The effect of drug loading on the outcome polymer charge distribution was quite understandable with propofol and griseofulvin formulations. Elevating the drug loading caused increasing the main charge of the polymer.

The essential reason for micelle formation is the achievement of a condition of minimum free energy. The free energy change,  $\Delta G$ , of a system is reliant on changes in both entropy,  $S$ , and enthalpy,  $H$ , which are associated with the expression ( $\Delta G = \Delta H - T\Delta S$ ). For a micellar system at normal temperatures the entropy term is by far the most crucial in deciding the free energy changes ( $T\Delta S$  comprises roughly 90-95% of the  $\Delta G$  value) (Gaucher *et al.* 2005).

The clarification most generally accepted for the entropy change is uptight alongside the form of water. Water obtains a comparably high degree of structure due to hydrogen connecting between abutting molecules. If an ionic or strongly polar solute is added to water it will rattle this structure, but the solute molecules

can form hydrogen connections alongside the water molecules that more than restitution for the disruption or deformity of the existing connections in pure water.

The propofol and griseofulvin loading drugs into PAA-Ox5 and carried out by exploiting hydrophobic drug encapsulated into hydrophobic core of amphiphilic polymer by preparing drug: polymer feed ratio 1:1,1:5 and 1:10 and quantified by high performance liquid chromatography. In general, all polymers encapsulated highest drug levels at higher polymer concentrations and at 10:1 initial drug feed: polymer concentration. Figure 2-30 shows the optimal loading concentrations of both Propofol and griseofulvin across the polymer molecular weights. Unfortunately at (900 kDa) the aggregates formed were too large to filter and hence this molecular weight was disregarded. The data showed that at increased molecular weight, increased drug loading was possible.

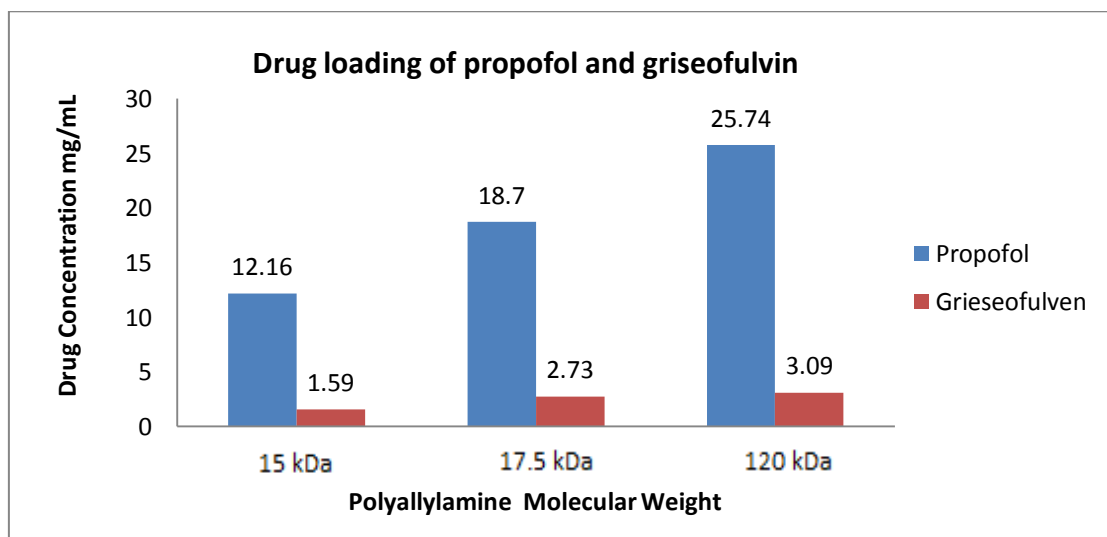


Figure 2-30: Drug loading of propofol and griseofulvin in 0.25 % with Poly (allylamine) PAA at R .T, (n=3,  $\pm$ SD)

Griseofulvin solubilisation results are lower than the propofol solubilisation. The reason for this is not clear, despite the fact it could be resulting in the height core enlargement upon drug loading due to in bigger accumulation which was then taken off during the filtering process (Barnett *et al.* 2013).

The drug release from nanoparticles depends on many factors such as diffusion from the polymer nanoparticles, desorption of the surface drug polymer nanoparticle and a combined degradation/diffusion process. Drug release and biodegradation are important in the development of drug delivery systems. A study by Barnett shows that drug release is a significant characteristic of a therapeutic system. Where scientists found a linear linker between the drug release and the absorption of the body. (Lu *et al.* 2011). In this work, the drug release was influenced by polymer molecular weight and drug loading. Polymers with higher molecular weight tend to possess slower drug release compared to lower molecular weight.

The molecular weight of the polymer can significantly affects the degree of aggregation, the solubility of higher molecular weight polymer in solvent was less than that of lower molecular weight polymer. Therefore, the heavier polymer would precipitate out faster and the molecular chain would be hardened by not allowing the intermolecular interaction of the drug layers around the particles which would cause aggregation (Kung ,1997).

Taking our findings into account, looking at the surface tension data, the aggregates formed at high molecular weight are likely to be more unstable upon dilution. Hence, it was decided to continue our studies throughout this thesis on PAA-Ox5

with molecular weight of PAA as 17,500 Da. This result may be due to the molecular weight of the drug propofol ( $M_w=178 \text{ g mol}^{-1}$ ) and griseofulvin ( $M_w= 353 \text{ g mol}^{-1}$ ) (Barnett *et al.* 2012).

In an identical experiment, Barnett and colleagues constructed PAA amphiphiles combined alongside oxadiazole in 5% mole grafting ratios. They proclaimed CAC values between  $0.02 \text{ mg mL}^{-1}$ -  $0.18 \text{ mg mL}^{-1}$  which were dependant on the polymer architecture. The factors influencing the value of CAC in a particular medium depend largely on the temperature and concentration of the material where Micelles is formed at a critical temperature.

The polydispersity indicator of the PAA-Ox5 demonstrates the monodispersity of the nano-aggregation is not dominating for a long time. PAA-Ox5 zeta potential calculated and displayed ranging between several values depending on the molecular weight of the PAA –OX5 and feed ratio of the hydrophobic drug.

*In vitro*, drug release analyses of propofol were completed under 'sink conditions' for all of the exquisite formulations Figure 2-30. The analyses were completed in a duration of 48 h (74.3%)for PAA-OX5 15 kDa, 4 h (53.54%) for PAA-OX5 17.5 kDa and 72 h (35.84%) for PAA-OX5 120 kDa.

Griseofulvin release pursued a very slow. The percentage released of (PAA-Ox5, 15 kDa) was 0.3314 % after 72 h. Unfortunately at (17.5 kDa) and (900 kDa) there was no records any result this due to the aggregates formed were too large to filter and hence this molecular weight was disregarded.

## **2.6 Conclusion**

For use as a universal drug solubilising agent PAA 17,500 Da was the optimal chain length to use as a PAA-Ox5 construct to give the most stable drug delivery system.

CHAPTER THREE

MAGNETIC IRON OXIDE GOLD

HYBRID NANOPARTICLE

FABRICATION AND

MAGNETOMICELLE FORMATION

### 3.1 Introduction

Magnetic iron oxide nanoparticles (MNPs) have been used as contrast agents for MRI due to their ability to improve the visualisation of various conditions particularly cancer. Scientific investigation is on-going to find an appropriate means to utilise MNPs in magnetic resonance imaging (MRI) motivated cellular hyperthermia. MNPs are the emphasis of interest in recent studies as a result of enormous biomedical applications (Acar *et al.* 2005). Among these are drug delivery, biological detection, magnetic bio-separation, imaging and targeted delivery. MNPs have larger surface range as compared to the ratios of volume as a result of their nano-size and the lower surface charge at physiological pH but they can quickly aggregate in solution because of their magnetic nature. Experiments have exploited the use of MNPs using both EPR effect (with passive targeting) as well as surface functionalization to confer site specific action to the tumour (active targeting) (Arruebo *et al.* 2007).

To reduce the inherent cytotoxicity of MNPs, they are commonly coated with materials such as poly(acrylic acid) PAA (Mak and Chen, 2005), dextran (Ciobanu *et al.* 2012), poly(ethylenimine) (PEI) (Wang *et al.* 2009), silica (Santra *et al.* 2001), carbon (Mendes *et al.* 2014) or precious metals (e.g. gold or silver) Figure 3-1 (Mandal *et al.* 2005).

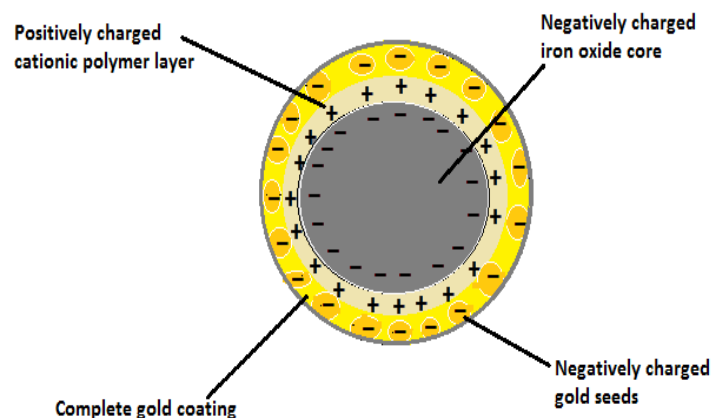


Figure 3-1: Schematic representation of gold Iron oxide hybrid nanoparticles

Gold coated hybrid nanoparticles (HNPs) have been shown as promising delivery vehicles for chemotherapeutics (Oluwasamni *et al.* 2017) including gemcitabine which is commonly used in pancreatic cancer therapy. The main downfall of HNPs is their reduced ability to carry drug cargo with hydrophobic qualities. The HNPs to date have reported only the delivery of hydrophilic compounds, this is because surface decoration of the metallic nanoparticles with high levels of lipophilic compounds results in them crashing out of solutions as precipitates. Therefore, the only way to utilise these nanoparticles and benefit from their inherent properties for lipophilic drug molecules is to incorporate into larger macromolecular systems such as amphiphilic polymers (Barnett *et al.* 2013).

### 3.1.1 Hybrid iron oxide core gold shell nanoparticles (HNPs)

The HNPs adopted in this study consist of both gold as the exposed shell and iron oxide as a core (Barnett *et al.* 2013; Hoskins *et al.* 2012): The magnetic aspect of the iron oxide core allows imaging potential whilst the gold shell which can be exploited

for its heating potential as well as allowing a biocompatible exterior for drugs to attach onto.

In order to achieve this core-shell structure a poly(ethylenimine) cushion is inserted between the iron oxide core and gold shell. PEI is a cationic polymer containing multiple amino groups each separated by two carbon atoms. Attachment of this cationic polymer onto the electronegative gold surface results in a positively charged surface, this allows attachment of tiny gold seeds before subsequent coating. However, PEI holds another purpose other than logistics. Studies have shown that the direct coating of gold onto the MNPs results in magnetic quenching possibly due to the electron migration of the gold coat into the iron oxide core. Hence, adding this polymer cushion maintains the inherent magnetism of the MNP core allowing exploitation in MR Imaging.

Gold nanoparticles have been widely reported in the literature for cancer therapy both as drug carriers and alternative approaches to cancer therapy. Colloidal gold possesses an interesting phenomenon known as surface plasmon resonance. At a specific wavelength irradiation of these particles with light results in the absorption and scattering of photons. The process of absorption results in a rapid transfer from light energy to heat energy. This results in the nanoparticle heating which is being investigated widely for thermal ablation. The HNPs we propose to use in this study exhibit this exciting potential, these can be irradiated by light within the near infrared wavelengths which allow focussed nanoparticle heating without destruction of local tissue. This heating can be tuned dependant on irradiation time and laser power, a characteristic which can be used to exploit release of drug compounds.

HNPs have shown to bind and release positively charged drug molecules upon heating (Malekigorji *et al.* 2017). In Malekigorji's study, bisnaphthalimido drug molecules with polyamine chains within the backbone were able to attach and release dependant on the extent of charge at elevated temperature. These findings will form the basis of our complex system. In our work we plan to fabricate the HNPs and incorporate them into an amphiphilic polymer for the delivery and triggered release of a doxorubicin analogue. The focus of this chapter will be the synthesis and characterisation of the HNPs and incorporation of these particles into the PAA based amphiphilic polymers developed in Chapter 2. For the purposes of this work and all ongoing work we chose to work with PAA-Ox5 with estimated molecular weight 17,500 kDa.

### **3.2 Research aims**

To synthesize hybrid iron oxide core gold shell nanoparticles (HNPs), monitoring their synthesis steps and characterise the final product. To incorporate the HNPs developed into the intrinsic PAA-Ox5 structure developed in Chapter 2.

### 3.3 Materials and methods

#### 3.3.1 Materials used

Table 3-1 shows the materials which is used in synthesis and description of hybrid iron oxide core gold shell nanoparticles.

Table 3-1 Explain the materials which is used in synthesis and description of hybrid iron oxide core gold shell nanoparticles

Item No	Material	Suppliers
1	Chloroform	Sigma-Aldrich Co., UK
2	Absolute ethanol	Sigma-Aldrich Co., UK
3	Copper grid	Agar Scientific Co., UK
4	Formvar	Agar Scientific Co., UK
5	Tetrachloroauric acid	Sigma-Aldrich Co., UK
6	Hydrochloric acid	Sigma-Aldrich Co., UK
7	Hydroxyl amine	Sigma-Aldrich Co., UK
8	Iron (II) sulphate	ACROS Organics Co., UK
9	Nitric acid	Sigma-Aldrich Co., UK
10	Polyethyleneimine (Mw = 750000 gmol <sup>-1</sup> )	Sigma-Aldrich Co., UK
11	Polyethyleneimine (Mw = 2000 gmol <sup>-1</sup> )	Sigma-Aldrich Co., UK
12	Potassium nitrate	ACROS Organics Co., UK
13	Sodium borohydrate	Sigma-Aldrich Co., UK
14	Sulfuric acid	Sigma-Aldrich Co., UK
15	Sodium hydroxide	Fisher Scientific Co., UK

### **3.3.2 Synthesis of iron oxide nanoparticles**

The techniques described by Goon and colleagues were used in this work to synthesize HNPs. The first step was to synthesise the iron oxide core through the co-precipitation technique (Goon *et al.* 2009).

A mixture of 1.03 g NaOH and 1.82 g KNO<sub>3</sub> was dissolved in 180 mL of deionised water. Nitrogen was bubbled over for 1 h. The mixture was heated to 90 °C with a stirrer.

3.89 g FeSO<sub>4</sub>·7H<sub>2</sub>O was dissolved in 20 mL H<sub>2</sub>SO<sub>4</sub> 0.01 M (with sonication). The solution was added to the reaction with stirring for 24 h. The particles were then magnetically separated from the solvent and washed 6 times with deionised water. The final particles were diluted in 25 mL H<sub>2</sub>O.

#### **3.3.2.1 Coating of iron oxide nanoparticles with Poly(ethylenimine)**

Poly(ethylenimine) (MW 750,000) has been previously utilized to electro- statically coat iron oxide NP between the negatively charged magnetic particles and cationic polymer. The layer of coating prevents the aggregation of the particles. Essentially, this involves adding 5 mgmL<sup>-1</sup> of PEI to 50 mL deionised water. This mixture was added to 5 ml of iron oxide. Thereafter, the mixture was sonicated for 1 h (using Soniprep 150 plus, MSS150.CX4.5, MSE Co). The particle was magnetically separated and washed consecutively 5 times in 30 mL of deionised water to eliminate excess PEI. The final particles Figure 3-2 were stored.

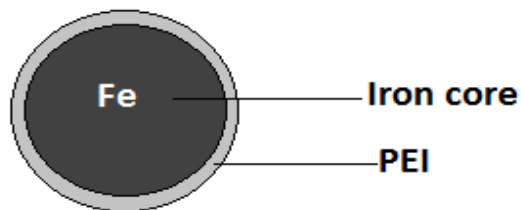


Figure 3-2: Schematic diagram of iron oxide NPS coated with PEI

### 3.3.2.2 Gold seeding step

Gold seeds (2 nm) were made by adding 375  $\mu\text{L}$  (4 %  $\text{HAuCl}_4$ ) and 500  $\mu\text{L}$  of 0.2 M potassium carbonate  $\text{K}_2\text{CO}_3$ . The 5 mL solution of sodium borohydride ( $0.5 \text{ mg mL}^{-1}$ ) was added separately 5 times to 100 mL icy cold water after 10 min. The yellow solution changed into a deep red solution. The gold (negatively charged) will interact electrostatically with PEI (positively charged) to reach the gold seeding formation. The solution was stirred on ice for a further 10 min and then stored in the fridge.

The gold seed solution (90 mL) was stirred at room temperature with 2 mL of  $\text{Fe}_3\text{O}_4$  of PEI solution temperature for 2 h. Then, the HNPs were magnetically separated from the solution and washed six times with deionised water. The product particles were diluted in 5 mL  $\text{H}_2\text{O}$ . Gold seeds were protected by stirring the particle with  $1 \text{ mg mL}^{-1}$  of PEI (2KD) polymer for 10 min. Particles were stirred with (20 mL,  $1 \text{ mg mL}^{-1}$ ) PEI (MW=2000) solution for 10 min to stabilize gold seeds. After this, particles were magnetically and washed six times in deionised water.

### **3.3.2.3 Gold coating process**

The last step of gold to complete coating was achieved by placing the particles in 110  $\mu\text{L}$  of (0.01 M) NaOH solution and stirring at 60 ° C. Hydroxylamine solution (750  $\mu\text{L}$ , 0.2M) was added followed by 1% HAuCl<sub>4</sub> (500  $\mu\text{L}$ ). After 10 min 250  $\mu\text{L}$  of NH<sub>2</sub>OH was added and followed by 500  $\mu\text{L}$  HAuCl<sub>4</sub> over four iterations.

The particles were washed 6 times and magnetically separated. The final particles resuspended in 5 mL H<sub>2</sub>O.

### **3.3.3 Hybrid nanoparticle characterisation**

#### **3.3.3.1 Transmission electron microscopy (TEM)**

Images of the nanoparticle products of every action in the synthesis of HNPs were attained by using a JEOL 1200 EX-FDL5000 microscope (Jeol, Japan) transmission electron microscope. Sample preparation involved diluting every sample in deionised water and a small amount (10  $\mu\text{L}$ ) was dropped onto a formvar coated copper grid (prepared earlier and dried for this objective) and permitted to dry at room temperature. The grids were situated into the TEM and directly imaged.

#### **3.3.3.2 Inductively coupled plasma –optical emission spectroscopy**

Inductively coupled plasma-optical emission spectroscopy (ICP/OES) was adopted to deduce the amount of both gold and iron in the hybrid nanoparticles formed. The instrument used was an Optima 7000 DV ICP-OES (PerkinElmer, Wokingham, UK). An acid digestion was performed on the models adopting a mixture of concentrated nitric acid and hydrochloric acid (1:1) with heating to 100 °C (1:5 modal: acid mixture).

The result was then diluted alongside deionised water (1:1000) preceding the analysis. A calibration was performed adopting usual iron and gold solutions ( $1000 \mu\text{g mL}^{-1}$ ) diluted alongside deionised water ( $10 \mu\text{g mL}^{-1}$  -  $0.05 \mu\text{g mL}^{-1}$ ).

### **3.3.3.3 UV/Visible spectroscopy**

Iron oxide nanoparticles, nanoparticles following the gold seed step and the final iron oxide core-gold shell hybrid nanoparticles (HNPs) were analysed using a Varian Cary 50 Bio Uv-Vis spectrophotometer over a wavelength range of 300 nm -700 nm in order to determine the  $\lambda_{\text{max}}$  of the HNPs which was indicative of the surface plasmon resonance for heating purposes. UV Peak absorbance was recorded for the aqueous samples in deionised water using quartz cuvettes. Uv-Vis absorption spectra were recorded in triplicate at room temperature and recorded as an average value.

### **3.3.3.4 Photon correlation spectroscopy and zeta potential measurement**

A diluted sample of nanoparticles in deionised water was arranged and sonicated in an ultrasonic bath preceding to analysis. Hydrodynamic diameter, polydispersity index (PDI) and zeta potential measurements were measured using a Zetasizer Nano-ZS, Malvern tools, UK. The calculations were administered at every action of the nanoparticle synthesis, all calculations were administered in triplicate at  $25^{\circ}\text{C}$  and an average value was reported.

### **3.3.4 Incorporation of HNPs into PAA-Ox5**

A 10 mL solution of  $5 \text{ mg mL}^{-1}$  PAA-OX5 was prepared with deionised water as the diluent. The polymer solution was probe sonicated for 10 min. To this solution 0.5 mL HNPs were added and the mixture was probe sonicated for a further 10 min.

### 3.3.5 Characterisation of PAA-Ox5 and PAA-Ox5-HNP Nano-aggregates

The macromolecular aggregates were characterised using photon correlation spectroscopy and zeta potential measurement as described above. The aggregation of these polymers were investigated using surface tension measurement as outlined in Chapter 2.

## 3.4 Results

### 3.4.1 Inductively Coupled Plasma-Optical Emission Spectroscopy (ICP- OES)

Metal content of the nanoparticles formed was quantified using the technique (ICP). The detection wavelengths for gold and iron were measured at 242.794 nm and 261.187 nm respectively. The  $R^2$  value of gold = (0.9999) and for iron =(0.9999) are shown in Figure 3-3. Three different batches of HNPs were measured giving the gold concentration was  $0.22 \mu\text{g/mL} \pm 0.1$  while the iron concentration was  $4.50 \mu\text{g/mL} \pm 0.41$  Figure 3-4.

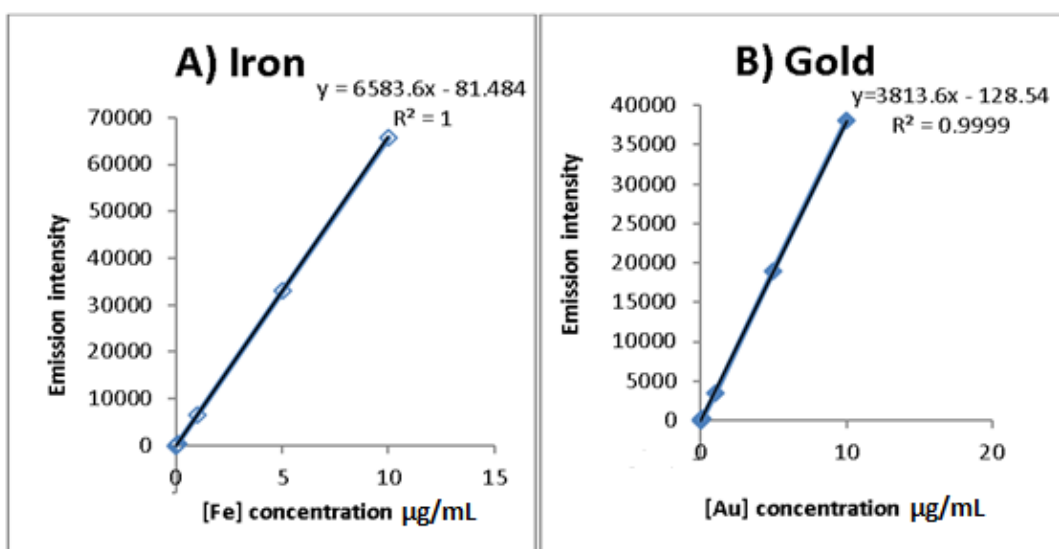


Figure 3-3: ICP/OES standard calibration curves for A ) Fe and B) Au

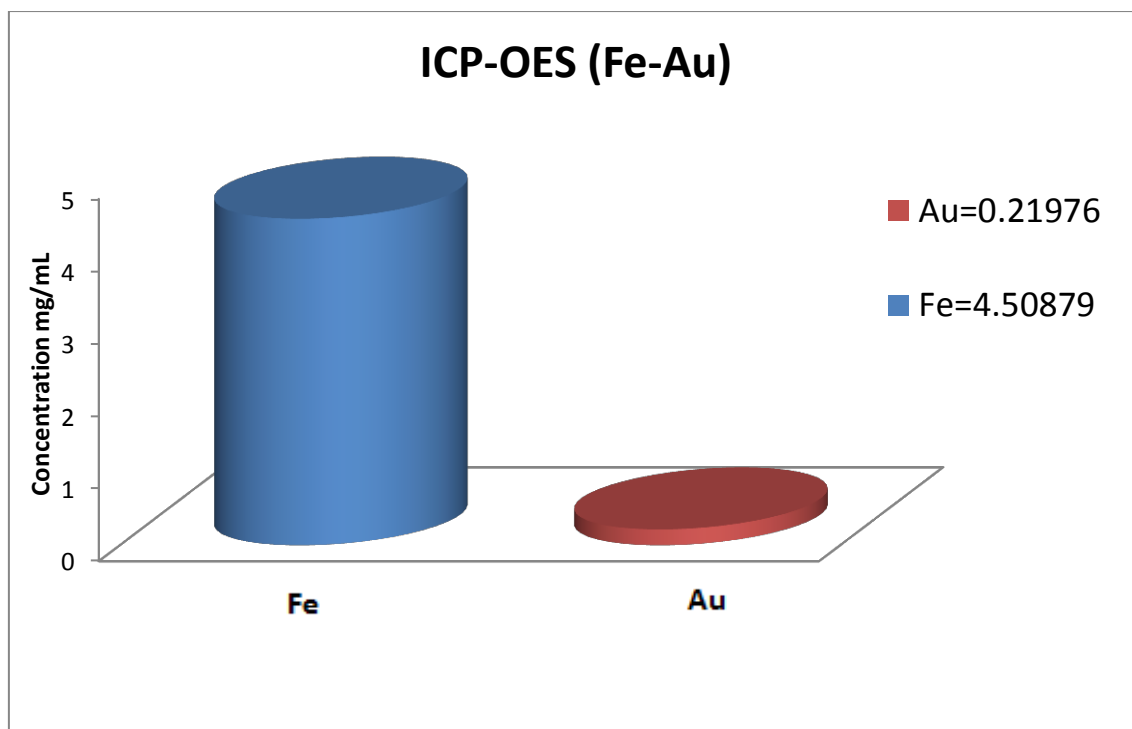


Figure 3-4: A graph viewing the concentrations of Au and Fe in HNPs identified by ICP-OES

### 3.4.2 UV/Visible spectroscopy

The absorption spectra of each formulated part in the HNPs was determined at the maximum absorption wave length in UV/Visible spectroscopy graph Figure 3-5. The MNPs ( $\text{Fe}_3\text{O}_4$ ) alone did not show any absorbance within the wavelengths tested.

The colloidal 2 nm gold seeds showed strong absorbance at around 480 nm. Once attached onto the  $\text{Fe}_3\text{O}_4$ -PEI a band shift was observed with a lambda max of approximately 540 nm. After subsequent coating the final HNPs showed a peak absorbance of 600 nm, this indicated that complete coating had formed Figure 2.7.

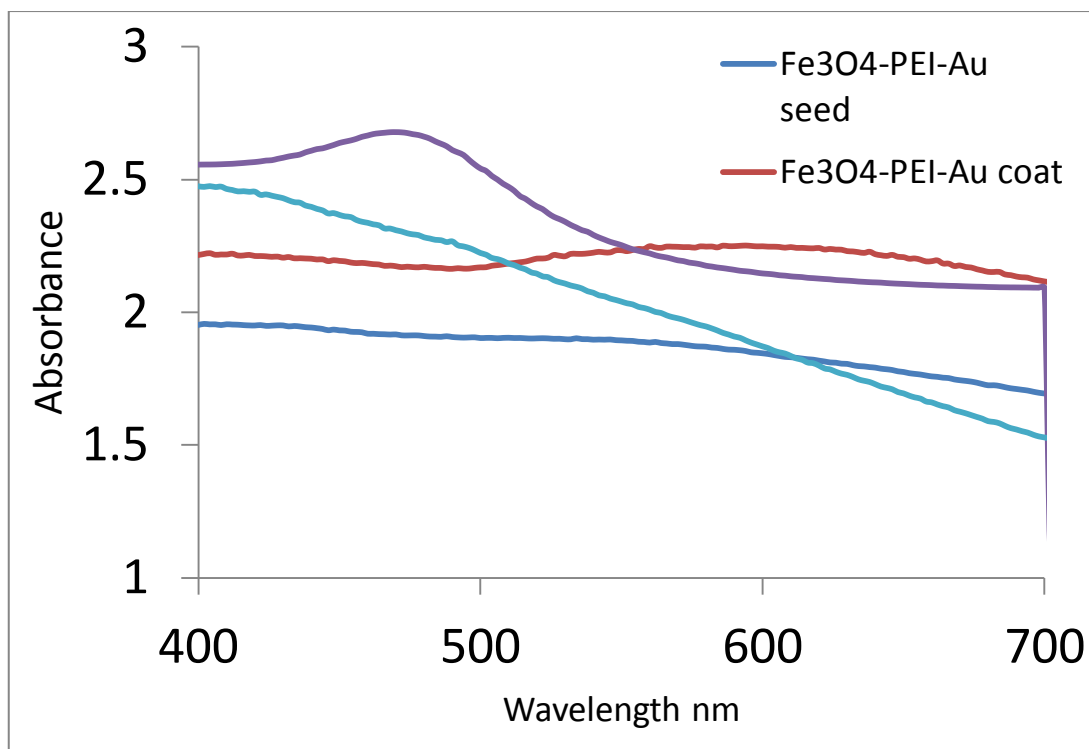


Figure 3-5: UV –Vis absorbance spectra of  $\text{Fe}_3\text{O}_4$ , Au seed ,  $\text{Fe}_3\text{O}_4$ -PEI and HNPs

### 3.4.3 Characterisation using TEM

Characterisation of products from each of the intermediate steps and of the final HNPs prepared was undertaken and is described below.

First step of hybrid nanoparticle formulation started with TEM imaging of iron core at 150K magnification to verify the average size and morphology which was recorded about 40 nm and spherical as shown in Figure 3-6.

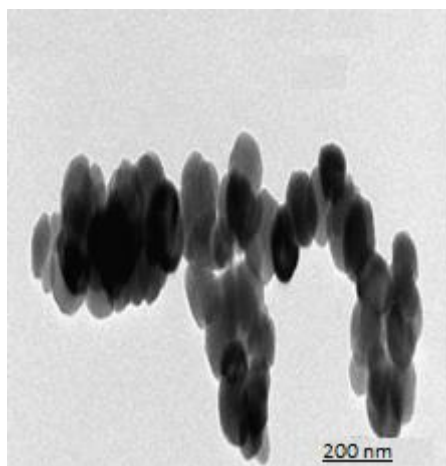


Figure 3-6: TEM images of A) iron oxide core

The next steps of hybrid nanoparticle formulation was PEI coating of iron core imaged at 120K as shown in Figure 3-7. These look similar to the uncoated iron oxide. This is because the electron dense metals appear dark on the TEM whereas polymers are less dense, hence it is very difficult to distinguish between these two samples.

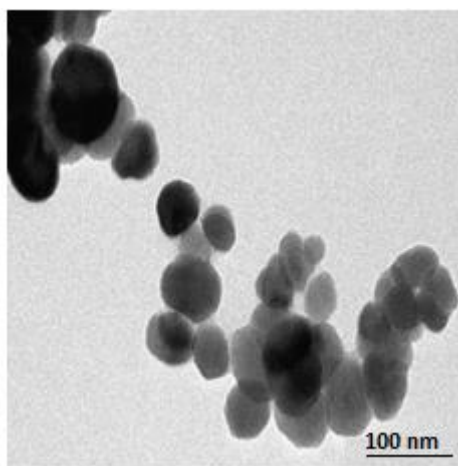


Figure 3-7: TEM images of iron core-PEI coating

The gold seeding processes was confirmed with 2 nm gold nanoparticles surrounding the iron core as shown in Figure 3-8 which appeared clearly on the surfaces of NPs at 200K magnification.

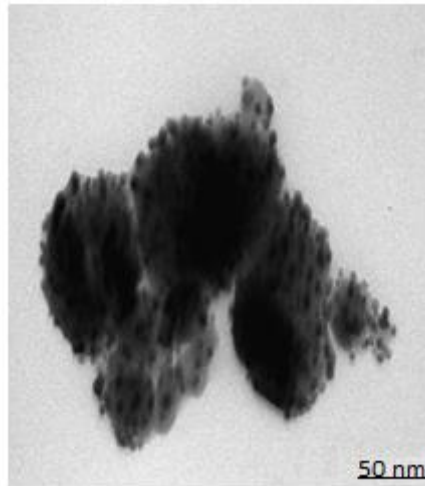


Figure 3-8: TEM image of gold seeded iron NPs

The final shape of HNPs was imaged at 100 K magnification and showed approximately particle size around 75 nm. The image of final particles was showed external smooth shape with fully gold coated layer and no more appearance was observed for the gold seeds Figure 3-9.

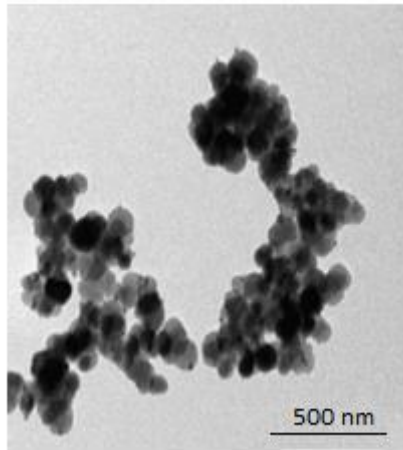


Figure 3-9: TEM image of final HNPs

### **3.4.4 Characterisation of PAA-Ox5-HNP**

#### **3.4.4.1 Surface tension**

The data from this test shows that the CAC for the PAA-Ox5 was  $0.3125 \text{ mgmL}^{-1}$  (Chapter 2 – Figure 2-16.) whilst the polymer aggregate incorporating the HNP containing amphiphile (PAA-Ox5-HNPs) decreased to  $0.039 \text{ mgmL}^{-1}$ . This suggested that the aggregates formed at lower concentration see Figure 3-10. This may be due to the magnetic nature of the HNPs bringing the hydrophobic pendant groups closer to one another hence resulting in earlier aggregation compared to the PAA-Ox5.

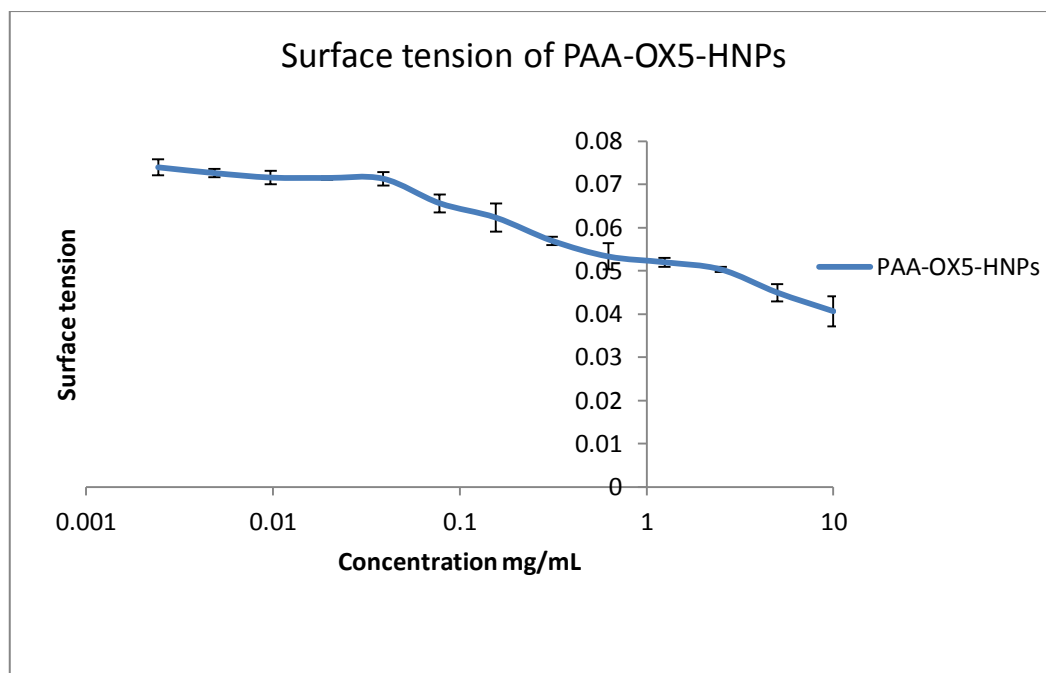


Figure 3-10: Surface tension (N/m) of PAA-Ox5-HNP(n=3, ave  $\pm$  SD)

#### 3.4.4.2 Photon correlation spectroscopy

The charge increased from -8 mV to +26 mV, due to the amine groups in the polymer (polycationic PEI) gives the positively charge; this large increase in surface charge is indicative of successful polymer attachment (Hoskins *et al.* 2012).

After gold seeding the zeta potential dropped to +11 mV and -6.4 mV respectively Table 3-2 owing to the electronegative charge on the colloidal gold. The final particles coating were recorded with remarkable decrease to -6.4mV and the final particles were visualised using TEM and the particle diameter was determined to be 1221 nm as a result of intrinsic magnetic iron particles.

Table 3-2 Zeta potential and PDI, hydrodynamic radius of nanoparticle solution of hybrid nanoparticle synthesis at different steps

Particles	Hydrodynamic radius/ nm	PDI	Zeta potential/mV
Iron oxide	1221	0.328	- 8
Iron oxide-PEI	800.7	0.420	+ 26
Gold seeded PEI coated iron oxide nanoparticles	649.6	0.587	+11
HNPs	173.3	0.185	-6.4

Therefore, the diameter of the particles remarkably decreased with the next formulation steps of polymer and gold coating related to aggregation reducing abilities of magnetic particles Table 3-2. The polydispersity index (PDI) of HNPs referred to the homogeneity rate of the distribution of the particles in the formulation, which here showed values near 0.3 that detect a good dispersity index rate of this formulation Table 3-2.

Presuming that one thiol aggregation only is tied up to one HNP committing low combination of HNP used in conjugation as well as the steric hindrance effect. HNP fixed to PAA-Ox5 approved by TEM images which detected as dark curtail parts inside nano aggregate Figure 3-11.

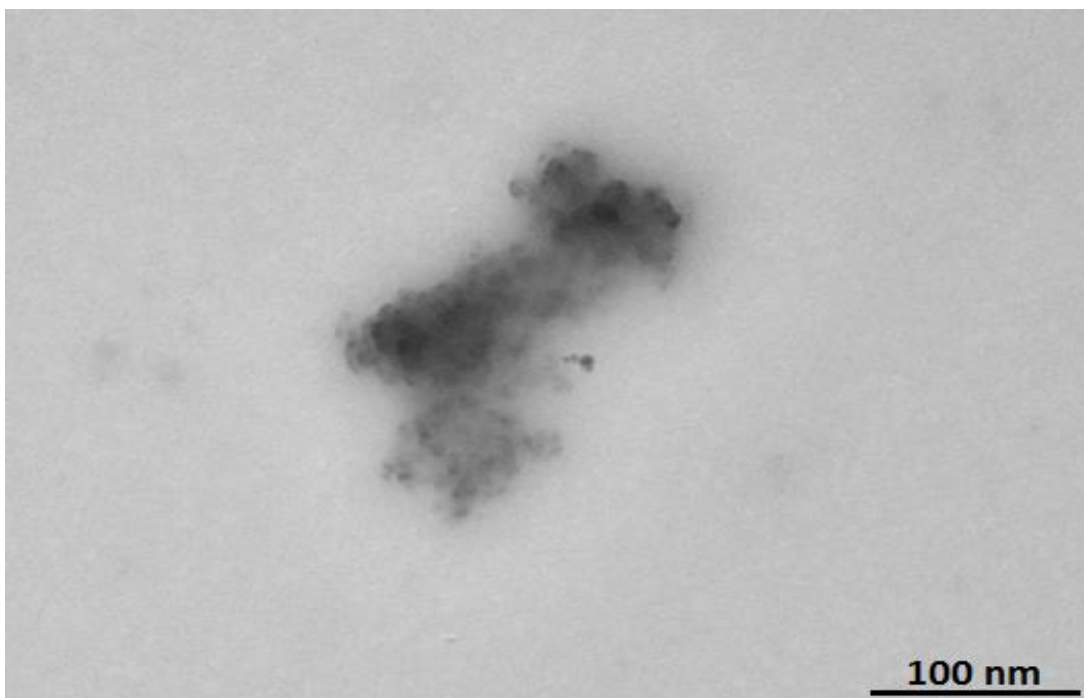


Figure 3-11: TEM image of PAA-Ox5-HNPs nano-aggregates

### 3.5 Discussion

One of the interesting emerging designs in polymer therapeutics is in the incorporation of HNPs within PAA-OX5 amphiphilic polymers for form magnetomicelle. These serve as multifunctional platforms for imaging and drug delivery (Barnett *et al.* 2013a). In this chapter, the potential of metallic amphiphilic polymer function was used as a drug carrier with the ability of incorporation of specific bio-particle to the surfaces of HNP.

The HNPs were incorporated into PAA-OX5 polymer via dative covalent bonding between the gold surfaces and thiol function group of the oxadiazole pendant group.

Several techniques were used to characterise the synthesis steps of polymer and HNP binding by  $^1\text{H}$  NMR, FTIR, TEM and zeta potential measurements as illustrated in Chapter 2.

Concerning the synthesis of the hybrid nanoparticles (HNPs), the information obtained supports the successful synthesis of the particles. The information created from the surface charge measurements correlate the expected pattern, from being negatively charged particles for the uncoated iron oxide core (notably, due to the surface associated sulphate (Hoskins *et al.* 2012)) to the positively charged PEI-coated iron oxide core, due to the positively charged amino groups inside the PEI construction which is covering the iron oxide core. Figure 3-12 displays an appropriate extent of particle separation as driven by the devaluation in hydrodynamic radius.

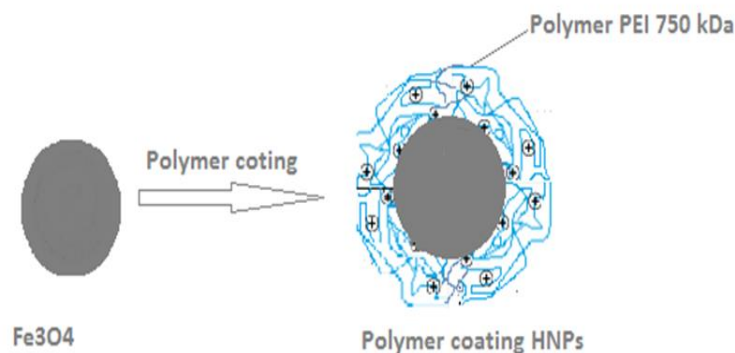


Figure 3-12: Explain PEI-coated iron oxide core

In addition to that, the contradictory charges between the iron oxide core and the PEI polymer selected a good sort of charge-charge interaction.

The reduction in surface charge after the inclusion of the small gold seed nanoparticles and after the final gold surface application advocates the successful coating of the gold outer layer.

Metal content of the HNPs was exposed by ICP-OES and counted the concentration of the gold and iron which is acknowledged as main crucial step in the next biological application of the new formulation. UV/Vis spectroscopy information was adopted to detect the existence of gold on the surface of the HNPs. Gold nanoparticles show an optical characteristic known as surface plasmon resonance (SPR) and the SPR wavelength for gold nanoparticles is an observed in the visible region (500 nm - 600 nm). The magnitude of the absorbing peak and the absorbing shifting was enormously dependent on the diameter and form of gold nanoparticles (the absorbing wavelength rises alongside a large and variable gold particles) (Huang *et al.* 2007; Hoskins *et al.* 2012). In the end, the TEM images of the starting, intermediate (gold seeding step) and the eventual HNPs confirm the successful synthesis. The TEM images also give supporting information for the resulting diameter and form of the HNPs: the final diameter of the HNPs appears to be inside the range of 100 nm-120 nm and the form was approximately stellar as pointed out by the image of the HNPs Figure 3-12. The results obtained in this study matched the others reported in the literature (Hoskins *et al.* 2012a).

### 3.6 Conclusion

Hybrid iron oxide-gold NPs have been successfully formulated and characterized by several methods such as PCS, UV–vis absorption and TEM. All the checking steps confirmed the successful formation procedure of hybrid nanoparticles. The magnetic iron core with 40 nm diameter was manufactured and other formulated layers were diagnosed as a poly(ethylenimine) intermediate layer and gold coating. The last size of HNPs was about diagnosed as 100 nm by TEM. These particles were successfully incorporated into the PAA-Ox5 structure. This will enable the controllable release of hydrophobic drugs through heat trigger. These drug analogues will be synthesized in Chapter 4.

Attachment of doxorubicin to the surface of the HNPs is worth exploring further. Sulfur forms dative bonds to the gold surface but it have been shown that electrostatic interactions can also be used to attach drug substances to gold. Irradiation of a formulation of a polyamine drug derivative coated onto HNPs with near infrared laser light triggers drug release.

CHAPTER FOUR

SYNTHESIS AND

CHARACTERISATION OF

DOXORUBICIN ANALOGUES

## 4.1 Introduction

Cancer is a devastating disease associated with high mortality rates. The main treatment methods for cancer are chemotherapy, surgical treatment, and radiation therapy, with the chemotherapy the most commonly used (Zuccala, 2016). In spite of this, there are more than 70 types of anticancer drugs which have been used, and a variation of new anticancer drug using in clinical trials. However there are many problems yet to be solved associated with these chemotherapies, such as aqueous drug solubility, side effects from systemic potency, the extend of premature drug degradation, and multidrug resistance. To enhance the targeting ability and drug solubility, improving the rate and therapeutic effect of the anticancer drugs, the design and discovery of reasonable nanocarriers and their targeting drug delivery system has received attention (Maeda, 2015).

### 4.1.1 Doxorubicin

Doxorubicin((7S,9S)-7-[(2R,4S,5S,6S)-4-amino-5-hydroxy-6-methyloxan-2-yl]oxy-6,-  
9,11-trihydroxy-9-(2-hydroxyacetyl)-4-methoxy-8,10-dihydro-7H-tetracene-5,12-dione

Figure 4-1 was first extracted from *Streptomyces Peucetius Var*. Doxorubicin is a drug used in therapies for the treatment of many diseases among them lymphoblastic leukaemia, non-Hodgkin's lymphoma and breast carcinoma (Reddy *et al.* 2005).

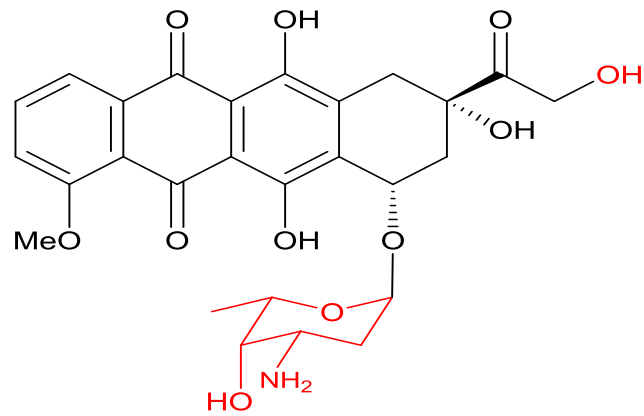


Figure 4-1: Structure of doxorubicin

Doxorubicin (Dox) is an anthracycline antibiotic which plays the role of a DNA intercalater to restrict topoisomerase II from isolating DNA double helix strands while reproducing and therefore stopping the duplication of cells Figure 4-2 (Swift *et al.* 2006). Dox is the most antineoplastic operator used in the treating paediatric and adult cancer, leukemia, lymphomas, breast carcinoma and many other cancerous tumours (Vincenzi *et al.* 2010) and (Hortobágyi,1997).

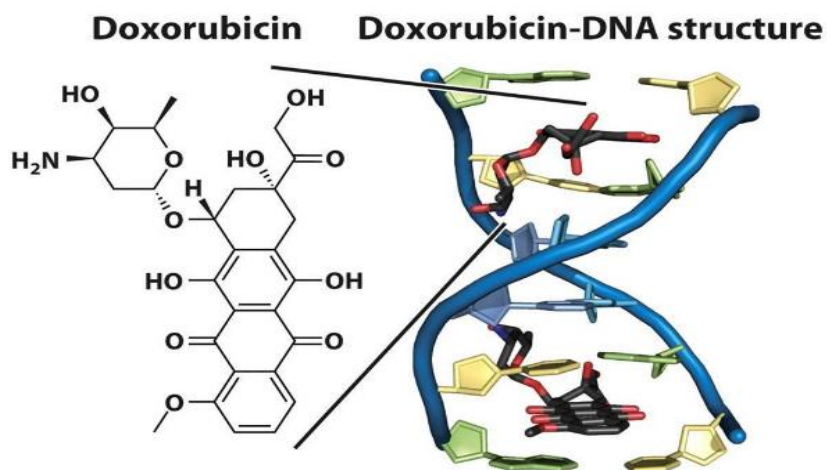


Figure 4-2: Doxorubicin intraction into DNA structure (Freeman ,2012)

Furthermore, the usage of Dox has been restricted for the dangerous side effects which include gastrointestinal disorders bone marrow toxicity, alopecia, stomatitis, acute and cumulative cardio-toxicity as well as extravasation (Octavia *et al.* 2012). However, to avoid these limitations and modify the therapeutic potential of Dox several approaches have been trialled such as chemical modification (Huang, 2012) and loading the drug molecules into nanocarriers such as polymeric micelles (Shan, 2011) vesicles, liposomes and nano gels (Bochot *et al.* 2012). The chemical modification of Dox forming analogues is crucial for the continued ability to use clinically as these analogues can overcome the undesirable side effects whilst maintaining clinical efficacy (Oh *et al.* 2008). The chemical modification can adjust the properties of Dox such as lipophilicity, cellular uptake and prolonged activity (Chhikara *et al.* 2010). Substantial work has been carried out in order to form more acceptable prodrug and analogue forms of Dox to date (Ding *et al.* 2012).

In the present study, we describe the preparation of new doxorubicin analogues by coupling of doxorubicin with lipoic acid and doxorubicin with spermine. The results are expected to exhibit better effective therapies than anything else previously develop

#### **4.1.2 Polyamines**

Polyamines are chain like structure which consists of two or more amines. The growth of polyamines occurs naturally or is produced by hormone treatment. The naturally arising amines (putrescine ( $C_4H_{12}N_2$ ), spermidine ( $C_7H_{19}N_3$ ) and spermine ( $C_{10}H_{26}N_4$ )). Figure 4-3 are derivatives resulting from the transglutaminase reaction take part in the active cell life circle. Polyamine balance within the active cell is related to the growth

estimation, therefore, fewer polyamine levels are identified by shrinkage of the cell growth (Nowotarski *et al.* 2013).

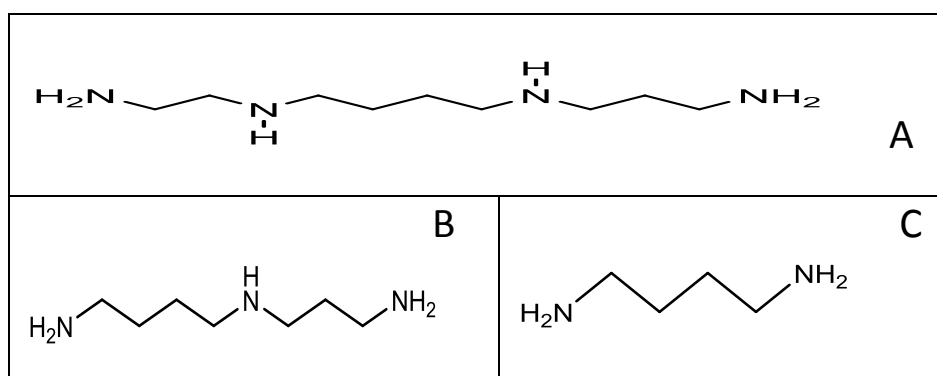


Figure 4-3: Structures of naturally occurring polyamines: A spermine ,B spermidine and C putrescine

In addition to that, cancer progression is subjected to be controlled by polyamines, as, the highest polyamines level is detected in cancer cells of breast and colon unlike normal cell; however, the higher polyamine levels were checked with patients with psoriasis, cystic fibrosis (Casero & Marton 2007). Protein synthesis have been shown to be triggered by polyamines through provocation of DNA and RNA synthesis due to its responsible for the organization and stabilization of the structure and efficacy of these biomolecules (Child *et al.* 2003) in addition to that stealth of reactive-oxygen species by polyamines guides to the conservation of DNA proteins and lipids (Nowotarski *et al.* 2013).

Scientists over the last two decades acknowledge the reticence of the anabolic pathways of polyamines. The prevention for anabolic enzymes in the biosynthetic pathway of polyamines was checked but none of them gets progressed due to their lower efficacy as anti-cancer operator (Casero & Woster 2001).

Profiting of polyamine carrier as an engine to develop the process of rising up of the promising anticancer agents by involving the polyamines in their building, was a taking a big part of researches pointing the goal to make analogues with better cytotoxic activity either added to or being apart from reticence of polyamines biosynthesis (Casero & Woster 2001; Muth *et al.* 2014).

#### **4.1.2.1 Spermine**

Spermine is a natural polyamine with the molecular formula  $C_{10}H_{26}N_4$ , which exists in many microorganisms as well as in all eukaryotic cells but in different species forms as well as different ranges of polyamines. Putrescine, spermidine and spermine are the only polyamines produced by mammals (Kusano *et al.* 2007).

The structure of spermine was first identified in 1926 by a group of scientists. Antonie van Leeuwenhoek had characterized crystals of spermine phosphate in human semen in early 1678, while the name spermine was adopted first in 1888 by Ladenburg and Abel. Spermine is considered as a polycation at physiological pH and it is the constituent that gives the semen fluid its characteristic smell (Pegg *et al.* 2009).

Aside from this biological activity spermine is a charged molecule. Its cationic nature arises from the amine groups within its backbone. These groups can be exploited for reversible binding on the hybrid nanoparticle systems for drug delivery. Malekigorji *et al.* reported the use of a bisnaphthalimido based drug separated by a spermine chain which shown reversible binding onto hybrid iron oxide-gold nanoparticles after laser irradiation. The system developed enhanced drug efficacy *in vivo* in pancreatic cancer tumours. In this work we adopt this strategy and attach the spermine residue into the

Dox molecule to act as a conjugation site for attachment onto the hybrid nanoparticles inside the PAA amphiphiles developed in Chapter 3.

### 4.1.3 Lipoic acid

$\alpha$ -Lipoic acid is a type of thioctic acid, consistently presenting aggregation. Lipoic acid Figure 4-4 is synthesised enzymatically from octanoic acid in the mitochondria but it can also be acquired from Alimentary sources. It has been found to congregate in many tissues for a precise period of time. The mixture takes an important role in energy metabolism as it performs as a critical co-factor for the  $\alpha$ -ketoacid dehydrogenase enzyme situated within the mitochondria. However, the data has been demonstrating that lipoic acid from dietary sources may not function as a metabolic determinant.

Lipoic acid from dietary supplement is hard to generate key biochemical operation which can lead to a possible therapeutic effect. In addition to the antioxidant effect of lipoic acid, the mixture has been expressed as part of an administration for controlling diabetes and as an aid to enhance age-associated cardiovascular, cognitive, and neuromuscular deficits. It has also been displayed to play as a modulator of various inflammatory signalling pathways (Biewenga *et al.* 1997 Packer *et al.* 1995; Shay *et al.* 2009; Goręca *et al.* 2011; Vallianou *et al.* 2009).

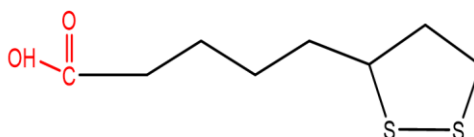


Figure 4-4: Chemical structure of lipoic acid

The conjugation of lipoic acid onto the Dox structure will allow for disulphide binding onto the hybrid nanoparticle surface which should break down at elevated temperatures.

## 4.2 Aims and Objectives

This project aims to synthesize two drug analogues of doxorubicin. The organic synthesis will be carried out using established protocols from the literature. Structural analysis of the compounds will be carried out using nuclear magnetic resonance, Fourier transforms infrared spectroscopy and thin-layer chromatography.

## 4.3 Materials and Methods

### 4.3.1 Materials

Table 4-1 shows the materials which is used to synthesize the doxorubicin analogues.

Table 4-1 Materials used in drug analogue synthesis.

	Materials	Supplier
1	Doxorubicin HCl	LC Laboratories (Woburn, USA)
2	Spermine	Alfa Aesar
3	Alpha Lipoic acid	Sigma Aldrich
4	N,N-Dicyclohexylcarbodiimide (DCC)	Acros organics
5	Dichloromethane (DCM)	Fisher Scientific, UK
6	Try ethyl amine (TEM)	Fisher Scientific, UK
7	Methanol	Fisher Scientific, UK
8	N-Hydroxy succinimide (NHS)	Alfa Aesar
9	Carbonyldiimidazole (CDI)	Alfa Aesar
10	Deuterated chloroform	Cambridge Isotope Laboratories, Inc.
11	Deuterated methanol	Cambridge Isotope Laboratories, Inc.
12	Deuterated dimethyl sulfoxide	Cambridge Isotope Laboratories, Inc.

## 4.3.2 Method

### 4.3.2.1 Coupling of doxorubicin to spermine

In a round bottom flask (RBF) 1, 1'-Carbonyldiimidazole (CDI) (1.9 mg, 12 mmol) and Dox (0.477mg, 878mmol) were dissolved in 50 mL of deionized water at 0 °C for 0.5 h . After this time spermine (2.4 mg, 12mmol) was added to the mixture and stirred at room temperature for 24 h. The reaction was monitored by TLC. The organic phase was evaporated to yield a dark red solid with a yield of 47 %., MP 174-175 ° C

Figure 4-5.

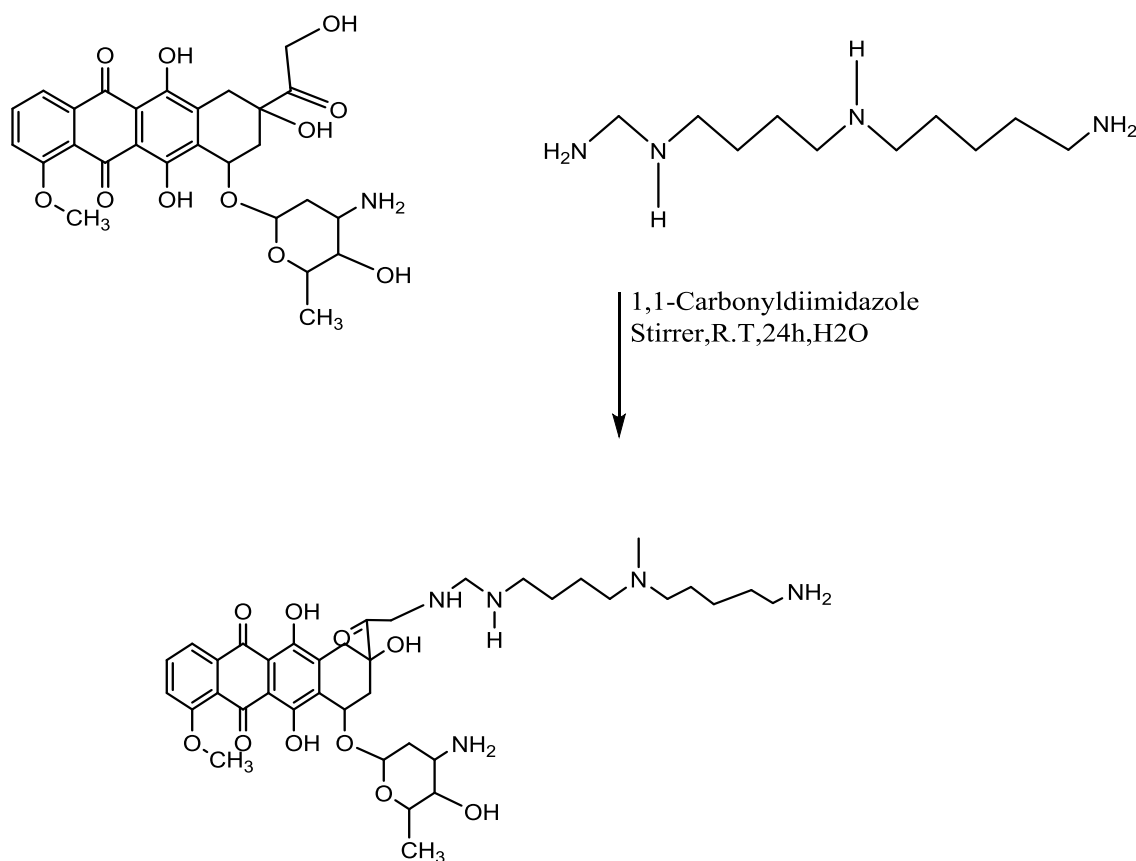


Figure 4-5: Synthesis of doxorubicin –spermine Reagents and conditions: deionized water, stirrer, 24 h

### 4.3.2.2 Coupling of lipoic acid to doxorubicin

This reaction has two steps, the first step was made to activated the lipoic acid.

#### 4.3.2.2.1 Activated the lipoic acid (step 1)

In a round bottom flask (RBF) lipoic acid (0.713mg, 3.45mmol) was dissolved in 20 mL dichloromethane (DCM). Dehydration agent N, N-Di cyclohexyl carbodiimide (DCC) (0.66 mg, 3.19 mmol) and (0.367 mg, 3.19 mmol) N-hydroxysuccinimide NHS were added to the mixture. The reaction was stirred for 24 h at room temperature. The result of the mixture was filtration to remove the solvents leaving a solid Yellow precipitate with yield 86% Figure 4-6.

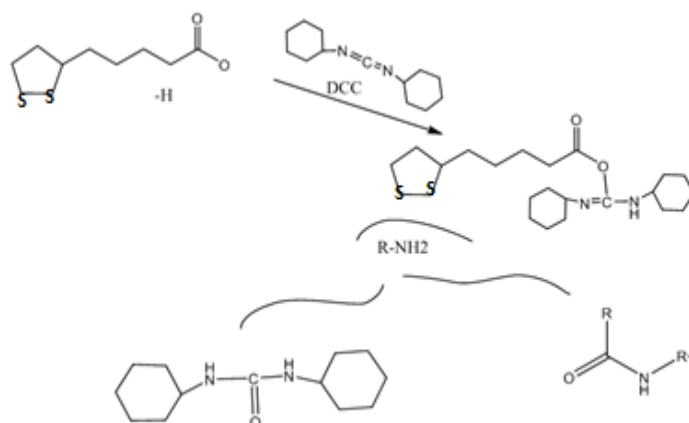


Figure 4-6: Activated the lipoic acid , Reagents and conditions: ethanol absolute reflux, stirrer, 24 h

#### 4.3.2.2.2 Doxorubicin coupling to lipoic acid (step2)

In a round bottom flask, doxorubicin (0.3258mg, 0.5994 mmol) was dissolved in 25 mL of MeOH and adding to the (0.182mg, 0.48 mmol) product (step1), the triethylamine (TEA) (0.32 mL) was added to drop wise the reaction mixture, and the reaction was

refluxed at R.T for 24 h. The solvent was removed leaving a solid dark red residue with yield 81% and MP 71-72 ° C Figure 4-7.

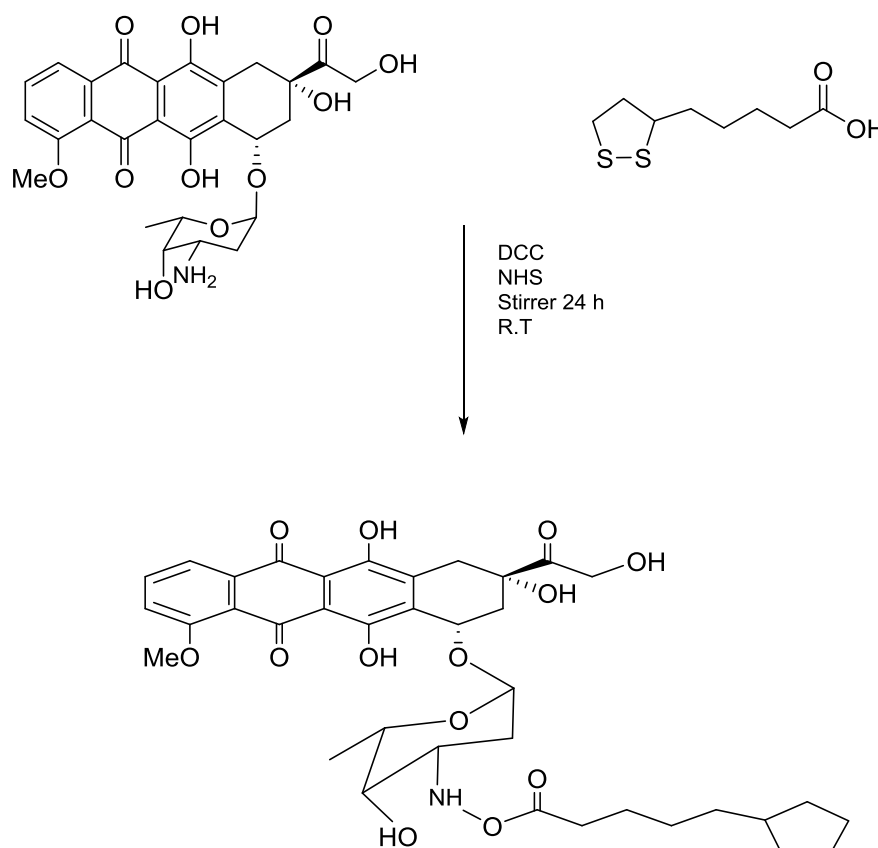


Figure 4-7: Reaction between doxorubicin and lipoic acid, Reagents and conditions: ethanol absolute reflux, stirrer, 24 h

### 4.3.2.3 Characterisation of Doxorubicin analogues

#### 4.3.2.3.1 Melting point

The melting point for each doxorubicin derivative was determined using an Advanced, Digital, Melting Point / SMP3 (Bibby Sterilin LTD, UK). Determination the melting point of each derivative was carried out in a pre-sealed (one end) capillary tube to hold

modals, full of 0.1 g-0.2 g of dry mixture. The sample tubes situated then in the melting point apparatus. The temperature was slowly elevated and the point at which the solid melted was recorded.

#### **4.3.2.3.2 Thin Layer Chromatography (TLC)**

Chromatography is a method used to separate chemical mixtures. There is a multitude forms of the chromatography such as: Thin layer chromatography (TLC), Gas chromatography (GC), Column liquid chromatography (CLC) and high performance liquid chromatography (HPLC) (Thammana, 2016).

TLC is a simple experiment which can be adopted in the laboratory to control reactions by checking whether the reaction is complete or not, decide the number of components in a blend, labelling of compounds or indicate their purity (Coskun, 2016, Yua *et al.* 2016). Chromatography contains a variety of the methods that depend on different distribution of the components of the substance to be separated into two phases: the first one stays fixed and called the stationary phase which can be either solid or liquid, and the second phase is called mobile phase which can be either liquid or a gas (Coskun, 2016).

TLC is carried out by spotting a sample on a silica gel coated sheet of aluminium as displayed in Figure 4-8. These TLC plates re then put in a shallow pool of an eluent solution to inspect the dissolution of materials within the response mixture. The retardation factor ( $R_f$ ), which describes in Equation 4-1, value was forecasted as the distance travelled by the unrecognized substance (a) detached by the distance travelled by the solvent through the TLC plate (b). Information attained with this

method was used to select the best solvent system for column chromatography (Coskun, 2016). Rf value is calculated as:

Equation 4-1 Retardation factor

$$R_f = \frac{\text{Distance travelled by compound}}{\text{Distance from baseline to solvent front}} \quad \text{--- (4-1)}$$

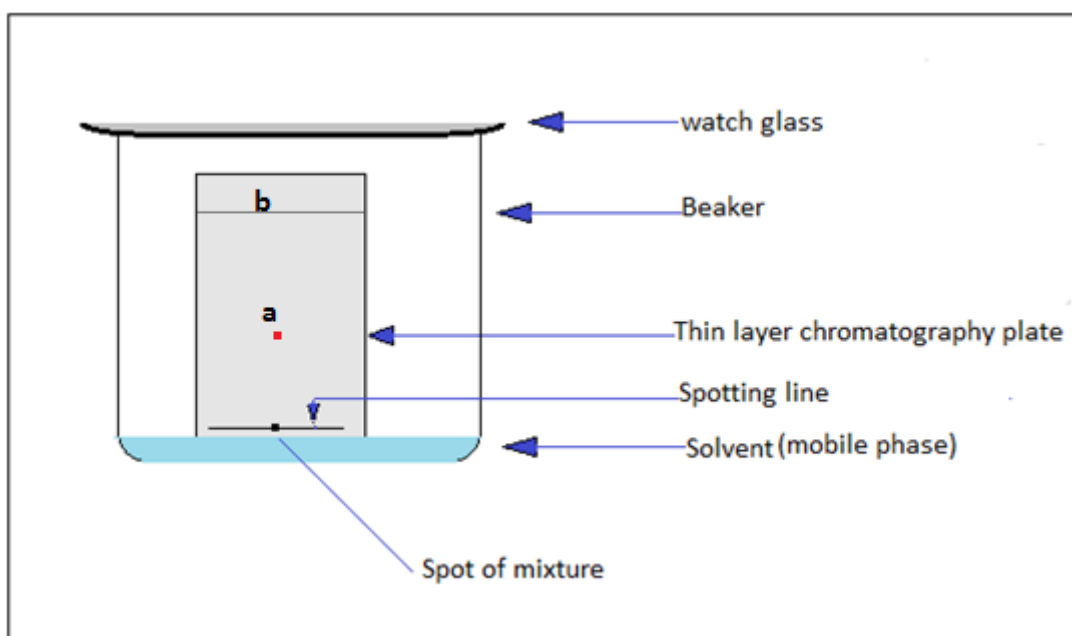


Figure 4-8: Diagram of TLC procedure

#### 4.3.2.3.3 <sup>13</sup>C NMR Spectrum

Carbon-13 (<sup>13</sup>C) nuclear magnetic resonance most commonly known as carbon-<sup>13</sup> NMR or <sup>13</sup>C NMR or often simply attributed as carbon NMR) is the usage of nuclear magnetic resonance (NMR) spectroscopy to carbon. It is analogous to proton NMR (<sup>1</sup>H NMR) and permit the labelling of carbon atoms in an organic molecule just as proton NMR

recognizes hydrogen atoms. As such  $^{13}\text{C}$  NMR is an essential tool in chemical structure explanation in organic chemistry.  $^{13}\text{C}$  NMR identify only the  $^{13}\text{C}$  isotope of carbon, whose natural abundance is only 1.1%, because the principal carbon isotope,  $^{12}\text{C}$  (Chemguide,2014).

#### **4.3.2.3.4 Mass Spectrometry**

The drug analogues were sent to Cardiff University and analysed by MALDI using a Bruker ultrafleXtreme instrument in positive-reflector mode with DCTB matrix (aprotic; molecular ions possible, any protonation could derive from HCl within the sample, any sodiation likely derives from ubiquitous sources). 1:1 MeCN: H<sub>2</sub>O solution.

### **4.4 Result**

#### **4.4.1 Characterisation of doxorubicin -spermine derivative**

##### **4.4.1.1 TLC analyses of doxorubicin-spermine**

TLC analysis of the DOX-SP mixture was carried out to clarify its purity. A drawing of the TLC plate is shown in Figure 4-9. The R<sub>f</sub> value of this compound is 0.66 mm in a methanol – dichloromethane (1:9) solvent system. A single spot indicate the reaction had reached completion and eliminated the need for further purification.

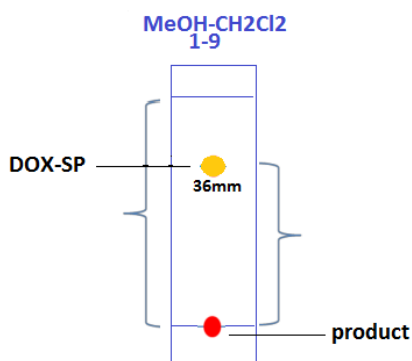


Figure 4-9: TLC plate of doxorubicin coupling to spermine (DOX-SP) post workup

#### 4.4.1.2 FT-IR spectrum of doxorubicin – spermine

Peak assignment of the FT-IR spectra obtained for the DOX-SP Figure 4-10 confirmed the coupling of the drug with spermine. This was due to the presence of the hydroxyl band at O-H ( $3254.09\text{ cm}^{-1}$ ) and the N-H ( $2937.64\text{ cm}^{-1}$ ) and  $2906.67\text{ cm}^{-1}$  of the primary amine, these groups were not present in the spectra for DOX alone and therefore this change in peak can be attributed to the drug molecule. Full peak assignment can be noticed in Table 4-2.

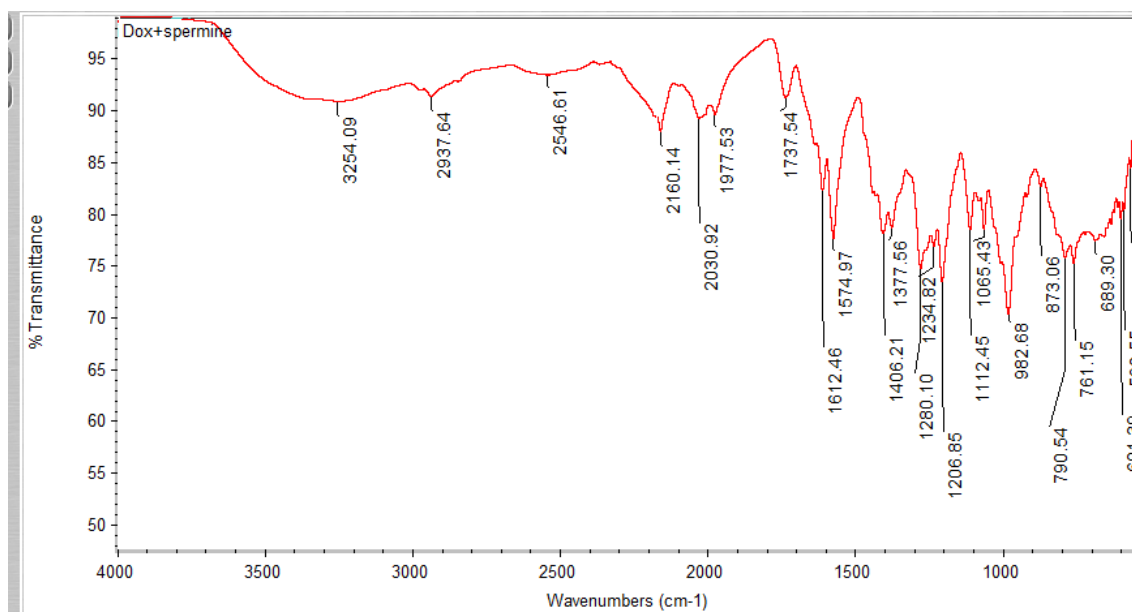


Figure 4-10: FT-IR spectra obtained for the DOX-Spermine

Table 4-2 Summary of functional of DOX-SP.

Compound code	Functional group	Bond	Frequency, $\text{cm}^{-1}$ Functional group
DOX-Spermine (DOX-SP)	Alcohol Secondary amines	O-H Stretch N-H Stretch	3254.09
	Alkanes	C-H Stretch	2906.67
			2937.64
	Carbonyl	C=O Stretch	1612.46
	Alkenes	-C=C- stretch	1638.99
	Secondary amines	N-H bend	1377.56
	Aromatics	C-C stretch (in-ring)	1574.97
	Alkenes	=C-H bend	1065.43
	Aromatic amines	C-N stretch	3000-3100
	Alkanes	C-H bend	850.22
	Aliphatic amines	C-N stretch	1280.10
Alkenes	=C-H bend	1406.21	

#### 4.4.1.3 $^1\text{H}$ NMR spectrum of Doxorubicin with spermine

The  $^1\text{H}$  NMR spectra Figure 4-11 of Dox-spermine show the spermine group at the following position: 1.1 ppm and 2.5 ppm. The spectrum displays Dox peaks at 7.5 ppm -8 ppm, corresponding to aromatic protons in Dox. The spectrum also indicates signal at 1.25 ppm which are characteristics of the methyl groups in Dox. The signals at 1.68 ppm, 1.88 ppm, 2.95 ppm, 4.75 ppm and 5.5 ppm were attributed to aliphatic cyclic protons.

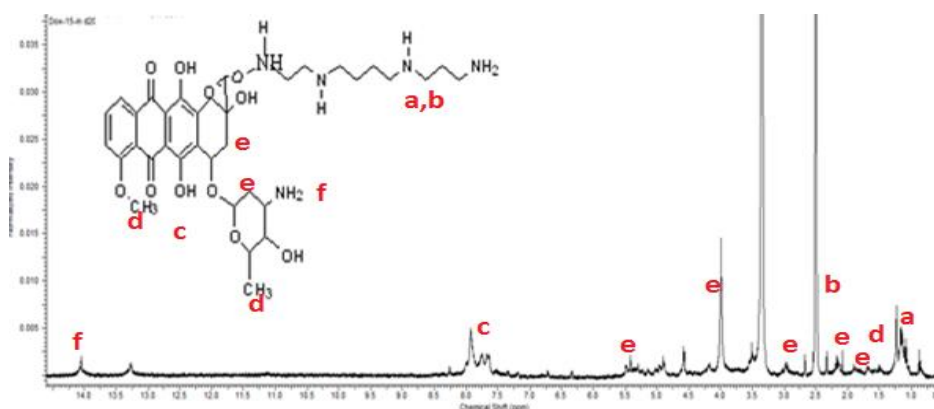


Figure 4-11:  $^1\text{H}$  NMR spectrum of doxorubicin with spermine in DMSO carried out using 400MHz NMR at 25 °C

#### 4.4.1.4 Mass Spectrometry

This sample Dox-SP Figure 4-12 was analysed by MALDI –Mass Spectrometry. In the spectra there is evidence for the expected molecule, MW=727, from the presence of a  $[\text{M}+\text{Na}]^+$  peak at  $m/z$  750.4 a.u., other species were observed which may have chlorine associated as would be expected from a polyamine Figure 4-13.

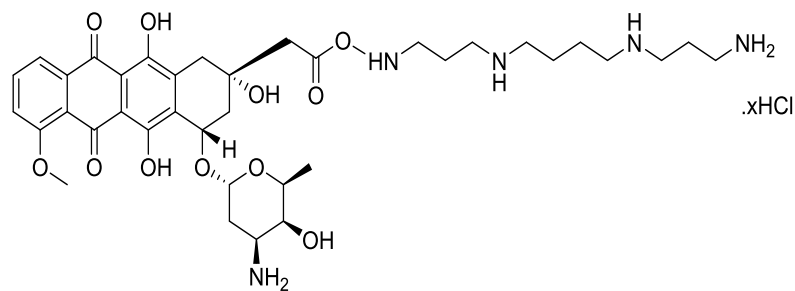


Figure 4-12: Doxorubicin coupling to spermine

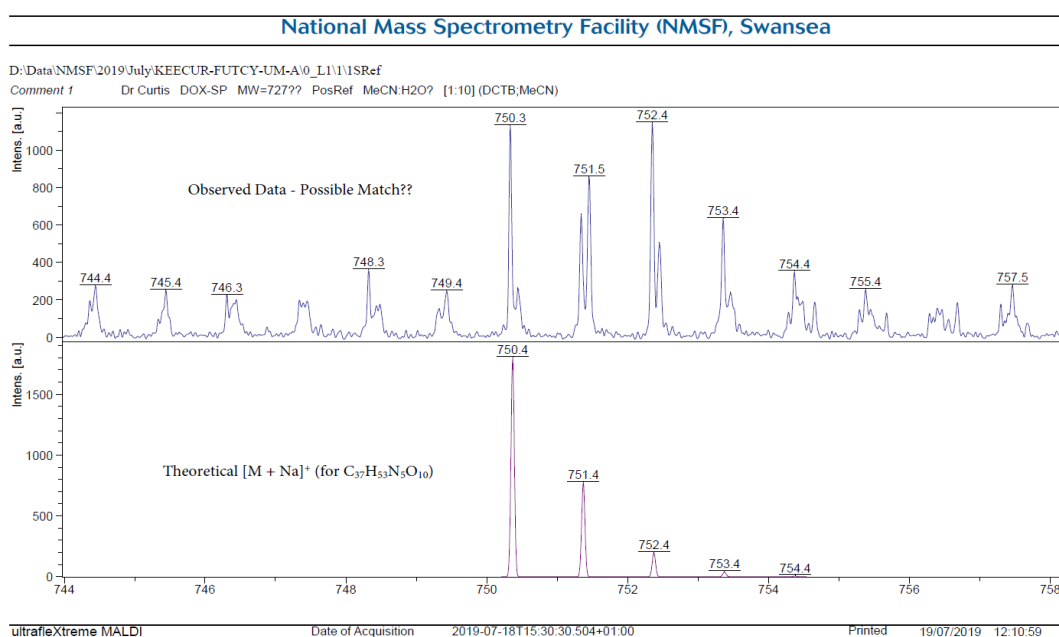


Figure 4-13: Mass spectra of DOX-SP

#### 4.4.1.5 <sup>13</sup>C NMR Spectrum of DOX- SP

The <sup>13</sup>C NMR Spectrum of DOX-spermine is shown in Figure 4-14-C. Aliphatic hydrocarbons (-CH<sub>2</sub>) were appearing between 23 ppm – 47 ppm Figure 4-14-a, aromatic carbons group between 121 ppm – 136 ppm. Amide group (O=C-N) was appear at 72 ppm Figure 4-14-b.

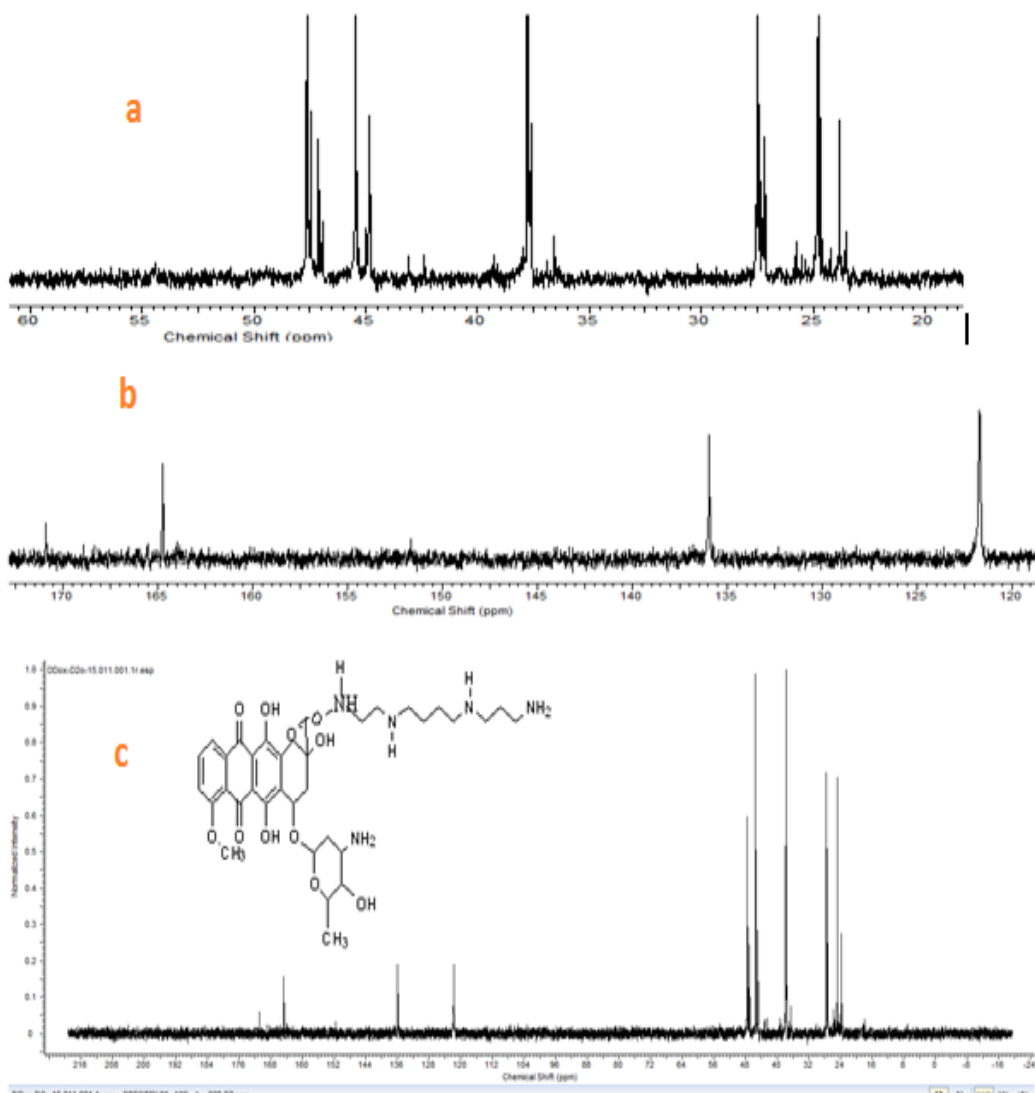


Figure 4-14:  $^{13}\text{C}$  NMR spectrum of (c) DOX-SP (c), (a) Aliphatic hydrocarbons, (b) Amide group of DOX in DMSO- carried out using 400MHz NMR at 25 °C

#### 4.4.2 Characterisation of Doxorubicin – lipoic acid derivative

##### 4.4.2.1 TLC analyses of doxorubicin-lipoic acid

TLC analysis of the DOX-LA combination post workup was carried out to explain its purity. An diagram of the TLC plate is showed in Figure 4-15. (A) Start materials which have two spots with two Rf. The Rf value of (B) mixture is 0.77 in an Ethyl Acetate - Petroleum Ether (6:1) solvent system.

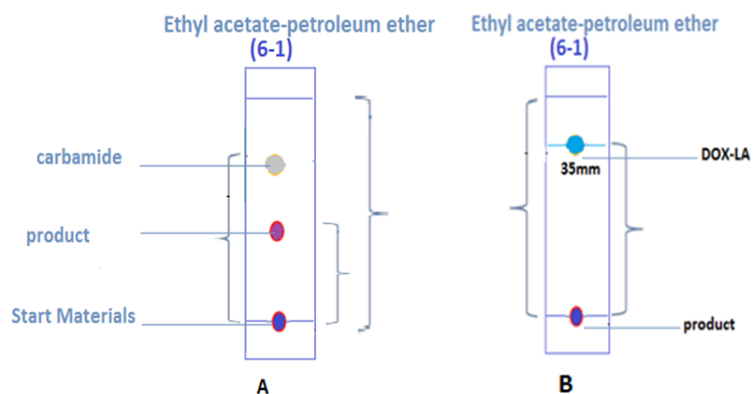


Figure 4-15: Chromatogram of TLC plate of DOX-LA,(A) step 1, (B) step 2

#### 4.4.2.2 FTIR spectrum of Doxorubicin – lipoic acid

FTIR has been utilized to study the coupling of DOX with lipoic acid. FTIR spectra of DOX-lipoic acid are presented in Figure 4-16 and characteristic peaks are tabulated in Table 4-3.

FTIR spectrum of DOX-coupling to lipoic acid shows the alcoholic O–H stretching band at  $3357.92\text{ cm}^{-1}$  and  $2936.18\text{ cm}^{-1}$ . The peaks of N–H stretching vibrations and O–H stretching vibrations intersect. From this FTIR result, it can be interpreted that attachment of DOX to lipoic acid occurs by the interaction of  $-\text{NH}_2$  groups of DOX with  $-\text{OH}$  groups of lipoic acid group hydrogen bonding.

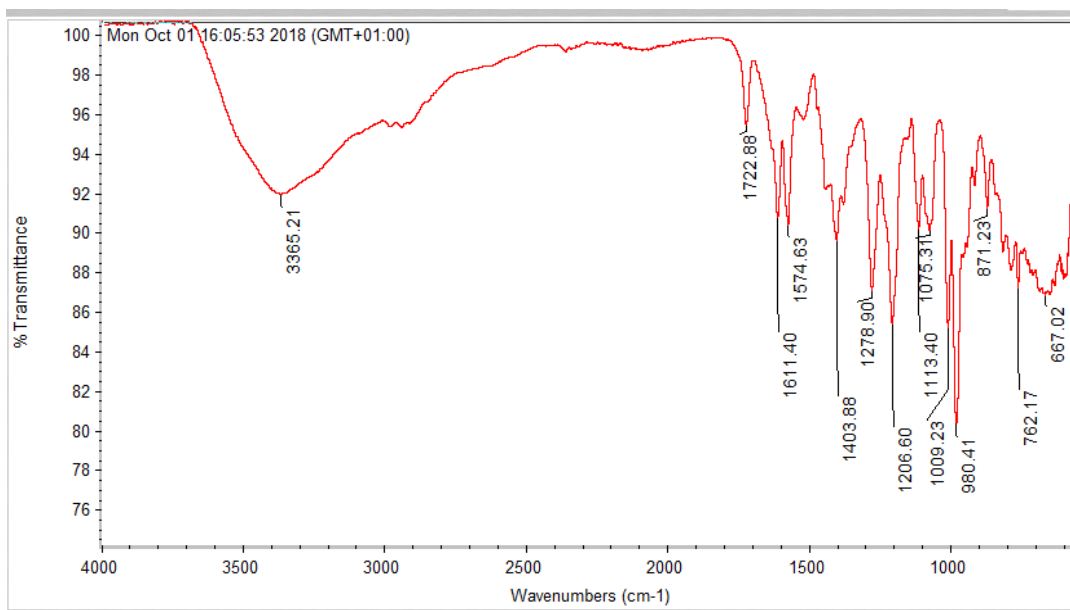


Figure 4-16: FT-IR spectra of doxorubicin with lipoic acid (DOX-LA)

Table 4-3 Summary of functional of DOX-LA.

Compound code	Functional group	Bond	Frequency, cm <sup>-1</sup> Functional group
DOX-lipoic acid (DOX-LA)	Alcohol Secondary amines	O-H Stretch N-H Stretch	3365.21
	Alkanes	C-H Stretch	2947.88
			2935.77
	Carbonyl	C=O Stretch	1722.88
	Alkenes	-C=C- stretch	1611.40
	Secondary amines	N-H bend	1403.88
	Aromatics	C-C stretch (in-ring)	1574.63
	Alkenes	=C-H bend	1085.37
	Aromatic amines	C-N stretch	3000-3100
	Alkanes	C-H bend	761.37
	Aliphatic amines	C-N stretch	1260.06
	Alkenes	=C-H bend	1340.33

#### 4.4.2.3 $^1\text{H}$ NMR spectrum of DOX-LA

Doxorubicin derivatives were characterised using  $^1\text{H}$  NMR spectroscopy. The  $^1\text{H}$  NMR spectrum Figure 4-17 of Dox-Lipoic acid shows the lipoic group at the following position: 1.4 ppm, 1.64 ppm, 1.5 ppm, 2.3 ppm, 2.4 ppm, 3 ppm, 3.5 ppm. The spectrum displays peaks at 7.5 ppm -8 ppm, corresponding to aromatic protons in Doxorubicin. The spectrum also indicates signal at 1.25 ppm which are characteristics of the methyl groups in doxorubicin. The signals at 1.68 ppm, 1.88 ppm, 2.95 ppm, 4.75 ppm and 5.5 ppm were attributed to aliphatic cyclic protons.

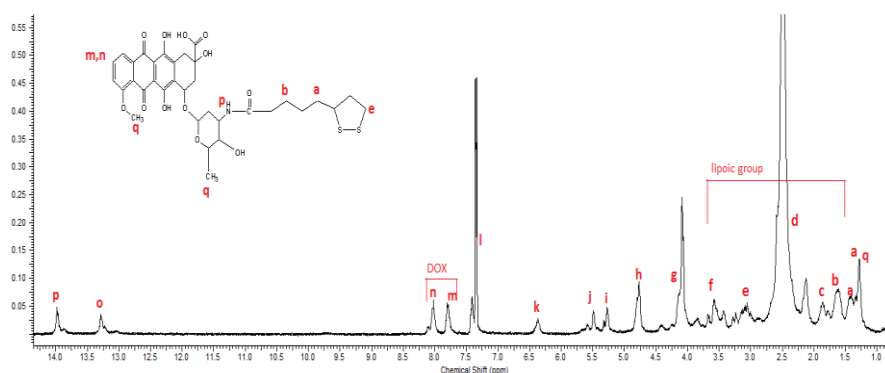


Figure 4-17:  $^1\text{H}$  NMR spectrum of doxorubicin-lipoic acid in DMSO carried out using 400 MHz NMR machine at 20 °C

#### 4.4.2.4 $^{13}\text{C}$ NMR Spectrum of Doxorubicin-lipoic acid (DOX-LA)

The  $^{13}\text{C}$  data acquired for DOX-LA Figure 4-18 aliphatic hydrocarbons ( $-\text{CH}_2-$ ) appear between 23 ppm – 48 ppm Figure 4-18-b with aromatic carbons group from the doxorubicin between 121 – 136 ppm. The amide groups ( $\text{N}-\text{C}=\text{O}$ ) were observed at 164 ppm Figure 4-18-a. The  $-\text{CH}_2-$  groups present in the lipoic acid were inverted, between

33 ppm – 40 ppm, and the quaternary carbons, for instance the carbonyl peak from the amide (164 ppm) had disappeared.

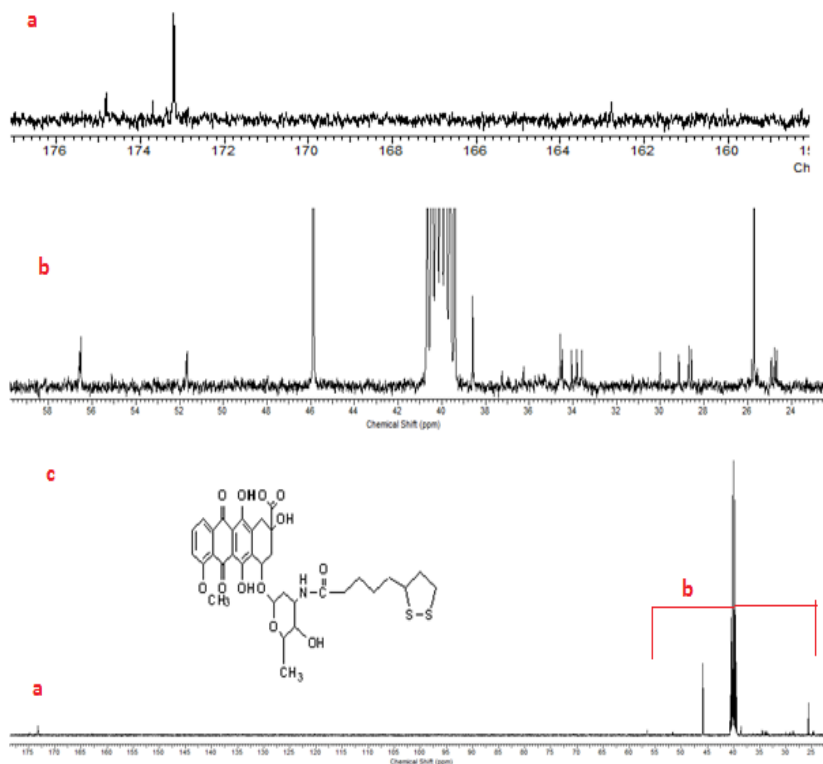


Figure 4-18:  $^{13}\text{C}$  NMR spectrum of (c) DOX-LA (c), (a) Aliphatic hydrocarbons, (b) Amide group of DOX in DMSO- carried out using 400MHz NMR at 25 °C

#### 4.4.2.5 Mass Spectrometry

Figure 4-19 shows the structure of the Dox-LA which was analysed using mass spectrometry.

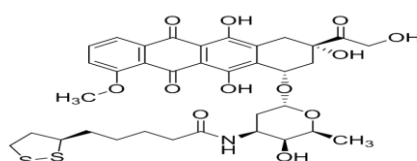


Figure 4-19: Chemical structure of coupling DOX-LA

This sample Figure 4-19 was analysed using a Waters Xevo G2-S instrument. There was evidence of a  $[M+H]^+$  signal at 732.2457 a.u. but this was accompanied by significant fragmentation using this solid insertion technique Figure 4-20.

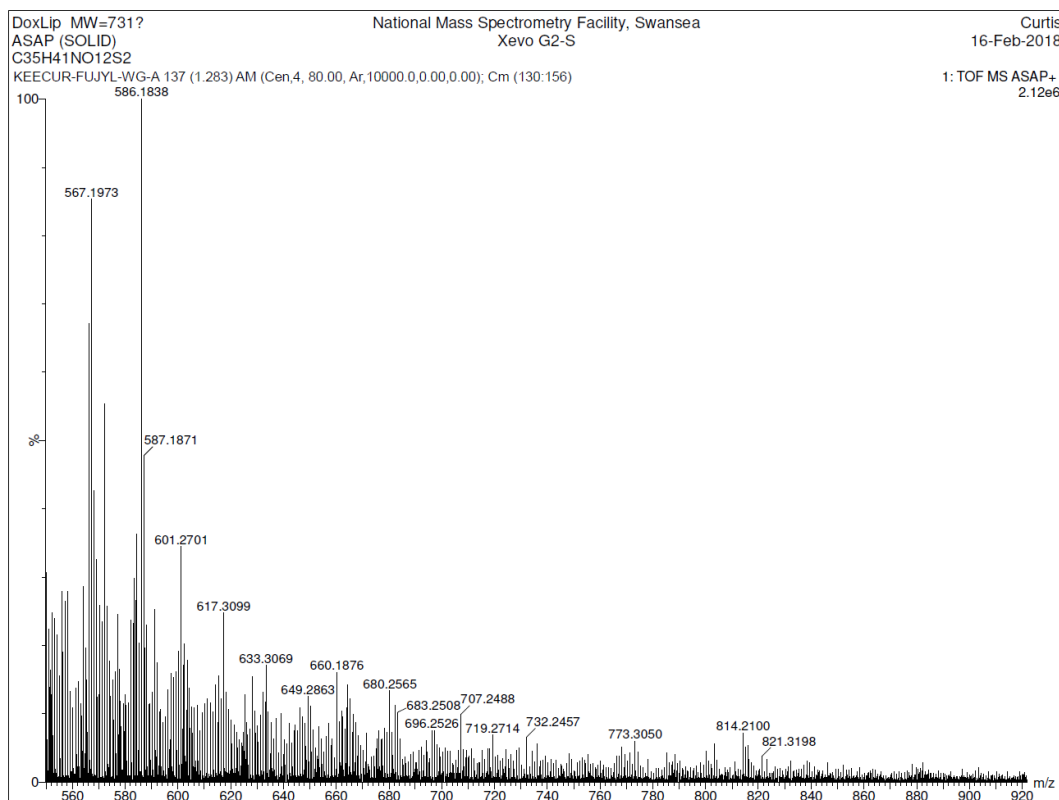


Figure 4-20: Mass spectra of coupling DOX-LA

## 4.5 Discussion

A multitude of other coupling reactions between doxorubicin and various linkers have been reported but unfortunately none of them resulted in favourable yields. Strategies for the formation of amide link bond coupling agents have been explored (Montalbetti & Falque 2005; Valeur & Bradley 2009) and a remarkable multitude of these procedures were adopted in small scale test in order to discover a strategy that gave

the elevated yield. These trials were in addition to the essential trial that had been tried to optimise the simple protocol applied originally in the synthesis of doxorubicin analogues.

The data presented shows that the two doxorubicin analogues in this work were successfully synthesized (PAA-Ox5-HNPs-DOX-SP and PAA-Ox5-HNPs-DOX-LA). Spermine was coupled with Dox by using a (1,1'-Carbonyldiimidazole) CDI as a coupling reagent using laboratory conditions and confirmed to be prepared to adopt NMR, FTIR, and  $^{13}\text{C}$  NMR with a yield (47 %).

Doxorubicin was also coupling with lipoic acid to obtain doxorubicin containing a combination of sulfur and (N,N'-Dicyclohexylcarbodiimide) DCC as a connecting operator. The preparation is confirmed utilizing FTIR, NMR, Mass, and  $^{13}\text{C}$  NMR measurements with yield (81%). The yields obtained in this work give promise to the field in the respect that it is possible to form doxorubicin analogues in sufficient quantities to make them worthwhile candidates for further evaluation as chemotherapies.

The doxorubicin analogues synthesised in this chapter will be used to couple onto the PAA-Oxadiazole-HNP magnetomicelles formed in Chapter 3 and their ability to encapsulated and release the analogues at varied temperatures will be evaluated in Chapter 5.

#### **4.6 Conclusion**

Synthesis and characterisation of doxorubicin analogues in sufficient yields was successful as characterised by various techniques. Subsequently these analogues will

be formulated and tested for their efficacy enhancement on pancreatic cancer cells *in vitro*.

CHAPTER FIVE

INCORPORATION OF

ANALOGUES INTO POLYMERIC

SYSTEMS AND POTENTIAL IN

CANCER THERAPY

## 5.1 Introduction

Cancer is a deadly disease characterised by uncontrolled tumour growth and spread to other parts of the body. Pancreatic cancer is particularly devastating due to its late diagnosis and lack of treatment options (Banerjee *et al.* 2005). Therefore, new treatment regimes are required. The scientific utility of doxorubicin (DOX) is limited by its serious side effects. Persisting efforts are pursued at evaluating effective DOX-delivery systems that might control the disadvantages of present ones. In the current report, we document a self assembling prodrug making elevated drug loading nanoparticles for DOX delivery (Gou *et al.* 2013).

One option for these is the use of amphiphilic polymers as drug carriers as discussed elsewhere in this thesis. One drawback to using this technology is its constant state of dynamic equilibrium, where control over release is unachievable. Often in the use of these technologies in cancer therapy, the phenomenon of enhanced permeability is relied on whereby the particles accumulate in the tumour tissues offering a degree of site specificity. In this chapter we incorporate the drug analogues synthesised in Chapter 4 into our amphiphilic poly(allylamine)-oxadiazole-HNP construct. This will allow for electrostatic binding of the drug molecule onto the HNP within the aggregate core, which can only be reversed at elevated temperatures. Hence this system will confer a greater degree of drug release. In order to achieve such elevated temperatures, our HNPs within the polymer constructs will be irradiated with laser, the ability of these HNPs to heat upon laser irradiation has been reported in the literature. (Malekigorji *et al.* 2014).

All new drug carriers or active ingredients are required to undergo a series of preclinical testing before they can be considered for *in vivo* and clinical trial (Aulton 2007). Hence, we carried out preliminary *in vitro* testing of our novel formulations on human pancreatic cancer cell lines. Such studies enable the elucidation of whether these new formulations are an improvement on the existing drug treatment options.

Biological systems are a group of intricate chemical systems and microenvironments which could possibly have effect on alive ingredients and their component. Hence, new drug formulations have to be noticed in chemical environments that can mimic these physiological conditions (Wijdeven *et al.* 2014; de la Escosura *et al.* 2015).

These environments might comprise the diverse biological pH's such as blood and the gastrointestinal tract (Lemke 2008; Aulton 2007). These are repeatedly examined separately to completely understand their effects on the drug formulation being examined without the intervention of different changing chemical, such as examining a new drug in a series of biological such as changing the temperature, concentration etc.

*In vitro* examinations which were established on adopting cell and tissue cultures that proliferate outside the body in laboratory environment are repeatedly used to check the toxicity and efficiency of potential drug or chemicals molecules (Sonali *etal*, 2015). However, *in vivo* examination is needed to appropriately identify the *in vitro* data inadequate (James, 2008).

In the current experiment, pancreatic cancer cells (BxPC-3) were adopted as a sample cancer in order to examine the capability of our copolymer formulations to boost cancer chemotherapy.

### 5.1.1 MTT assay

The MTT(3-(4,5-dimethylthiazol-2-yl)-2,5-diphenyltetrazolium bromide) tetrazolium reduction assay is a commonly used assay in the cytotoxicity evaluation of new drug entities. The MTT assay used to assess cytotoxicity, activation and proliferation by measuring the signal resulting from living cells, which is dependent on the level of activation of the cells (Mosmann, 1983, Terry et al., 2013, Kumaravel and Begum, 2015).

The MTT assay Figure 5-1 is based on the conversion of MTT into formazan crystals by living cells which determines mitochondrial activity.

In most cell populations, the total mitochondrial activity is linked to the number of viable cells. This assay is used to measure the *in vitro* cytotoxic effects of drugs on cell lines or essential patient cells.

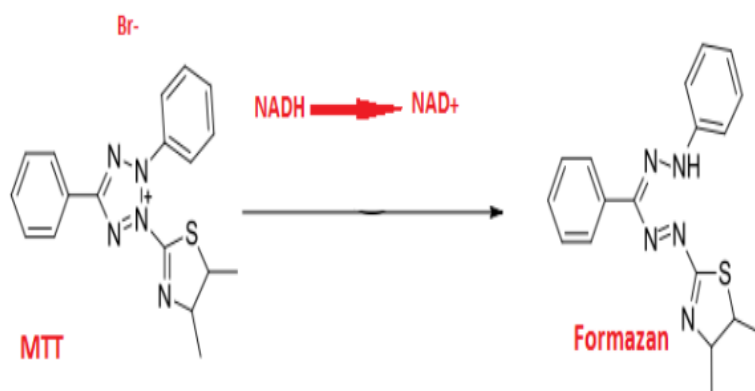


Figure 5-1: Chemical structure of MTT

## 5.2 Research aims

The objective of this chapter is to Incorporation of analogues doxorubicin into polymeric systems and analyse the interaction of doxorubicin-spermine and doxorubicin-lipoic acid along the surface gold of the HNPs. Subsequent examination into the potential for the nanoparticulate formulation to heat responsive drug delivery system *in vitro* necessary drug loading and drug release experiments to be set in motion, monitored by HPLC and potential in cancer therapy. To determine the cytotoxicity effect of formulations of HNPs, PAA-OX5-DOX-LAHNPs and PAA-OX5-DOX-Spe-HNPs on the BxPC-3 pancreatic cell lines utilizing the MTT assay.

## 5.3 Materials and Methods

### 5.3.1 Materials used

Table 5-1 shows the materials used in corporation of analogues into polymeric and biological investigations.

Table 5-1 Materials used in corporation of analogues into polymeric and biological investigations.

	<b>Materials</b>	<b>Suppliers</b>
1	Doxorubicin (DOX)	LC Laboratories (Woburn, USA)
2	DOX-Spermine	Synthesised in Chapter Four
3	DOX-Lipoic acid	Synthesised in Chapter Four
4	Poly(allylamine) PAA 17.5 kDa	Synthesised in Chapter two
5	Orthophosphoric acid	Sigma-Aldrich Co., UK
6	Acetonitrile	Sigma-Aldrich Co., UK
7	PRMI culture medium	Life technologies Co., UK
8	Trypsin-EDTA 0.05	Life technologies Co., UK
19	Foetal bovine serum	Fisher Scientific, UK
10	Penicillin streptomycin	Life technologies Co., UK
11	Cell freezing medium	Sigma-Aldrich Co., UK
12	3-[4,5-dimethylthiazol-2-yl]-2,5-diphenyl tetrazolium bromide (MTT)	Sigma-Aldrich Co., UK
13	of dimethyl sulfoxid DMSO	Fisher Scientific, UK
14	Hybrid nanoparticles (HNPs)	Synthesised in Chapter Three
15	BxPC-3 cell line (Passage number:10)	LGC Standards Co., UK
16	Phosphate buffered saline	Fisher Scientific, UK

## 5.3.2 Methods

### 5.3.2.1 Drug conjugation

### 5.3.2.2 HNP-DOX-Spermine and HNP-DOX-Lipoic acid loading into polymer

A 10 mL solution of  $5\text{mgmL}^{-1}$  PAA-Ox5 was prepared with deionised water as a diluent. The polymer solution was probe sonicated for 10 min. To this solution, 500  $\mu\text{L}$  of HNP-DOX- Spermine and HNP-DOX-Lipoic acid were added separately and the mixture was probe sonicated for 10 min. The resultant solution was filtered using 0.45  $\mu\text{m}$  syringe filters and preparing to additional analysis. The drug loading of each formulation was calculated by using HPLC analysis.

### 5.3.2.3 Quantification of doxorubicin

An accurate amount of doxorubicin hydrochloride was weighed in order to prepare 1  $\text{mgmL}^{-1}$  stock standard solution in methanol Figure 5-2.

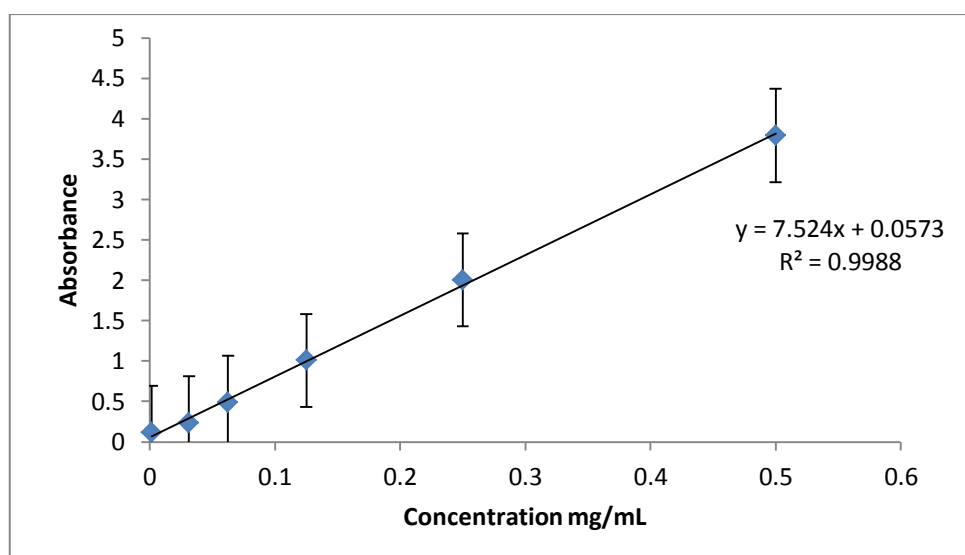


Figure 5-2: Calibration curve of doxorubicin at R.T

To identify the optimal loading concentration of every drug on the HNPs, the amount of drug attachment was quantified by reverse phase high performance liquid chromatography RP-HPLC (Prominence, DEGASSER, LC20AD, SHIMADZU) utilizing a fluorescence indicator at 480 nm (Excitation) and 560 nm (Emission) (Jasco, PU-980, Japan; column C18(2), 150 mm ×4.60 mm 5 micron, flow rate: 1 mLmin<sup>-1</sup>, injection volume: 20 µL). The buffer applied in HPLC mobile phase was arranged by adding 10 mmol ammonium hydrogen phosphate((NH<sub>4</sub>)<sub>2</sub>HPO<sub>4</sub>)(to boost the retention) and 5mL trimethylamine(C<sub>3</sub>H<sub>9</sub>N) to 200 mL of deionised water. Then the pH of the solution was adjusted to 4.0 with orthophosphoric acid (H<sub>3</sub>PO<sub>4</sub>). The mobile phase was a mixture of buffer pH 4.0/acetonitrile(C<sub>2</sub>H<sub>3</sub>N )/methanol(CH<sub>3</sub>OH) (60:24:16, V/V/V), sonicated for 10 min (Toshniwal ultrasonic cleaner, India) and filtered through 0.45 µm filter. R<sup>2</sup>0.9988. the regression equation obtained is:  $y = 7.524X + 0.0573$ .

#### **5.3.2.4 *In vitro* drug release study in aqueous media**

Formulations (2 mL, 0.5 mgmL<sup>-1</sup>) were placed into visking tubing (12-14 KDa) and dialysed against 100 mL deionised water at different temperature (20 °C, 37°C, 44°C) along stirring. The volume of dialysis fluid was in excess to mimic the 'sink' setting examined after injection into the blood stream (Barnett *et al.* 2013a). At chosen time points (1 min, 5 min, 10 min, 0.5 h, 1 h, 2 h, 3 h, 4 h and 24 h) a sample of the exterior solution (1 mL) was taken off and changed with 1 mL deionised water at the stated time points previously described. All models were diluted with 1 mL of deionizes water and drug concentrations were examined via HPLC. The investigation was carried out in triplicate and the peak area was compared to a calibration of the free drug.

### 5.3.3 Biological characterisation of nano-aggregates and formulation

#### 5.3.3.1 MTT([3-(4,5-Dimethylthiazol-2-yl)2,5DiphenyltetrazoliumBromide])

##### cytotoxicity assay

Human pancreatic adenocarcinoma BxPC-3, cells (3 mL, 15000 cells/well) in their exponential growth phase were seeded into 96-well plates and incubated for 24 h at 37 °C with 5 % CO<sub>2</sub>. A 20 mgmL<sup>-1</sup> stock solution was prepared of each DOX formulation (and free drug). From this stock solution eight dilutions (0.1 mgmL<sup>-1</sup> - 1×10<sup>-5</sup> mgmL<sup>-1</sup>) using media as the diluent were prepared Table 5-2.

Table 5-2 Preparation of Excipient Solutions for MTT assay

Drug concentration (mgmL <sup>-1</sup> )	Volume of 20 mgmL <sup>-1</sup> drug stock solution (µL)	Total volume of media (mL)
0.1	22.5	4.5
0.05	11.5	4.5
0.025	6.5	4.5
0.01	2.25	4.5
0.005	1.125	4.5
*0.001	90	4.5
*0.0001	9	4.5
*0.00001	1	4.5

\* Sample was made from 0.05 mgmL<sup>-1</sup> concentration as a stock solution.

After 24 h, the formulations were removed and replaced with fresh media (100  $\mu\text{L}$ ). MTT 3-[4, 5-dimethylthiazole-2-yl]-2, 5-diphenyl tetrazolium ( 50  $\mu\text{L}$ , 5  $\text{mgmL}^{-1}$  in PBS) was added to the wells and then the plate was incubated (37  $^{\circ}\text{C}$  with 5 %  $\text{CO}_2$ ) for 4 h. Next, the solution of MTT was removed from the wells. The purple formazan was remaining complexes were dissolved in (100  $\mu\text{L}$ ) DMSO. At 570 nm, the absorbance of the plates was read using a microplate reader (Tecan, infinite 200 pro, GmbH 5082, Australia).  $\text{IC}_{50}$  and Percentage cell viability was calculated relative to the negative and positive controls (no cell treatment and complete cell lysis using 2% Triton-X). All studies were run in triplicate (n=3) and the average values were recorded.

### **5.3.3.2 *In vitro* thermo-responsive cytotoxicity assay**

To indicate whether laser irradiate could be used for triggered drug release the MTT assay was repeated with one amendment. After exposure to formulation (1 h), the plates were incubated at 44 $^{\circ}\text{C}$  (as a thermal variant that can mimics the heat generated by the surface plasmon resonance (SPR) of laser irradiated HNP gold coatings) for 0.5 h, before being replaced into the incubator at 37  $^{\circ}\text{C}$  with 5 %  $\text{CO}_2$  for rest of the 24 h period.

## **5.4 Results**

### **5.4.1 Drug conjugation**

Conjugation of drugs by electrostatic attachment onto the surface of HNPs has been previously reported. The conjugation of DOX-SP and DOX-LA onto the HNPs in the presence of PAA-Ox5 was achieved successfully. The drug loading of each formulation

was calculated by using HPLC analysis. The value loading of HNP-DOX-SP to the PAA-Ox5 was 3.301 and for the HNP-DOX-LA loading to the PAA-Ox5 were 3.7.

#### 5.4.2 Drug release of PAA-Ox5-HNPs- DOX-SP at different temperatures

Conjugation of drugs by electrostatic attachment on the surface of HNPs is a new strategy to transfer therapeutic agents towards their site of action. The drug release profile was at first decided at 20°C before conducting analysing the effect of heat on the release profile of doxorubicin analogue from the PAOx5-HNPs-DOX-SP and PAA-Ox5-HNPs-DOX-LA structures.

The percentages of burst release in the first hour of the analysis display there is no release in the drug at 20 °C Figure 5-3. Then one hour later the percentages of drug release had started to appear, at 4 h was (2.16 %), the drug release was reported (3.38 %) the utmost drug release occurred at 24 h.

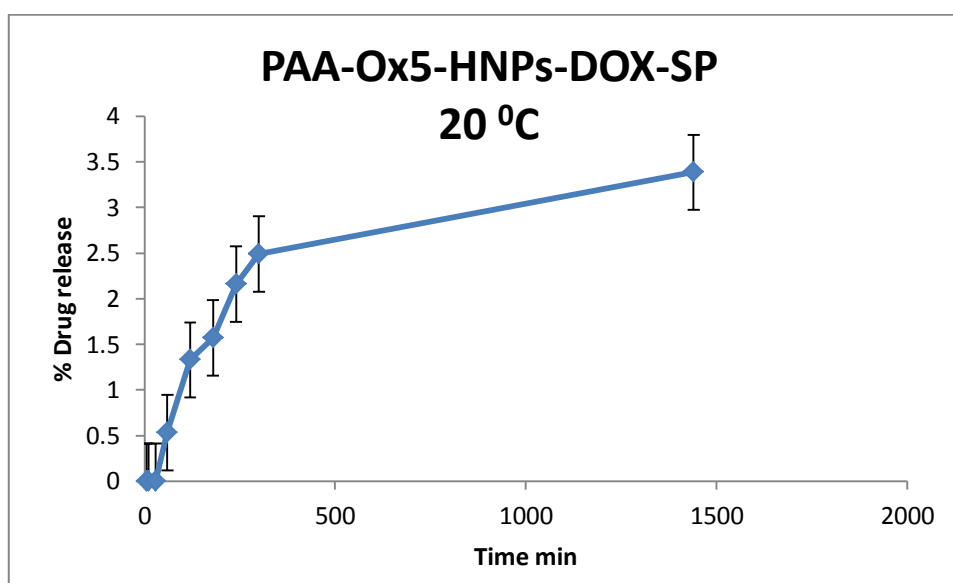


Figure 5-3: Drug release of PAA-Ox5-HNPs-DOX-SP at 20 °C over 24 h(n=3)(SD±)

At 37 °C the percentage of drug release was recorded (17.15 %) after only 4 h. At 24 h the percentages of drug release was recorded (30%) which was the highest concentration at 37 °C Figure 5-4.

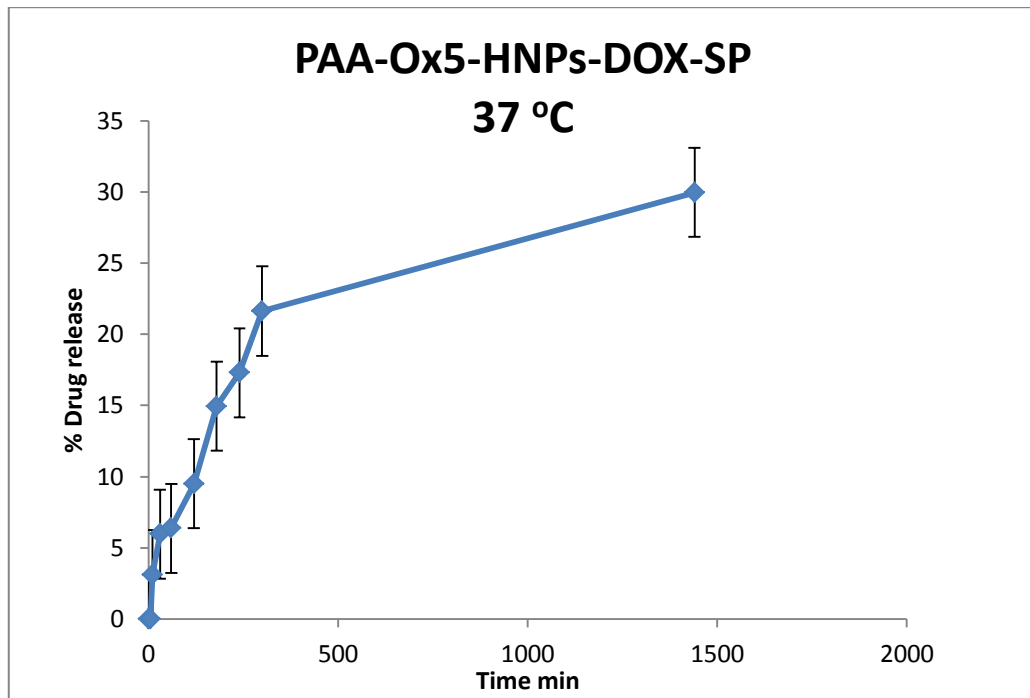


Figure 5-4: Drug release of PAA-Ox5-HNPs-DOX-SP at 37 °C over 24 h (n=3) (SD±)

At 44 °C the percentage of drug release was shown (23.72 %) after 4 h, at 24 h the percentages of drug release was recorded (49.11%) Figure 5-5. This result was indicating the effect of heat in drug release formulation of PAA-Ox5-HNPs-DOX-SP.

However, this was not notably enhanced compared with those release profiles at body temperature.

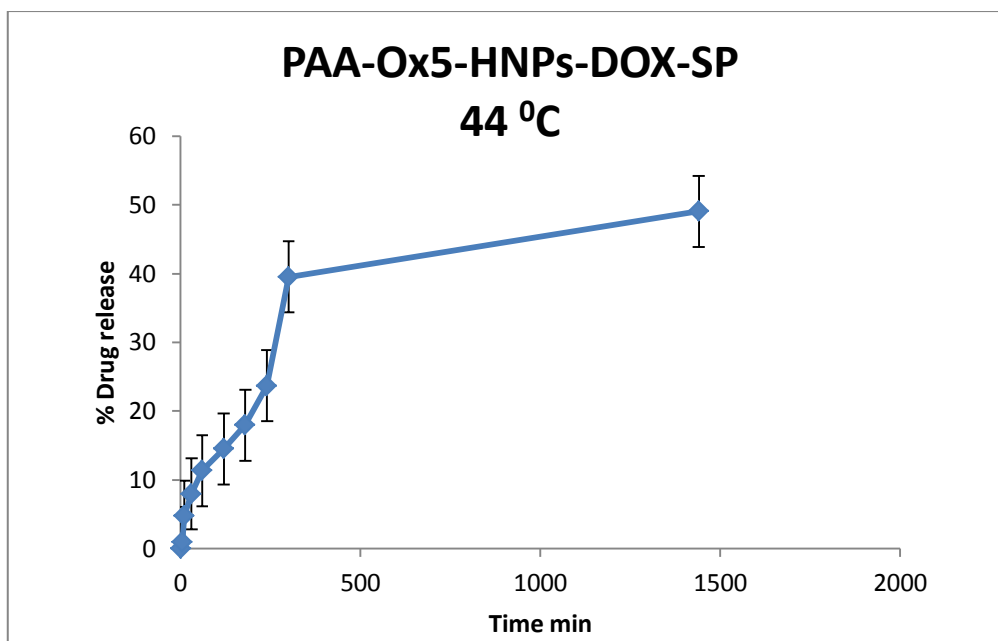


Figure 5-5: Drug release of PAA-Ox5-HNPs-DOX-SP at 44 °C for 24 h (n=3)(SD±)

#### 5.4.3 Drug release of PAA-Ox5-HNPs- DOX-LA at different temperatures

Drug release for formulation of PAA-Ox5-HNPs-DOX-LA was recorded lower percentages than drug release for formulation of PAA-Ox5-HNPs-DOX-SP , this was due to the number of amine group of spermine N-H.

At 20 °C the percentage of drug release was shown (1.16 %) after 4 h . After 24 h the percentages of drug release was recorded (1.98 %) which was the highest concentration at 20 °C Figure 5-6.

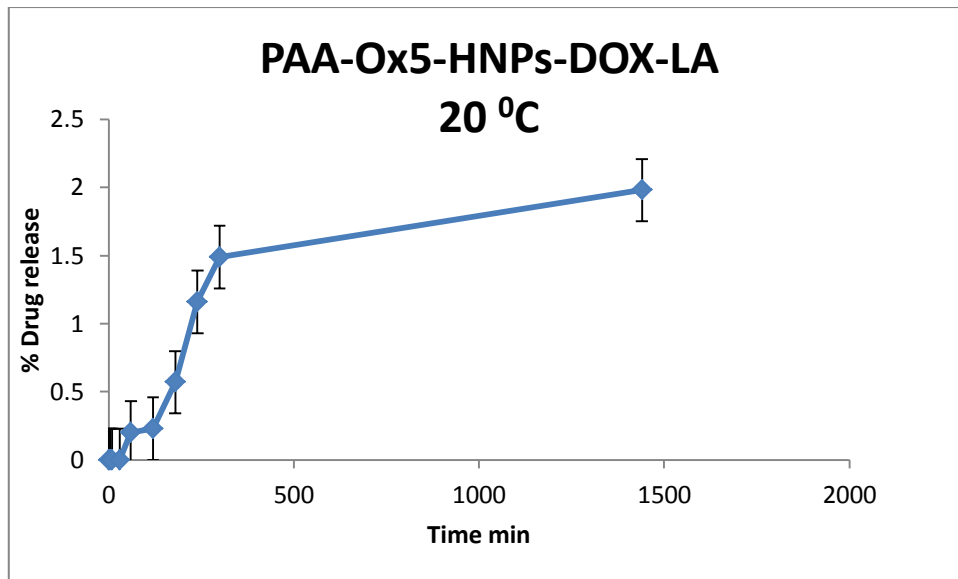


Figure 5-6: Drug release profile of PAA-Ox5-HNPs-DOX-LA at 20°C over 24 h (n=3)(SD±)

Figure 5-7 shows the highest percentage of drug release at 37 °C was noted (23.64 %) after 24 h. This was greatly reduced compared with the spermine-DOX release profile.

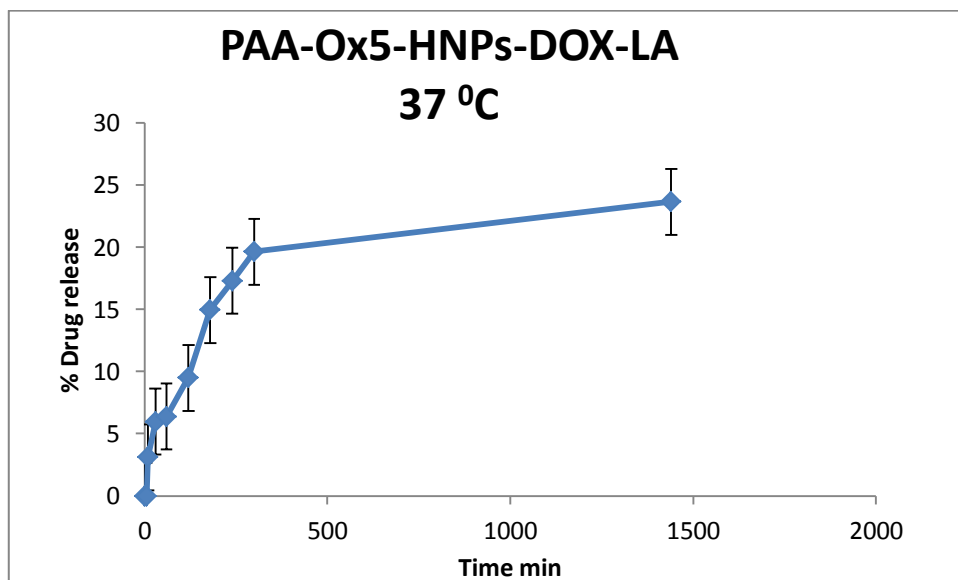


Figure 5-7: Drug release profile of PAA-Ox5-HNPs-DOX-LA at 20°C over 24 h (n=3) (SD±)

Doxorubicin analogues release was analysed at 44 °C to mimic the temperature of the environment around HNPs and after laser irradiation with near-infrared light. Figure 5-8 shows the drug release of PAA-Ox5-HNPs-DOX-LA at 44 °C which is recorded the higher release rates of doxorubicin at (39.64%) over 24 h.

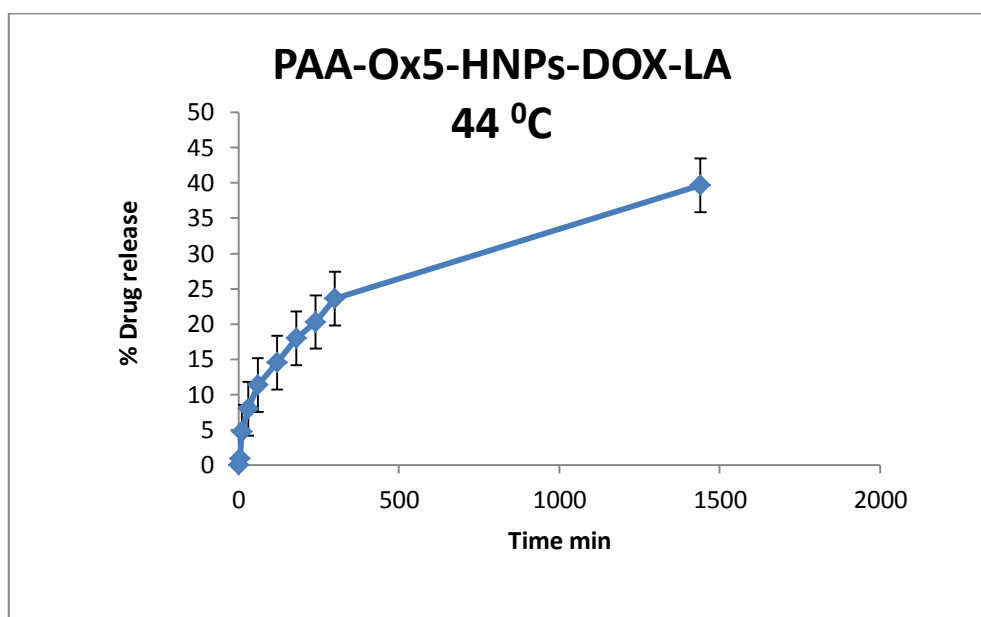


Figure 5-8: Drug release profile of PAA-Ox5-HNPs-DOX-LA at 20°C over 24 h (n=3)(SD±)

#### 5.4.4 Biological characterisation of nano-aggregates and formulation

Cell viability of BxPC-3, incubated with unloaded HNPs was determined using the MTT assay. The MTT assay is a commonly used assay in the cytotoxicity evaluation of new drug entities. The concentrations displayed in the chart for HNPs are identical to the concentration of hybrid formulations but evidently without drug (the concentrations of Fe in HNP and hybrid formulations are similar). Overall, both cytotoxic evaluations show comparable results and the HNPs did not demonstrate a cytotoxic effect on cell viability over the concentration ranges tested.

Percentage cell viability for PAA-Ox5-HNPs, doxorubicin alone, PAA-Ox5-HNPsDOX-SP and PAA-Ox5-HNPs-DOX-LA at 24 h were compared. Figure 5-9 shows there was no  $IC_{50}$  observed for PAA-Ox5-HNPs after 24 h. There was however a reduction in cell viability at the higher concentrations possibly due to the cationic nature of the PAA conferring a slight degree of cytotoxicity.

The  $IC_{50}$  observed for PAA-Ox5-HNPs-SP after 24 h was  $48 \mu\text{g mL}^{-1}$ , while the  $IC_{50}$  obtained for PAA-Ox5-HNPs-LA after 24 h was  $53.3 \mu\text{g mL}^{-1}$ . This was an improvement compared to the free drug which did not present any  $IC_{50}$  value. This increase in cytotoxicity compared with the free drug is possibly due to the cellular uptake of the drug in greater quantities once inside the PAA nanoaggregates. Multiple studies have shown that once encapsulated inside polymeric micelles, endocytosis enables greater quantities of cellular uptake of drugs compared with the unformulated molecules.

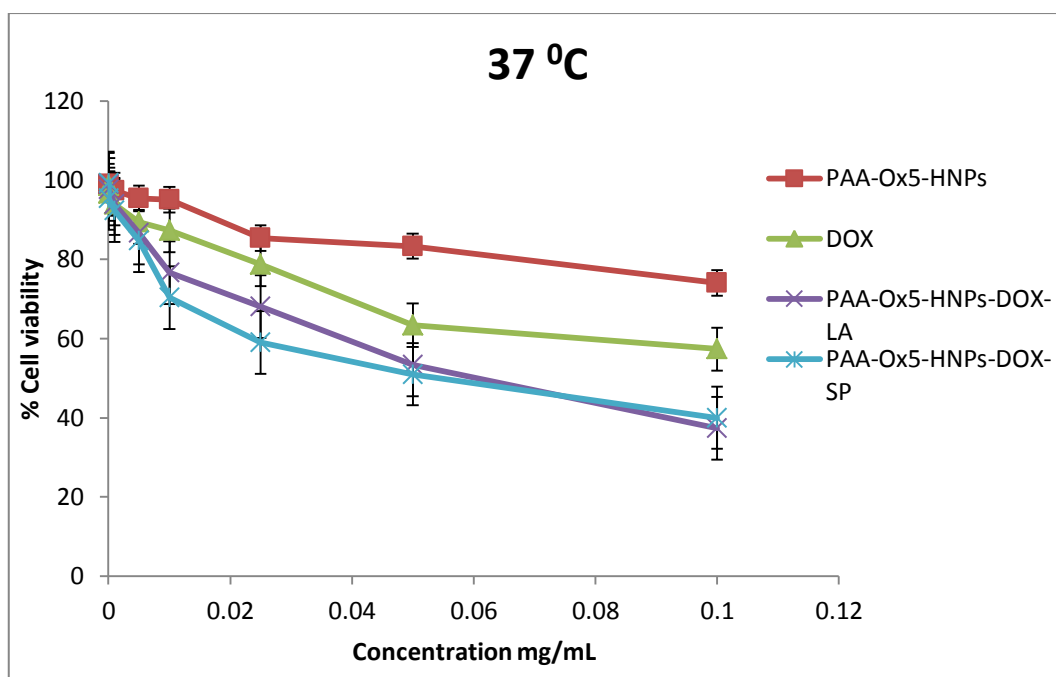


Figure 5-9: MTT assay graph show the effect of various concentrations of doxorubicin, PAA-Ox5-HNPs ,PAA-Ox5-HNPs-DOX-SP and PAA-Ox5-HNPs-DOX- on BxPC-3 cells in 37 ° C at 24 h time points (n=3) ( $\pm 23\%$ )

At high temperature 44° C Figure 5-10, the cell viability for PAA-Ox5-HNPs resulted in an unexpectedly large reduction in the cell viability, the reason for which is unknown, further studies are needed in order to validate this finding. PAA-Ox5-HNP-DOX-SP possessed a notable reduction in the cell viability, where an  $IC_{50}$  was observed at 25  $\mu\text{g mL}^{-1}$  after 24 h, which was a 2-fold reduction compared to the value observed at body temperature. This indicated that the threshold energy required to break the electrostatic binding between the HNP and drug had occurred resulting in the free drug being able to exert its toxic effect on the cell more efficiently.

Similarly, PAA-Ox5-HNPs-DOX-LA showed a 2-fold improvement in  $IC_{50}$  at 0.025  $\mu\text{g mL}^{-1}$  at 44 °C temperature, whilst the free drug possessed an  $IC_{50}$  at much higher concentration of 85  $\mu\text{g mL}^{-1}$ . Both formulations showed a great improvement compared to DOX at both temperatures observed indicating that the formulation has

potential in pancreatic cancer therapy. However, more work is required to further understand the biological interactions with cells both *in vitro* and *in vivo*.

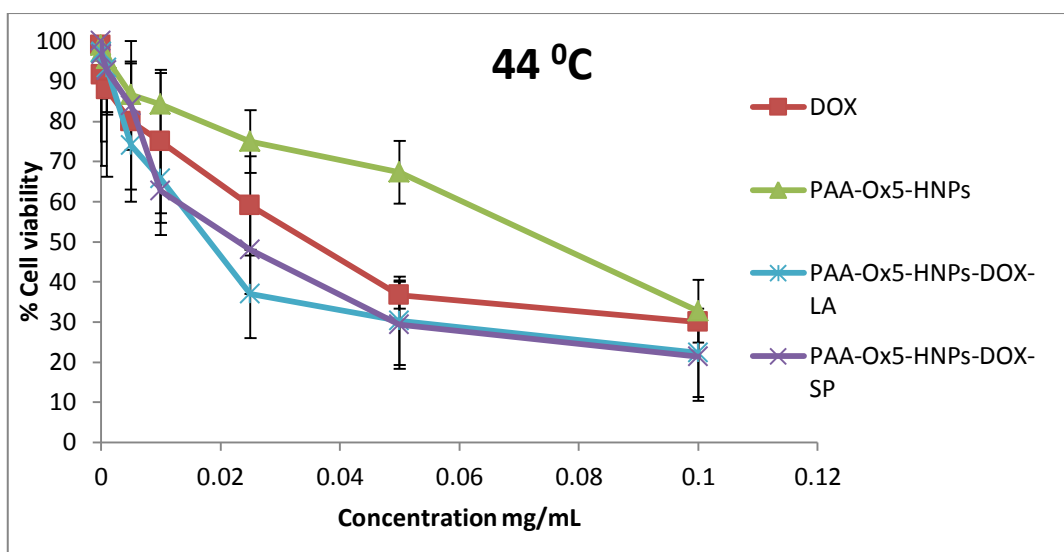


Figure 5-10: MTT assay graph show the effect of various concentrations of doxorubicin, PAA-Ox5-HNPs ,PAA-Ox5-HNPs-DOX-SP and PAA-Ox5-HNPs-DOX-LA on BxPC-3 cells in 44 °C at 24 h time points (n=3) ( $\pm 23\%$ )

## 5.5 Discussion

Polly(allylamine) amphiphiles have been reported for drug solubilisation previously. However, conferring heat triggered release into these systems have not yet been explored. Conjugation of drugs by electrostatic attachment onto the surface of HNPs has been previously reported. In this work we combined the use of PAA amphiphiles with HNPs.

In a different experiment, Barnett and co-workers made and assessed a new class of (PAA) polymer conjugated with hydrophobic oxadiazole (Ox5) pendant group.

They advised that the thiol-containing pendant group can augment the attachment of HNPs by dative covalent connection. Various drugs were conjugated along with direct

conjugation of hydrophilic and encapsulation of hydrophobic drugs. In contrast with the free drug, the conjugated drugs had remarkable elevated drug uptake with diminished  $IC_{50}$  (Barnett *et al.* 2012) Figure 5-11 and Figure 5-12.

In order to deliver doxorubicin analogues in the treatment of pancreatic cancer. Drug loading into the amphiphiles was achieved as confirmed by HPLC. Generally speaking, loading capacity of drugs is affected by a number of determinants such as feeding concentration, the number of amine group, the existence of thiol group and PAA and the type of interaction between drug and HNPs (electrostatic or covalent). In a different experiment, Aslam and co-workers clarified that gold has a strong affinity about the amino group (Aslam *et al.* 2004).

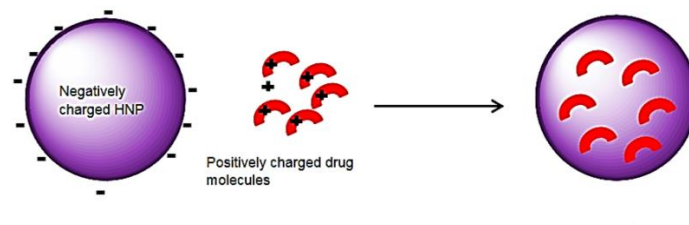


Figure 5-11: Explain interaction of positive amine groups of doxorubicin with the gold coating

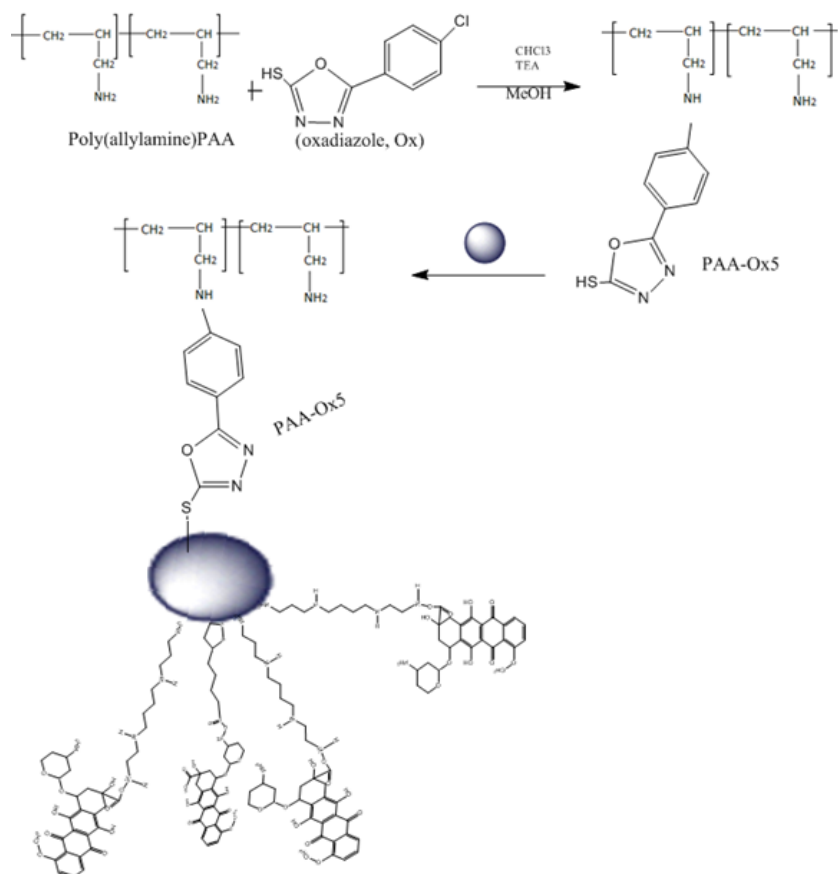


Figure 5-12: Theoretical imagination of doxorubicin –spermine and -lipoic acid coupling to the surface of the hybrid iron oxide core gold shell nanoparticles

The drug release profiles were observed at varied temperatures from the PAAOx5-HNPs-DOX-SP and PAA-Ox5-HNPs-DOX-LA structures. *In vitro* heat treatment and drug release of the drug analogues formulated into PAA-Ox5-HNPs-DOX-SP was attained, 3.38 % of release DOX was released over 24 h at room temperatures. The particles displayed Fickian dispersal release kinetics, 49.11% was the maximum drug released noticed at 44 °C after 24 h. *In vitro* analysis displayed also presented that 42.12. % of the total drug content was released after 24 h at 37°C (Purushotham *et al.* 2009)

Figure 5-13.

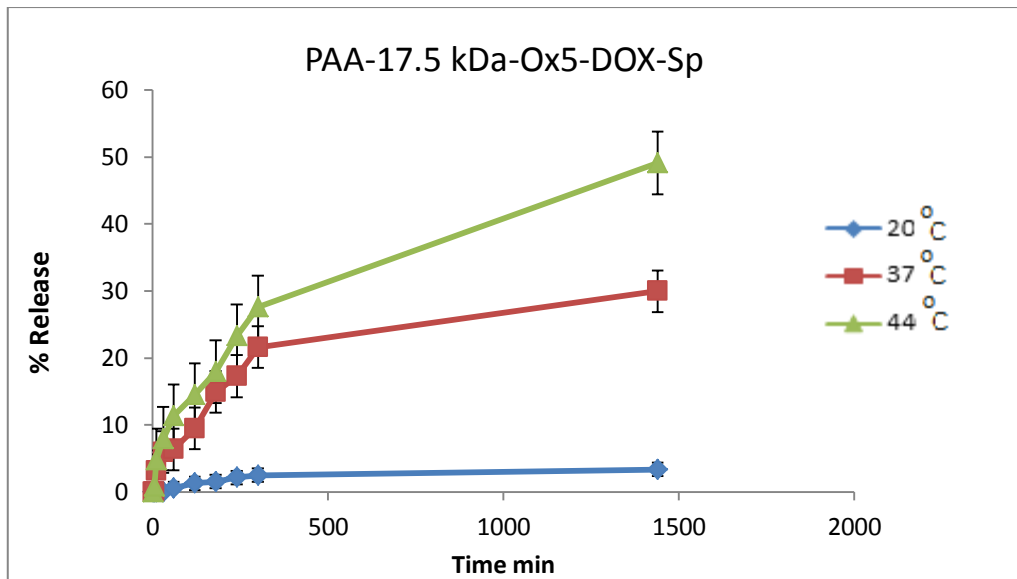


Figure 5-13: Drug release of PAA-Ox5-HNPs-DOX-SP in different temperature (n=3) (SD±)

The formulation of PAA-Ox5-HNPs-DOX-LA was recorded 1.98% of release dox was released over the period of 24 h at room temperatures Figure 5-14. The particles displayed Fickian dispersal release kinetics, 38.64% was the maximum drug release noticed at 44 °C after 24 h. *In vitro* analysis displayed also presented that 23.64 % of the total drug content was released after 24 h at 37°C (Purushotham *et al.* 2009).

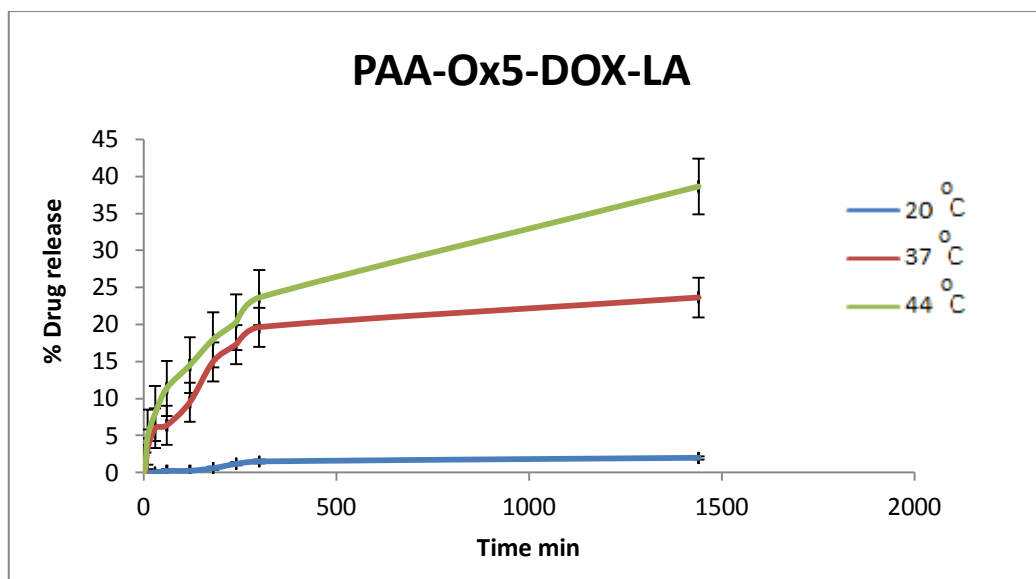


Figure 5-14: Drug release of PAA-Ox5-HNPs-DOX-LA in different temperature (n=3) (SD±)

MTT assay was used to determine the cytotoxicity of the doxorubicin analogue on human pancreatic adenocarcinoma (BxPC3) cells. The unloaded nano-aggregates were incubated for 24 h with the cells and the cell viability was compared to control wells. The result revealed that 50% of the total cell number was viable ( $IC_{50}$ ) at  $50 \text{ mg mL}^{-1}$  (PAA-Ox5-HNPs). These values revealed that the incorporation of the metallic HNPs into the polymer backbone did not result in any significant increase in toxicity ( $p > 0.001$ ).

MTT assays were achieved on doxorubicin, PAA-Ox5-HNP, formulation of (PAA-Ox5-DOX-SP-HNP and PAA-Ox5-DOX-LA-HNP construction to decide if the formulation of doxorubicin analogues were able of transfer cytotoxic drugs into the cells, thus boosting their therapeutic effect. To decide if the novel formulation boosted the therapeutic effect of their anticancer drug, they were encapsulated at the polymer  $IC_{90}$  concentration (the concentration at which 90% of cells were viable).

In order to examine the effect of temperature on cell cytotoxicity, the  $IC_{50}$  was decided for the heat operating plates and compared to the non-operating plates. In general, heat treatment did not conclude in a significant effect on cytotoxicity of PAA-OX5-HNPs. This work confirms the heat triggered system developed resulted in more efficient DOX delivery compared to free drug and drug at body temperature. Due to the detrimental side effects experienced after DOX administration it often cannot be used in already ill pancreatic cancer patients. Therefore, this work offers an exciting alternative where drug can be tracked real-time using MRI guidance and laser irradiation could be used to release the drug localised within its desired site hence reducing systemic toxicity and side effects. More work is needed *in vitro* to further elucidate cellular response as well with laser irradiation to further investigate the systems potential.

## **5.6 Conclusion**

Doxorubicin with amine group was able to conjugate with HNP; however, stronger interaction of drug-NPs was achieved by increasing the number of amine from doxorubicin to DOX-SP (four amine groups). Conjugation of DOX-LA with HNPs confirmed that exploiting Au-S chemistry is possible for conjugation of a molecule possessing thiol group to the gold coating surface. By connecting doxorubicin to lipoic acid to afford a method to connect the prodrug to the gold surface of the HNPs nano particles may offer various advantages. It may heighten the action of doxorubicin as a result of site-specific activity or augmenting the amount of drug entering the circulation considering the overall physicochemical properties of the drug analogue. In addition to that, the effect applied by the lipoic acid residue of the prodrug might influence the activity of the prodrug and the quantity of doxorubicin released

(Geromichalou *et al.* 2015). The addition of polyamine (spermine) or lipoic acid and coupling of the PAA-Ox5 to the HNPs could improve the efficacy of doxorubicin therapy. The data showed that the coupling of doxorubicin to spermine resulted in an increase in the rate of drug application also.

# CHAPTER SIX

## GENERAL CONCLUSION

## 6.1 General Conclusion

This study showed that hydrophobic oxadiazole groups were capable of attachment onto via conjugation to the primary amines of a PAA backbone.

Many studies have been carried out in the literature regarding other cationic polymers such as poly(ethylenimine) and their role in self-assembly after modification of hydrophobic subunits. However, little has been explored for PAA. Preliminary work in this study showed that in general increasing molecular weight of polymer resulted in a higher extent of drug loading as tested at 15 kDa, 17.5 kDa, 120 kDa and 900 kDa PAA. This finding was in agreement with other studies reported on other cationic polymers. (Shen et al, 2015). However, with higher drug loading comes other properties such as larger sizes, instability of aggregates, release profiles, etc. A study by Barnett shows that drug release is a significant characteristic of a therapeutic system (Barnett *et al.* 2013). Where scientists found a linear linker between the drug release and the absorption of the body. (Lu *et al.* 2011). In this work, the drug release was influenced by polymer molecular weight and drug loading. Polymers with higher molecular weight tend to possess slower drug release compared to lower molecular weight. The molecular weight of the polymer can significantly effect the degree of aggregation, the solubility of higher molecular weight polymer in solvent was less than that of lower molecular weight polymer. Therefore, the heavier polymer would precipitate out faster and the molecular chain would be hardened by not allowing the intermolecular interaction of the drug layers around the particles which would cause aggregation (Kung, 1997).

Taking our findings into account, looking at the surface tension data, the aggregates formed at high molecular weight are likely to be more unstable upon dilution. Hence, it was decided to continue our studies throughout this thesis on PAA-Ox5 with molecular weight of PAA as 17,500 kDa.

The rationale for using oxadiazole within the polymer comb structure was in order to later attach inorganic nanoparticles into the system. These hybrid iron oxide-gold nanoparticles (HNPs) have previously been exploited for thermally triggered thermo-responsive drug delivery applications (Malekigorji *et al.* 2017). However, due to the weight and solution stability of these molecules, such applications could only be exploited for aqueous soluble compounds.

Barnett *et al.* showed that these HNPs could be irreversibly be incorporated into the core of the core-shell polymeric aggregates in aqueous environments via dative covalent binding between the thiol residue in the oxadiazole and the gold HNP surface (Barnett *et al.* 2013). Once the HNP was located within the newly formed magnetomicelle structure this could be exploited as a site of attachment for insoluble drug compounds within the lipophilic core of the polymeric aggregate. Hence this system was developed in order to give safe-passage of the doxorubicin analogues created enabling a heat triggered mechanism for site specific delivery of this highly toxic molecule.

The synthesis of the HNPs was shown to be successful by determining the physicochemical features of the particles, size, shape and efficient coating of the iron oxide core of the hybrid system by using multitude techniques that include photon

correlation spectroscopy, zeta potential dimensions, inductively coupled plasma-optical emission spectroscopy (ICP-OES) and transmitting electron microscopy (TEM).

Another objective was to synthesis of two doxorubicin derivatives. The synthesis of a doxorubicin derivative supporting a cationic polyamine chain (spermine) designed following on from the Malekigorji work (Malekigorji *et al.* 2014) Here they reported the use of electrostatic chains in the reversible heat cleavable binding of novel drug molecules – with a bisnaphthalimido based drug with a spermine linker being the most successful. Hence, spermine was used to conjugate onto the doxorubicin for the initial drug analogue. Malekigorji *et al.* (2017) indicated that the effect of heat (44° C) might shift the drug HNPs binding if the connection was an electrostatic charge interaction (Malekigorji *et al.* 2017).

The analogue was successfully synthesised and analysed using FTIR, NMR <sup>13</sup>C NMR and Mass spectroscopy with a yield of 47%. The goal of the synthesis of the DOX-SP was to supply an arm with doxorubicin to actively cohere to the gold surface of the HNPs while granting the ability of the system DOX-SP-HNPs-PAA-OX5 to operate as a stimuli-responsive carrier.

The second analogue was based on the conjugation of lipoic acid onto the doxorubicin. In previous studies in our group lipoic acid was shown to form a disulphide linkage with the gold HNP surface which cleaved at elevated temperature and reduced pH (data not published). In this work, synthesis of the doxorubicin analogue bearing a sulfur-containing residue was achieved by using amide bond union of doxorubicin to lipoic

acid. The profitable synthesis and reaction level up was completed by using simple two steps reaction and the prime conditions for the reaction were concluded. The region selectivity of the union of doxorubicin to lipoic acid by amide bond structure was one of the advantages of utilizing DCC as a unifying operator that supplied only one product with a just yield of 81%. The aim of the synthesis of the DOX-LA was to supply an arm with doxorubicin to actively cohere to the gold surface of the HNPs, while granting the capability of the system DOX-LA-HNPs-PAA-OX5 to operate as a stimuli responsive carrier.

Loading of the DOX-SP and DOX-LA onto the surface gold of the HNPs was tested at various concentration ratios and a maximum loading concentration of 5 mg of DOX-per 1 mg HNPs (Fe) and 5 mg of DOX-LA per 1 mg HNPs (Fe) was accomplished successfully. *In vitro* heat treatment and drug release of the drug analogues formulated into PAA-Ox5-HNPs-DOX-SP was attained, 3.38 % of released DOX was released over 24 h at room temperatures Figure 5. 14. The particles displayed Fickian dispersal release kinetics, 49.11% was the maximum drug release noticed at 44 °C after 24 h. *In vitro* analysis displayed also presented that 42.12. % of the total drug content was released after 24 h at 37 °C. The formulation of PAA-Ox5-HNPs-DOX-LA was registered 1.98% of release dox was released over the duration of 24h at room temperatures. The particles displayed Fickian dispersal release kinetics, 39.64% was the maximum drug release observed at 44 °C after 24h. *In vitro* analysis showed also demonstrate that 23.64 % of the total drug content was released after 24 h at 37 °C.

The final formulations acquired in the biological part of this experiment were used. MTT assay was adopted to decide the cytotoxicity of the doxorubicin analogue on

human pancreatic adenocarcinoma (BxPC-3) cells. The unloaded nano-aggregates were incubated for 24 h with the cells and the cell viability was set to manage wells. The outcome displayed that 50% of the total cell number was active ( $IC_{50}$ ) at  $50 \text{ gmL}^{-1}$  (PAA-Ox5-HNPs). These values displayed that the unification of the metallic HNPs into the polymer backbone did not issue in any remarkable increase in toxicity.

MTT assays were used to evaluate the change in viability of BxPC-3 cells after exposure to the novel formulation and the effect of temperature on cell cytotoxicity. The  $IC_{50}$  was determined for the heat activated plates and compared to the non-activated plates. In general, the data showed that the heat activation resulted in more efficient drug efficacy compared to free drug and drug at body temperature with no associated toxicity from the HNPs – experiments were carried out at the polymer  $IC_{90}$ . Due to the damaging side effects DOX induces in pancreatic cancer patients, it often cannot be used as a treatment option. Therefore, this work provides an interesting alternative where drug can be tracked real-time using MRI instruction and laser irradiation could be employed to release the drug situated within its desired site hence reducing systemic toxicity and side effects.

This study serves as a proof of principle, however a lot more work is required to further understand and optimise these systems before clinical translation could occur. The drug loading/release profiles required further tailoring in order to improve drug efficacy *in vitro* and a greater improvement on heat activation would possibly result – helping to provide further rationale for using this complex system. Repeatable scale-up of the preparation is required, perhaps this could be achieved through the use of microfluidics which seems to be revolutionising the liposome domain. More work is

required *in vitro* to further interpret cellular response as well with laser irradiation to further examine the potential of the system. Additional cell lines would be required such as Panc-1, pancreatic panel cell lines as well as healthy cell lines and fibroblasts which may mimic better the extracellular matrix. *In vivo* target ability, permeability, accumulation and fate are ultimately required which could be conducted using xenograft mice similar to Malekigorji's work. Finally, GMP good manufacture Practice must be employed in order to produce suitable formulations for clinical trial.

# REFERENCES

## References

Bochot,A., & Fattal, E. J. **Controlled Release**, 2012,161, 628–634.

Acar, H.Y.C., Garaas, R.S., Syud, F., Bonitatebus, P. & Kulkarni, A.M., 2005. **Magnetism and Magnetic Materials**, **293**(1), pp. 1-7.

Aguilar, Z. P. (2013). **Targeted Drug Delivery**. *Nanomaterials for Medical Applications*, 181–234.doi:10.1016/b978-0-12-385089-8.00005-4.

Alexis, F., Pridgen, E., Molnar, L. K., & Farokhzad, O. C. (2008). **Factors affecting the clearance and biodistribution of polymeric nanoparticles**. *Molecular pharmaceutics*, 5(4), pp.505-515.

Aliabadi, H.M., Shahin, M., Brocks, D.R. and Lavasanifar, A. (2008) Disposition of Drugs in Block Copolymer Micelle Delivery Systems. **Clinical Pharmacokinetics**, **47**(10), pp. 619-634.

Allen, L.V. & Ansel, H.C. (2014) **Ansel's Pharmaceutical Dosage Forms And Drug Delivery Systems**. 10th edn. Baltimore, U.S.: Wolters Kluwer Health.

Almoguera, C., Shibata, D., Forrester, K., Martin, J., Arnheim, N., & Perucho, M. (1988). **Most human carcinomas of the exocrine pancreas contain mutant c-K-ras genes**. *Cell*, 53(4), 549–554. doi:10.1016/0092-8674(88)90571-5

Almoguera, C., Shibata, D., Forrester, K., Martin, J., Arnheim, N. And Perucho, M., 1988. **Most Human Carcinomas Of The Exocrine Pancreas Contain Mutant C-K- Ras Genes**. *Cell*, 53(4), Pp. 549-554.

Alves, A. C., Magarkar, A., Horta, M., Lima, J. L. F. C., Bunker, A., Nunes, C., & Reis, S. (2017). **Influence Of Doxorubicin On Model Cell Membrane Properties: Insights From In Vitro And In Silico Studies**. *Scientific Reports*, 7(1).doi:10.1038/s41598-017-06445-z url to share this paper: [sci-hub.tw/10.1038/s41598-017-06445-z](https://doi.org/10.1038/s41598-017-06445-z)

Aminabad, N. S., Farshbaf, M., & Akbarzadeh, A. (2018). **Recent Advances of Gold Nanoparticles in Biomedical Applications: State of the Art**. *Cell Biochemistry and Biophysics*. Doi:10.1007/s12013-018-0863-4 url to share this paper:

Antipov, A; Gleb B. Sukhorukov; Edwin Donath; Helmuth Moehwald (2001). "**Sustained Release Properties of Polyelectrolyte Multilayer Capsules**". *J. Phys. Chem. B*. 105: 2281–2284.

Aulton M E (Ed ), 2002. **Pharmaceutics : The Science Of Dosage Form Design. 2 Edn. London.**

Aulton.M.E, Pharmaceutics, **The Science Of Dosage Form Design**, China, Churchill  
Avendano, C. And Menendez, J.C., 2015. *Medicinal Chemistry Of Anticancer Drugs*. 2 Ed. Edn. San Diego, Ca, Usa: Elsevier Science.

Azimuddin, K. And Chamberlain, R.S., 2001. **The surgical management of pancreatic neuroendocrine tumors**. *Surgical clinics of north america*, 81(3), pp. 511-525.

B. S. Chhikara and K. Parang, *Expert Opin. Drug Delivery*, 2010,7, 1399–1414.

Bair, H.E. And Salovey, R., 1969. **The Effect Of Molecular Weight On The Structure And Thermal Properties Of Polyethylene**. *Journal of macromolecular science, part b*, 3(1), pp. 3-18.

Bardeesy, N. & Depinho, R. A, 2002. **Pancreatic Cancer Biology And Genetics.**

Christopher M.

Barnett, C. M., Lees, M. R., Curtis, A. D. M., Lin, P. K. T., Cheng, W. P. and Hoskins, C.

(2013) **Poly(allylamine) Magnetomicelles for Image Guided Drug Delivery.**

*Pharmaceutical Nanotechnology*, 1, pp.1-15.

Barnett, C., Gueorguieva, M., Lees, M., Mcgarvey, D. & Hoskins, C., (2013) **Physical**

**stability, biocompatibility and potential use of hybrid iron oxide-gold nanoparticles**

**as drug carriers.** *Journal of Nanoparticle Research*, 15(6), pp. 1-14.

Basu, H.S., Feuerstein, B.G., Deen, D.F., Lubich, W.P., Bergeron, R.J., Samejima, K. and

MARTON, L.J., 1989. **Correlation between the Effects of Polyamine Analogues on DNA**

**Conformation and Cell Growth.** *Cancer Research*, 49(20), pp. 5591.

Basu, H.S., Marton, L.J., Pellarin, M., Deen, D.F., Mcmanis, J.S., Liu, C.Z., Bergeron, R.J.

& Feuerstein, B.G., 1994. **Design And Testing Of Novel Cytotoxic Polyamine**

**Analogues.** *Cancer Research*, 54(23), Pp. 6210-6214.

Bergeron, R.J. et al., 1988. **Synthetic polyamine analogues as antineoplastics.** *Journal*

*of medicinal chemistry*, 31(6), pp.1183–90. Available at: [http://www.ncbi.nlm.nih.gov/](http://www.ncbi.nlm.nih.gov/pubmed/3373487)

[pubmed/3373487](http://www.ncbi.nlm.nih.gov/pubmed/3373487).

Berridge, M. et al., 1996. **The biochemical and cellular basis of cell proliferation**

**assays that use tetrazolium salts.** *Biochemica*, (4), pp.4–9.

Berridge, M.V. & Tan, A.S., 1993. **Characterization of the Cellular Reduction of 3(4,5-**

**dimethylthiazol-2-yl)-2,5-diphenyltetrazolium bromide (MTT):** Subcellular

Localization, Substrate Dependence, and Involvement of Mitochondrial Electron

Transport in MTT Reduction. Archives of Biochemistry and Biophysics, 303(2), pp.474–482.

Bi, D., Zhao, L., Yu, R., Li, H., Guo, Y., Wang, X., & Han, M. (2018). **Surface Modification Of Doxorubicin-Loaded Nanoparticles Based On Polydopamine With Ph-Sensitive Property For Tumor Targeting Therapy.** Drug Delivery, 25(1), 564–575. doi:10.1080/10717544.2018.1440447

Biewenga, G.P., Haenen, G.R.M.M. & Bast, A., 1997. **The Pharmacology Of The Antioxidant: Lipoic Acid.** General Pharmacology, 29(3), pp.315–331.

Bildstein, L., Dubernet, C. & Couvreur, P., 2011. **Prodrug-based intracellular delivery of anticancer agents.** Advanced Drug Delivery Reviews, 63(1–2), pp.3–23.

Boyer, C., Teo, J., Phillips, P., Erlich, R. B., Sagnella, S., Sharbeen, G., & Kavallaris, M. (2013). **Effective delivery of siRNA into cancer cells and tumors using well-defined biodegradable cationic star polymers.** Molecular pharmaceutics, 10(6), pp.2435-2444.

Brana, M.F. et al., 2001. **Intercalators as Anticancer Drugs | BenthamScience. Current Pharmaceutical Design, 7(17), pp.1745–1780. Available at: <http://www.eurkaselect.com/65102/article>.**

Brigger, I., Dubernet, C. & Couvreur, P., 2012. **Nanoparticles In Cancer Therapy And Diagnosis.** Advanced drug delivery reviews, 64, pp. 24-36.

C.Y.Zhang,Y.Q.Yang,T.X.Huang,B.Zhao,X.D.Guo, J.F.WangandL.J.Zhang ,**Biomaterials**, 2012, 33, 6273–6283.

Cabral, H. et al., 2011. **Accumulation of sub-100 nm polymeric micelles in poorly permeable tumours depends on size.** *Nature Nanotechnology*, 6(12), pp.815– 823.

Available at: <http://dx.doi.org/10.1038/nnano.2011.166>.

Cai, W. et al., 2008. **Applications of gold nanoparticles in cancer nanotechnology.** *Nanotechnology, science and applications*, 1, pp.17–32. Available at:

<http://www.pubmedcentral.nih.gov/articlerender.fcgi?artid=3781768&tool=pmc>

CancerResearch, 2016. **Cancer statistics for the UK.** *Cancer Research UK*, pp.1– 4.

Available at: <http://www.cancerresearchuk.org/health-professional/cancer-statistics>.

Cao-Milán, R. & Liz-Marzán, L.M., 2014. **Gold nanoparticle conjugates: recent advances toward clinical applications.** *Expert opinion on drug delivery*, 11(5), pp.741–

52. Available at: <http://www.ncbi.nlm.nih.gov/pubmed/24559075>.

Carradori, d., gaudin, a., brambilla, d. & andrieux, k., 2016. **Application of nanomedicine to the cns diseases.** *International review of neurobiology*, 130, pp. 73.

Casals, E., Gonzalez, E. And Puentes, V.F., 2012. **Reactivity Of Inorganic Nanoparticles In Biological Environments: Insights Into Nanotoxicity Mechanisms.** *Journal of physics d: applied physics*, 45(44), pp. 443001.

Block, Seymour Stanton (2001). *Disinfection, Sterilization, & Preservation*. Lippincott Williams & Wilkins. p. 631. ISBN 9780683307405. Archived from the original on 2016-12-20.

Casero, J.A. & Woster, P.M., 2001. **Terminally alkylated polyamine analogues as chemotherapeutic agents.** *Journal of Medicinal Chemistry*, 44(1), pp.1–26.

Casero, R. a & Marton, L.J., 2007. **Targeting polyamine metabolism and function in cancer and other hyperproliferative diseases.** Nature reviews. Drug discovery, 6(5), pp.373–390.

Casero, R.A. & Pegg, A.E., 2009. **Polyamine catabolism and disease.** *The Biochemical journal*, 421(3), pp.323–338. Available at: <http://www.pubmedcentral.nih.gov/articlerender.fcgi?artid=2756025&tool=pmc+entrez&rendertype=abstract>.

Chacko, r.t., ventura, j., zhuang, j. & thayumanavan, s., 2012. **Polymer nanogels: a versatile nanoscopic drug delivery platform.** *Advanced drug delivery reviews*, 64(9), pp. 836-851.

Chang, Y., Liu, N., Chen, L., Meng, X., Liu, Y., Li, Y. & Wang, J., 2012. **Synthesis And Characterization Of DOX-Conjugated Dendrimer-Modified Magnetic Iron Oxide Conjugates For Magnetic Resonance Imaging, Targeting, And Drug Delivery.** *Journal of Materials Chemistry*, 22(19), pp. 9594-961.

Cheng, Y., Xu, Z., Ma, M. & Xu, T. (2007) **Dendrimers As Drug Carriers: Applications In Different Routes Of Drug Administration.** *Journal of pharmaceutical sciences*, 97(1), pp. 123-143.

Cherukuri, P., Glazer, E.S. & Curley, S.A., 2010. **Targeted hyperthermia using metal nanoparticles.** *Advanced Drug Delivery Reviews*, 62(3), pp.339–345.

Chiellini, F. et al., 2016. **Modelling of Pancreatic Ductal Adenocarcinoma *in Vitro* with Three-Dimensional Microstructured Hydrogels.** *RSC Advances*, 6, pp.54226–54235. Available at: <http://dx.doi.org/10.1039/C6RA08420F>

Childs, A.C., Mehta, D.J. & Gerner, E.W., 2003. **Polyamine-dependent gene expression. Cellular and Molecular Life Sciences**, 60(7), pp.1394–1406.

Cobley, C.M. et al., 2010. **Targeting gold nanocages to cancer cells for photothermal destruction and drug delivery.** *Expert opinion on drug delivery*, 7(5), pp.577–587.

Corr, S. A., Rakovich, Y. P., & Gun'ko, Y. K. (2008) **Multifunctional Magnetic-fluorescent Nanocomposites for Biomedical Applications.** *Nanoscale Research Letters*, 3(3), pp.87–104.

Cui, h., chen, z., zhong, s., wooley, k.l. & pochan, d.j., 2007. **Block copolymer assembly via kinetic control.** *Science*, 317(5838), pp. 647-650.

Curtis, A. et al., 2015. **Heat Dissipation of Hybrid Iron Oxide-Gold Nanoparticles in an Agar Phantom.** *J Nanomed Nanotechnol*, 6. Available at: <http://dx.doi.org/10.4172/2157-7439.1000335>.

da Costa, A.O. et al., 1999. **Comparative analysis of three methods to assess viability of mammalian cells in culture.** *Biocell*, 23(1), pp.65–72. Available at: <http://www.ncbi.nlm.nih.gov/pubmed/10904534>.

David, K.I., Jaidev, L.R., Sethuraman, S. & Krishnan, U.M. (2015) **Dual drug loaded chitosan nanoparticles—sugar-coated arsenal against pancreatic cancer.** *Colloids & Surfaces B: Biointerfaces*, 135, pp. 689-698.

Day, E.S. et al., 2010. **Antibody-conjugated gold-gold sulfide nanoparticles as multifunctional agents for imaging and therapy of breast cancer.** *International Journal of Nanomedicine*, 5(1), pp.445–454.

De Ilarduya, C. T. D. & Gonzalez-Aseguinolaza, G. (2012) '**Nanocarriers For Gene Delivery**', In R. Srirajakanthan And V. R. Preedy. *Nanomedicine and cancer*. Enfield: Science publishers.

Dimou, A., Syrigos, K. N., & Saif, M. W. (2012). **Overcoming the stromal barrier: technologies to optimize drug delivery in pancreatic cancer**. *Therapeutic Advances in Medical Oncology*, 4(5), 271–279.

Ding, j., shi, f., li, d., chen, l., zhuang, x. & chen, x., 2013. **Enhanced endocytosis of acid-sensitive doxorubicin derivatives with intelligent nanogel for improved security and efficacy**. *Biomater. Sci*, 1(6), pp. 633-646.

Does Not Equal Cure. *Surgery*, 152(3 Suppl 1), pp.S43-9. Available at: Ferrone, C.R. et al., 2012. **Pancreatic Ductal Adenocarcinoma: long-term survival**.

Dreaden, E.C. et al., 2012. **Size matters: gold nanoparticles in targeted cancer drug delivery**. *Therapeutic Delivery*, 3(4), pp.457–478.

Dreher, M.R. et al., 2006. **Tumor vascular permeability, accumulation, and penetration of macromolecular drug carriers**. *Journal of the National Cancer Institute*, 98(5), pp.335–344.

Du, Yinfeng|Chen, Wei|Zheng, Meng|Meng, Fenghua|Zhong, Zhiyuan, 2012. **PH-Sensitive Degradable Chimaeric Polymersomes For The Intracellular Release Of Doxorubicin Hydrochloride**. *Biomaterials*, 33(29), pp. 7291-7299.

Duncan, R. (2006) **Polymer conjugates as anticancer nanomedicines**. *Nature Reviews Cancer*, 6(9), pp. 688-701.

Emanuela, B. et al., 2012. **Synthetic polyamines as potential amine oxidase inhibitors: A preliminary study.** *Amino Acids*, 42(2–3), pp.913–928.

entrez&rendertype=abstract.

Ernst, R.R., Bodenhausen, G. & Wokaun, A., 1987. **Principles of nuclear magnetic resonance in one and two dimensions.** In *Principles of Nuclear Magnetic Resonance in One and Two Dimensions*. pp. 50–60.

Feng, X., Lv, F., Liu, L., Tang, H., Xing, C., Yang, Q. & Wang, S. (2010) **Conjugated Polymer Nanoparticles for Drug Delivery and Imaging.** *Applied materials & interfaces*, 2(8), pp. 2429-2435.

Ferreira, D., Adegá, F. & Chaves, R., 2013. **The Importance of Cancer Cell Lines as *in vitro* Models in Cancer Methylation Analysis and Anticancer Drugs Testing.** In *Oncogenomics and Cancer Proteomics - Novel Approaches in Biomarkers Discovery and Therapeutic Targets in Cancer*.

Feuerstein, B.G., Williams, L.D., BASU, H.S. & Marton, L.J., 1991. **Implications and concepts of polyamine-nucleic acid interactions.** *Journal of cellular biochemistry*, 46(1), pp. 37-47.

Fonseca, A. C., Serra, A. C., & Coelho, J. F. (2015). **Bioabsorbable polymers in cancer therapy: latest developments.** *EPMA Journal*, 6(1), pp.1-18.

Gad, A., Kydd, J., Piel, B. & Raj, P., 2016. **Targeting Cancer Using Polymeric Nanoparticle Mediated Combination Chemotherapy.** *International Journal Of Nanomedicine And Nanosurgery*, 2(3),.

Garrec, D. L., Ranger, M. & Leroux, J. (2004) **Micelles in Anticancer Drug Delivery**. *Healthcare Technology Review*, 2(1), pp.15-42.

Gaucher.G, Dufresne.M-H, Sant.V.P, King.N, Maysinger.D, Leroux. J-C, 2005, **Block Copolymer Micelles**: preparation, characterization and application in drug delivery, *Journal of Controlled Release*, 109, pp 169-188. doi:10.1016/j.jconrel.2005.09.034.

Geall, A.J. & Blagbrough, I.S., 2000. **Homologation of polyamines in the rapid synthesis of lipo spermine conjugates and related lipo plexes**. *Tetrahedron*, 56(16), pp.2449–2460.

Gibaldi, M., 1991. **Biopharmaceutics And Clinical Pharmacokinetics**. United states

Gil, E. S. & Hudson, S. M. (2004) **Stimuli-responsive polymers and their bioconjugates**. *Progress in polymer science*, 29, pp. 1173-1222.

Gohy, I.;F. (N.D.). **Block Copolymer Micelles**. *Advances in polymer science*, 65–136. Doi:10.1007/12\_048 Url to share this paper: [sci-hub.tw/10.1007/12\\_048](http://sci-hub.tw/10.1007/12_048)

Goon, I.Y. *et al.*, 2009. **Fabrication and dispersion of gold-shell-protected magnetite nanoparticles**: Systematic control using polyethyleneimine. *Chemistry of Materials*, 21(4), pp.673–681

Gorąca, A. *et al.*, 2011. **Lipoic Acid - Biological Activity And Therapeutic Potential**. *Pharmacological reports* : PR, 63(4), pp.849–58. Available at: <http://www.ncbi.nlm.nih.gov/pubmed/22001972>.

Govender, T., Stolnik, S., Garnett, M.C., Illum, L. & Davis, S.S., 1999. **Nanoparticles Prepared By Nanoprecipitation**: Drug Loading And Release Studies Of A Water Soluble Drug. *Journal Of Controlled Release*, 57(2), pp. 171-185.

Greco, F. And Vicent, M.J. (2009) **Combination therapy**: Opportunities and challenges for polymer–drug conjugates as anticancer nanomedicines. *Advanced Drug Delivery Reviews*, **61**(13), pp. 1203-1213.

Gu, J., Cheng, W.P., Hoskins, C., Lin, P.K.T., Zhao, L., Zhu, L., Qu, X. And Yang, Z. (2011) **Nano self-assemblies based on cholate grafted poly-L-lysine enhanced the solubility of sterol-like drugs**. *Journal of microencapsulation*, **28**(8), pp. 752-762.

Gu, X. F., Karnik, R., Wang, A. Z., Alexis, F., Levy-Nissenbaum, E., Hong, S., Robert S. Langer, R.S., & Omid C. Farokhzad, O.C. (2007) **Targeted nanoparticles for cancer therapy**. *Nanotoday* 2(3), pp.14-21.

Guo, Y. *et al.*, 2013. **Photothermal ablation of pancreatic cancer cells with hybrid iron-oxide core gold-shell nanoparticles**. *International Journal of Nanomedicine*, 8, pp.3437–3446.

Hart, K.E., Abbott, L.J., Lísal, M. And Colina, C.M. (2014) **Morphology and molecular bridging in comb- and star-shaped diblock copolymers**. *Journal of Chemical Physics*, **141**(20), pp. 1-9.

He, C. & Li, W. (2015) **Hybrid Nanoparticles For Cancer Imaging And Therapy**. In: C.A.Mirkin *et al.* (eds). *Nanotechnology-Based precision for the Detection and Treatment of Cancer*. Cancer Treatment and Research.

Hermanson, G. T. (2013). Zero-Length Crosslinkers. *Bioconjugate Techniques*, 259–273. doi:10.1016/b978-0-12-382239-0.00004-2.

Hezel, A.F. *et al.*, 2006. **Genetics and biology of pancreatic ductal adenocarcinoma**. **Genetics and biology of pancreatic ductal adenocarcinoma**. *Genes & Development*, 1(30), pp.1218–1249. Available at:

<http://genesdev.cshlp.org/content/20/10/1218.full.pdf+html>.

Hidalgo, M. (2010). **Pancreatic Cancer**. *New England Journal of Medicine*, 362(17), 1605–1617. doi:10.1056/nejmra0901557

Hillaireau, H. & Couvreur, P. (2006) '**Polymer Nanoparticles As Drug Carriers**'. In: F. I. Uchegbu and A. G. Schätzlein. Eds. *Polymers In Drug Delivery*. Boca Raton, FL: CRC/Taylor & Francis.

Hortobágyi, g., 1997. **Anthracyclines in the treatment of cancer**. *Drugs*, 54(s4), pp. 1-7.

Hoskins, C. *et al.*, 2012. **Hybrid gold-iron oxide nanoparticles as a multifunctional platform for biomedical application**. *Journal of Nanobiotechnology*, 10(27), pp.1–12.

Hoskins, C., 2010. **The Use Of Novel Poly(Allylamine) Based Amphiphilic Polymers For Drug Delivery**, Proquest Dissertations Publishing.

Hoskins, C., Cuschieri, A. and Wang, L. (2012) **The cytotoxicity of polycationic iron oxide nanoparticles**: Common endpoint assays and alternative approaches for improved understanding of cellular response mechanism. *Journal of Nanobiotechnology*, **10**(1), pp. 1-11.

Hoskins, C., Cuschieri, A., Wang, L. (2012a). **Cytotoxicity of polycationic iron oxide nanoparticles: Common endpoint assays and alternative approaches for improved understanding of cellular response mechanism**. *J Nanobiotechnol*, 10:15.

Hoskins, C., Min, Y., Gueorguieva, M., McDougall, C., Volovick, A., Prentice, P., Wang, Z., Melzer, A., Cuschieri, A., Wang, L. (2012b). **Hybrid gold-iron oxide nanoparticles as a multifunctional platform for biomedical application.** *Journal of Nanobiotechnology*, 10:27.

Hoskins, C., Ouaisi, M., Lima, S., Cheng, W., Loureiro, I., Mas, E., Lombardo, D., Cordeiro-Da-Silva, A., Ouaisi, A. And Kong Thoo Lin, P. (2010) ***In vitro* and *In vivo* Anticancer Activity of a Novel Nano-sized Formulation Based on Self-assembling Polymers Against Pancreatic Cancer.** *Pharmaceutical research*, 27(12), pp. 2694-2703.

Hoskins, C., Yue Min, Gueorguieva, M., Mcdougall, C., Volovick, A., Prentice, P., Wang, Z., Melzer, A., Cuschieri, A. and Wang, L. (2012) **Hybrid gold-iron oxide nanoparticles as a multifunctional platform for biomedical application.** *Journal of Nanobiotechnology*, 10(1), pp. 27-38.

Hoskins, C., Lin, P., Tetley, L. And Cheng, W., 2012. **The Use Of Nano Polymeric Self-Assemblies Based On Novel Amphiphilic Polymers For Oral Hydrophobic Drug Delivery.** *Pharmaceutical research*, 29(3), pp. 782-794.

<http://www.ncbi.nlm.nih.gov/pubmed/22763261><http://www.pubmedcentral.nih.gov/articlerender.fcgi?artid=2756025&tool=pmc>

<http://www.pubmedcentral.nih.gov/articlerender.fcgi?artid=2756025&tool=pmc>

entrez&rendertype=abstract.

Huang, X. *et al.*, 2007. **Gold nanoparticles: interesting optical properties and recent applications in cancer diagnostics and therapy.** *Nanomedicine* (London, England), 2(5), pp.681–693.

Hruban, R. H., Fukushima, N., & Wilentz, R. E. (2009). Pancreas. Modern surgical pathology, 867–901. Doi:10.1016/b978-1-4160-3966-2.00026-6

J. C. Zhang, J. X. Ding, C. S. Xiao, C. L. He, X. L. Zhuang, Y. N. Yang & X. S. Chen, Chem. J. Chin. Univ., 2012,22, 2809–2815.

J. K. Oh, R. Drumright, D. J. Siegwart & K. Matyjaszewski, **Prog.Polym. Sci.**, 2008,33, 448–477.

JAMBHRUNKAR, S., QU, Z., POPAT, A., KARMAKAR, S., XU, C. & YU, C., 2014. **Modulating *In Vitro* Release And Solubility Of Griseofulvin Using Functionalized Mesoporous Silica Nanoparticles.** *Journal Of Colloid And Interface Science*, 434, pp. 218-225.

James, H, P., John, R., Alex, A. & Anoop, K.R. (2014) **Smart polymers for the controlled delivery of drugs – a concise overview.** *Acta Pharmaceutica Sinica B*, 4(2), PP.120–127

Jawhar Jawahar, N & Meyyanathan, SN. (2012) **polymeric nanoparticles for drug delivery and targeting: a comprehensive review.** *International Journal of Health & Allied Sciences*, 1 (4), PP.217-223.

Jeffrey D Clogston & Anil K Patri, 2011. **Zeta Potential Measurement.** *Methods In Molecular Biology* (Clifton, N.J.), 697, pp. 63-70.

Jeong, B. and Gutowska, A. (2002) Lessons from nature: **stimuli-responsive polymers and their biomedical applications.** *Trends in biotechnology*, 20(7), pp. 305-311.

Jiang, P., Yu, C., Yen, C., Woo, C.W., Lo, S., Huang, Y., Hong, J. & Chiang, C. (2015) **Irradiation Enhances the Ability of Monocytes as Nanoparticle Carrier for Cancer Therapy.** *PLoS ONE*, 10(9), pp. 1-15.

Kaur, P. I., Bhandari, B. R., Bhandari, B. S., Kaur, P. K.V., Bhandari, R., Bhandari, S., & Kakkar, V. (2008) **Potential of solid lipid nanoparticles in brain targeting.** *Journal of Controlled Release* 127 (2008) 97–109.

Kesharwani, P., Xie, L., Banerjee, S., Mao, G., Padhye, S., Sarkar, F.H. & Iyer, A.K. (2015) **Hyaluronic acid-conjugated polyamidoamine dendrimers for targeted delivery of 3,4-difluorobenzylidene curcumin to CD44 overexpressing pancreatic cancer cells.** *Colloids and Surfaces B: Biointerfaces*, **136**, pp. 413-423.

Khan, D.R. (2010) The Use of **Nanocarriers for Drug Delivery in Cancer Therapy.** *Journal of Cancer Science & Therapy*, 2, pp.058-062. doi:10.4172/1948-5956.1000024.

Khan, S., Chauhan, N., Yallapu, M.M., Ebeling, M.C., Balakrishna, S., Ellis, R.T., Thompson, P.A., Balabathula, P., Behrman, S.W., Zafar, N., Singh, M.M., Halaweish, F.T., Jaggi, M. & Chauhan, S.C. (2015) **Nanoparticle formulation of ormeloxifene for pancreatic cancer.** *Biomaterials*, **53**, pp. 731-743.

Kim, B.-S., Qiu, J.-M., Wang, J.-P., and Taton, T. A. (2005) **Magnetomicelles: Composite Nanostructures from Magnetic Nanoparticles and Cross-Linked Amphiphilic Block Copolymers.** *Nano Letters*, **5**(10), pp. 1987-1991.

Kim, G., Li, Y., Chu, Y., Cheng, S., Zhang, X. and Zhuo, R. (2008) **A nano-sized, thermo-sensitive drug carrier: self-assembled Fe.** *Journal of Biomaterials Science -- Polymer Edition*, **19**(9), pp. 1249-1259.

Kim, J.O., Oberoi, H.S., Desale, S., Kabanov, A.V. And Bronich, T.K. (2011) **Polypeptide nanogels with hydrophobic moieties in the cross-linked ionic cores: synthesis, characterization & implications for anticancer drug delivery to Tumors.** *Journal of drug targeting*, **21**(10), pp. 981-993.

Kirkwood, J. M., Butterfield, L. H., Tarhini, A. A., Zarour, H., Kalinski, P., & Ferrone, S. (2012). **Immunotherapy of cancer in 2012**. *CA: A Cancer Journal for Clinicians*, 62(5), 309–335. doi:10.3322/caac.20132

Kumar, A., 2013. **Nanomedicine in drug delivery**. Boca Raton, Florida: CRC Press.

Kung,H.H.,1997. **Effects Of Molecular Weight, Polydispersity And Solution Viscosity Of Cellulose Acetate Butyrate On Properties And Release Characteristics Of Ascorbyl Palmitate Microcapsules**.

Kusano, T. *et al.*, 2007. Advances in polyamine research in 2007. *Journal of Plant Research*, 120(3), pp.345–350.

LAKANEN, J.R., COWARD, J.K. and PEGG, A.E., 1992. **alpha.-Methyl polyamines: metabolically stable spermidine and spermine mimics capable of supporting growth in cells depleted of polyamines**. *Journal of medicinal chemistry*, 35(4), pp. 724-734.

Larson, N. & Ghandehari, H. (2012) **Polymeric Conjugates for Drug Delivery**. *Chemistry of Materials*, 24(5), pp. 840-853.

Lee, W., Loo, C., Traini, D. & Young, P.M. (2015) **Inhalation of nanoparticle-based drug for lung cancer treatment: Advantages and challenges**. *Asian Journal of Pharmaceutical Sciences*, 10(6), pp. 481-489.

Li, C. & Wallance, S. (2007) **Polymer-drug conjugates: Recent development in clinical oncology**. *Advanced drug delivery reviews*, (doi:10.1016/j.addr.), 886-898.

Li, L., Wang, Y., Ji, F., Wen, Y., Li, J., Yang, B. & Yao, F. (2014) **Synthesis and characterization of dendritic star-shaped zwitterionic polymers as novel anticancer**

**drug delivery carriers.** *Journal of Biomaterials Science -- Polymer Edition*, **25**(14/15), pp. 1641-1657.

Lin, C. & Symchowicz, S., 1975. **Absorption, Distribution, Metabolism, And Excretion Of Griseofulvin In Man And Animals.** *Drug Metabolism Reviews*, 4(1), pp. 75-95.

Lin, C., & Symchowicz, S. (1975). **Absorption, Distribution, Metabolism, and Excretion of Griseofulvin in Man and Animals.** *Drug Metabolism Reviews*, 4(1), 75–95.

Liu, Y., Miyoshi, H. & Nakamura, M. (2007) **Nanomedicine for drug delivery and imaging:** A promise avenue for cancer therapy and diagnosis using targeted functional nanoparticles. *Int. J. Cancer*, 120, 2527-2537.

Livingstone, 1998 .

Loo, C., Lin, A., Hirsch, L., Lee, M., Barton, J., Halas, N., West, J. & Drezek, R., 2004. **Nanoshell-Enabled Photonics-Based Imaging And Therapy Of Cancer.** *Technology In Cancer Research & Treatment*, **3**(1), pp. 33-40.

Louquet, S., Rousseau, B., Epherre, R., Guidolin, N., Goglio, G., Mornet, S., Duguet, E., Lecommandoux, S. & Schatz, C., 2012. **Thermoresponsive Polymer Brush-Functionalized Magnetic Manganite Nanoparticles For Remotely Triggered Drug Release.** *Polymer chemistry*, **3**(6), pp. 1408-1417.

Lü T., Shan G., Shang S. **Stability of two-phase polymerization of acrylamide in aqueous poly(ethylene glycol) solution** . *Journal of Applied Polymer Science*, 2011, 122(2): 1121-1133

LU, X., WU, D., LI, Z. and CHEN, G., 2011. **Polymer Nanoparticles. Progress in Molecular Biology and Translational Science.** Netherlands: pp. 299-323.

Lu, X., Wu, D., Li, Z. & Chen, G., 2011. **Polymer Nanoparticles. Progress In Molecular Biology And Translational Science.** Netherlands: pp. 299-323.

Maeda, H. (2015). **Toward a full understanding of the EPR effect in primary and metastatic tumors as well as issues related to its heterogeneity.** *Advanced Drug Delivery Reviews*, 91, 3–6. doi:10.1016/j.addr.2015.01.002.

Malekigorji, M., Curtis, A. DM & Hoskins, C. (2014) **The Use of Iron Oxide Nanoparticles for Pancreatic Cancer Therapy.** *Journal of Nanomedicine Research* 1(1), pp.1-12.

Maltesh, C., Xu, Q., Somasundaran, P., Benton, W.j. and Nguyen Hung, 1992. **Aggregation Behavior Of And Surface Tension Reduction By Comblike Amphiphilic Polymers.** *Langmur* , 8(6), pp. 1511-1513.

Malvezzi, M., Bertuccio, P., Rosso, T., Rota, M., Levi, F., La Vecchia, C. & Negri, E., 2015. **European Cancer Mortality Predictions For The Year 2015: Does Lung Cancer Have The Highest Death Rate In Eu Women?** *Annals Of Oncology : Official Journal Of The European Society For Medical Oncology*, 26(4), Pp. 779-786.

MASKOS, M. and STAUBER, R., 2011. **Characterization of Nanoparticles in Biological Environments.**

Maskos, M., & Stauber, R. H. (2011). Characterization of Nanoparticles in Biological Environments. *Comprehensive Biomaterials*, 329–339. *Nature reviews. Cancer*, 2(12), pp.897–909.

Mccarroll, J., Teo, J., Boyer, C., Goldstein, D., Kavallaris, M. & Phillips, P.A. (2014) **Potential applications of nanotechnology for the diagnosis and treatment of pancreatic cancer.** *Frontiers in Physiology*, **4/5**, pp. 1-10.

Meng, H. & Li, G. (2013) **A review of stimuli-response shape memory polymer composites.** *Polymer*, **54**, pp. 2199-2221.

Miragoli, M., Ceriotti, P., Iafisco, M., Vacchiano, M., Salvarani, N., Alogna, A., Carullo, P., Ramirez-Rodríguez, G.B., Patrício, T., Esposti, L.D., Rossi, F., Ravanetti, F., Pinelli, S., Alinovi, R., Erreni, M., Rossi, S., Condorelli, G., Post, H., Tampieri, A. & Catalucci, D., 2018. **Inhalation Of Peptide-Loaded Nanoparticles Improves Heart Failure.** *Science Translational Medicine*, **10(424)**, Pp. Ean6205.

Mishra, A.K. (2013) **Nanomedicine for drug delivery and therapeutics.** Beverly: Scrivener Publishing.

Moiseeva, E.P. & Manson, M.M., 2009. **Dietary Chemopreventive Phytochemicals: Too Little Or Too Much?.**

Montalbetti, C.A.G.N. & Falque, V., 2005. Amide bond formation and peptide coupling. *Tetrahedron*, **61(46)**, pp.10827–10852.

Mordente, A., Meucci, E., Silvestrini, A., Martorana, G.E. & Giardina, B., 2009. **New Developments In Anthracycline-Induced Cardiotoxicity.**

Moreira, J.C. & Demarquette, N.R., 2001. **Influence Of Temperature, Molecular Weight, And Molecular Weight Dispersity On The Surface Tension Of Ps, Pp, And Pe.** I. Experimental. *Journal of applied polymer science*, **82(8)**, pp. 1907-1920.

Mura, s., Nicolas, j. & Couvreur, p., 2013. **Stimuli-responsive nanocarriers for drug delivery.**

Muth, A. *et al.*, 2014. **Polyamine transport inhibitors: Design, synthesis, and combination therapies with difluoromethylornithine.** *Journal of Medicinal Chemistry*, 57(2), pp.348–363.

Neha, M.D., Pranav, B.P., Anita, P.A. & Vilasrao, J.K. (2013) **Polymeric micelles as a drug carrier for tumor targeting.** *Chronicles of Young Scientists*, 4(2), pp . 94-101.

Nicholson, J.W. & Royal Society of Chemistry. (2012) **The Chemistry Of Polymers. 4th Edn. Cambridge: Royal Society of Chemistry.**

Nowotarski, S.L., Woster, P.M. & Casero, R.A., 2013. **Polyamines And Cancer: Implications For Chemoprevention And Chemotherapy.**

Octavia, y., moens, a.l., krijns, h.j., tocchetti, c.g., gabrielson, k.l. & janssens, s., 2012. **Doxorubicin-induced cardiomyopathy: from molecular mechanisms to therapeutic strategies.** *Journal of molecular and cellular cardiology*, 52(6), pp. 1213-1225.

Pan, x., wang, G., Lay, C.l., Tan, B.H., He, C. & liu, y., 2013. **Photoluminescence From Amino-Containing Polymer In The Presence Of Co<sub>2</sub>: Carbamate Anion Formed as a Fluorophore.** *Scientific reports*, 3(1), pp. 276.

Paramjot, Khan, N.M., Kapahi, H., Kumar, S., Bhardwaj, T.R., Arora, S. And Mishra, N. (2015) **Role of polymer-drug conjugates in organ-specific delivery systems.** *Journal of drug targeting*, 23(5), pp. 387-416.

Park, H., Park, C.b., Tzoganakis, C. & Chen, P., 2007. **Effect Of Molecular Weight On The Surface Tension Of Polystyrene Melt In Supercritical Nitrogen**. *Industrial & engineering chemistry research*, 46(11), pp. 3849-3851.

Parveen, S., & Sahoo, S. K. (2010). **Evaluation of cytotoxicity and mechanism of apoptosis of doxorubicin using folate-decorated chitosan nanoparticles for targeted delivery to retinoblastoma**. *Cancer Nanotechnology*, 1(1-6), 47–62.

Patri, A.K., Majoros, I.J. & Baker Jr, J.R. (2002) **Dendritic polymer macromolecular carriers for drug delivery**. *Current opinion in chemical biology*, 6(4), pp. 466-471.

Peer, D., Karp, J.M., Seungpyo Hong, Farokhzad, O.C., Margalit, R. & Langer, R. (2007) **Nanocarriers as an emerging platform for cancer therapy**. *Nature Nanotechnology*, 2(12), pp. 751-760.

Pegg, a.e., 1988. **Polyamine metabolism and its importance in neoplastic growth and as a target for chemotherapy**. *Cancer research*, 48(4), pp. 759-774.

Peng Zhang, Qinglin Guo, Jinglin Tao, Dehua Ma & Yedan Wang, 2019. **Aging Mechanism Of A Diatomite-Modified Asphalt Binder Using Fourier-Transform Infrared (FTIR) Spectroscopy Analysis**. *Materials*, 12(6), pp. 988.

Perera-Bel, J., Hutter, B., Heining, C., Bleckmann, A., Fröhlich, M., Fröhling, S., ... Beißbarth, T. (2018). **From somatic variants towards precision oncology: Evidence-driven reporting of treatment options in molecular tumor boards**. *Genome Medicine*, 10(1). doi:10.1186/s13073-018-0529-2

Phillips, W.T., Bao, A., Brenner, A.J. & Goins, B.A. (2014) **Image-Guided Interventional Therapy For Cancer With Radiotherapeutic Nanoparticles**. *Advanced Drug Delivery Reviews*, **76**, pp. 39-59.

Pinkernelle, J., Calatayud, P., Goya, G. F., Fansa, H. & Keilhoff, G. (2012) **Magnetic nanoparticles in primary neural cell cultures are mainly taken up by microglia**. *BMC Neuroscience*, **13**(1), pp. 32-48.

Prabhu , R. H., Patravale , V.B., & Joshi, M. D. (2015). **Polymeric nanoparticles for targeted treatment in oncology: current insights**. *International Journal of Nanomedicine* ,pp.1001-1018

Rangel-Yagui, C. O., Hsu, H. W. L., Pessoa-Jr, A., & Tavares, L. C. (2005). **Micellar solubilization of ibuprofen**: influence of surfactant head groups on the extent of solubilization. *Revista Brasileira de Ciências Farmacêuticas*,**41**(2), pp.237-246.

Reckamp, K. L., Melnikova, V. O., Karlovich, C., Sequist, L. V., Camidge, D. R., Wakelee, H., ... Gadgeel, S. (2016). **A Highly Sensitive and Quantitative Test Platform for Detection of NSCLC EGFR Mutations in Urine and Plasma**. *Journal of Thoracic Oncology*, **11**(10), 1690–1700.

Reddy, L.H., Meda, N. & Murthy, R.R., 2005. **Rapid And Sensitive Hplc Method For The Estimation Of Doxorubicin In Dog Blood--The Silver Nitrate Artifact**. *Acta Pharmaceutica* (Zagreb, Croatia), **55**(1), pp. 81.

Roach, P., MCGarvey, D.J., Lees, M.R. & Hoskins, C. (2013) **Remotely Triggered Scaffolds for Controlled Release of Pharmaceuticals**. *International Journal of Molecular Sciences*, **14**(4), pp. 8585-8602.

Robinson, B. J., Ebert, T. J., O'Brien, T. J., Colinco, M. D., & Muzi, M. (1997). **Mechanisms whereby Propofol Mediates Peripheral Vasolidation in Humans.** *Anesthesiology*, 86(1), 64–72.

Rozga-Wijas, K., Stanczyk, W.A., Kurjata, J. & Kazmierski, S. (2015) **Star-Shaped and Linear POSS-Polylactide Hybrid Copolymers.** *Materials (1996-1944)*, 8(7), pp. 4400-4420.

RYAN, D.P., HONG, T.S. & BARDEESY, N., 2014. **Pancreatic adenocarcinoma.** *The New England journal of medicine*, 371(11), pp. 1039-1049.

Santos M. S, Tavares F. W, Biscaia Jr E. C, (2016), **Molecular thermodynamics of micellization: micelle size distributions and geometry transitions**, *Brazilian Journal of Chemical Engineering*, Volume 33, Issue 3, 515 – 523.

Satchi-Fainaro, R. & Duncan, R. (2006) **Polymer therapeutics II; polymers as drugs, conjugates and gene delivery systems.** Berlin: Springer.

SAVJANI, K.T., GAJJAR, A.K. & SAVJANI, J.K., 2012. **Drug Solubility: Importance And Enhancement Techniques.** *ISRN pharmaceutics*, 2012, pp. 195727.

Schimdt, C. & Bodmeier, R. (1999) **Incorporation of polymeric nanoparticles into solid dosage forms.** *Journal of controlled release*, 57, pp. 115-125.

Schmaljohann, D. (2006) **Thermo- and pH-responsive polymers in drug delivery.** *Advanced drug delivery*, 58, pp.1655-1670.

Schmaljohann, D., 2006. **Thermo- And Ph-Responsive Polymers In Drug Delivery.** *Advanced Drug Delivery Reviews*, 58(15), pp. 1655-1670.

Sebel, PS; Lowden, JD (1989). "**Propofol: A New Intravenous Anesthetic**". **Anesthesiology**. 71 (2): 260

Seiler, n., 2005. **Pharmacological aspects of cytotoxic polyamine analogs and derivatives for cancer therapy**. *Pharmacology and therapeutics*, **107**(1), pp. 99-119.

Shah, M., Agrawal, Y.K., Garala, K. And Ramkishan, A. (2012) **Solid Lipid Nanoparticles of a Water Soluble Drug, Ciprofloxacin Hydrochloride**. *Indian Journal of Pharmaceutical Sciences*, **74**(5), pp. 434-442.

Shen, S., Du, X., Liu, J., Sun, R., Zhu, Y. And Wang, J. (2015) **Delivery of bortezomib with nanoparticles for basal-like triple-negative breast cancer therapy**. *Journal of Controlled Release*, **208**, pp. 14-24.

Shrikhande, S. V., Kleeff, J., Reiser, C., Weitz, J., Hinz, U., Esposito, I., ... Büchler, M. W. (2006). **Pancreatic Resection for M1 Pancreatic Ductal Adenocarcinoma**. *Annals of Surgical Oncology*, 14(1), 118–127. doi:10.1245/s10434-006-9131-8.

Shroff, K. & Vidyasagar, A. (2013) **Polymer Nanoparticles: Newer Strategies Towards Targeted Cancer Therapy**. *Physical chemistry and Biophysics*, 3(4), pp. 1-3.

Siegel, R. L., Miller, K. D., & Jemal, A. (2016). **Cancer statistics, 2016**. *CA: A Cancer Journal for Clinicians*, 66(1), 7–30. doi:10.3322/caac.21332

Silverman, R.B. And Holladay, M.W. (2014) **The organic chemistry of drug design and drug action**. 3 edn. San Diego, CA: *Academic Press*.

Singh, R., & Lillard, J. W. (2009). **Nanoparticle-based targeted drug delivery**. *Experimental and molecular pathology*, 86(3), pp.215-223.

SONG, H., BAO, J., WEI, Y., CHEN, Y., MAO, X., LI, J., ... XUE, Y. (2014). **Kaempferol inhibits gastric cancer tumor growth: An *in vitro* and *in vivo* study.** *Oncology Reports*, 33(2), 868–874. doi:10.3892/or.2014.3662

Soppimath, K. S., Aminabhavi, T. M., Kulkarni, A. R. & Rudzinski, W. E. (2001) **Biodegradable polymeric nanoparticles as drug delivery devices.** *Journal of controlled release*, 70, pp.1-20.

Srinivasan, M., Rajabi, M. & Mousa, S.A., 2015. **Multifunctional Nanomaterials And Their Applications In Drug Delivery And Cancer Therapy.** *Nanomaterials (Basel, Switzerland)*, 5(4), pp. 1690-1703.

Sun, H., Meng, F., Cheng, R., Deng, C. & Zhong, Z., 2014. **Reduction-Responsive Polymeric Micelles And Vesicles For Triggered Intracellular Drug Release.** *Antioxidants & Redox Signaling*, 21(5), pp. 755-767.

Surh, Y., 2003. **Cancer Chemoprevention With Dietary Phytochemicals.** *Nature Reviews Cancer*, 3(10), Pp. 768-780.

Swift, I.p., rephaeli, a., nudelman, a., phillips, d.r. & cutts, s.m., 2006. Doxorubicin-dna adducts induce a non-topoisomerase ii-mediated form of cell death. *Cancer research*, 66(9), pp. 4863-4871.

Tansik, G., Yakar, A. & Gündüz, U. (2014) **Tailoring magnetic PLGA nanoparticles suitable for doxorubicin delivery.** *Journal of Nanoparticle Research*, 16(1), pp. 1-13.

Thompson, Ding.C, Qu.X, Yang.Z, Uchegby.I.F, Tetley.L, Cheng.W.P, 2008, **The Effect Of Polymer Architecture On The Nano Self-Assemblies Based On Novel Combshaped Amphiphilic Poly(Allylamine),** *Colloid Polymer Science*, 286, pp 1511-1526

Timothy P. Lodge. (2003) **Block Copolymers: past success and Future Challenges**. *Macromolecular Chemistry and Physics Journal*, 204 (2), pp.2652-73.

Torchilin, V. P. (2006) '**Polymeric Micelles as Pharmaceutical Carriers**'. In: F. I. Uchebue & A. G. Schätzlein. Eds. *Polymers in drug delivery*. Boca Raton, FL: CRC/Taylor & Francis.

Trimaille, T., mondon, k., Gurny, R. & Möller, M., 2006. **Novel Polymeric Micelles For Hydrophobic Drug Delivery Based On Biodegradable Poly(Hexyl-Substituted Lactides)**. *International journal of pharmaceutics*, 319(1), pp. 147-154.

Uchebue, I.F. & Schätzlein, A.G. (2006) **Polymers in drug delivery**. Boca Raton, FL: CRC/Taylor & Francis.

url to share this paper: [sci-hub.tw/10.1016/b978-0-12-382239-0.00004](https://doi.org/10.1016/b978-0-12-382239-0.00004)

Valeur, E. & Bradley, M., 2009. Amide bond formation: beyond the myth of coupling reagents. *Chem Soc Rev*, 38(2), pp.606–631. Available at: <http://www.ncbi.nlm.nih.gov/pubmed/19169468>.

Vicent, M. J., Dieudonne, L., Carbajo, R. J. & Pineda-Lucena, A. (2008) **Polymer conjugates as therapeutics: future trends, challenges and opportunities**. *Informa healthcare review*, 5(5), pp. 593-614.

Vicent, M.J. (2007) **polymer-drug conjugates as modulators of cellular apoptosis**. *The AAPS Journal*, 9(2), pp. E200-E206.

Vicent, M.J. & Duncan, R. (2006) **Polymer conjugates: nano-sized medicines for treating cancer**. *Trends in biotechnology*, 24(1), pp. 39-47.

Vincenzi, B., Frezza, A.M., Santini, D. & Tonini, g., 2010. **New therapies in soft tissue sarcoma**. *Expert opinion on emerging drugs*, 15(2), pp. 237-248.

Vittorio, O., Voliani, V., Faraci, P., Karmakar, B., Iemma, F., Hampel, S., Kavallaris, M. & Cirillo, G. (2014) **Magnetic catechin-dextran conjugate as targeted therapeutic for pancreatic tumour cells**. *Journal of drug targeting*, 22(5), pp. 408-415.

Wang, B., Siahaan, T. & Soltero, R. (2005) **Drug delivery;principles and applications**. Hoboken, N.J.: Wiley-Interscience.

Weidner,N, Hasteh,F. **Modern Surgical Pathology** (Second Edition), 2009.

Wissing, S. ., Kayser, O., & Müller, R. . (2004). **Solid lipid nanoparticles for parenteral drug delivery**. *Advanced Drug Delivery Reviews*, 56(9), 1257–1272. doi:10.1016/j.addr.2003.

Wong, R. S. H., & Dodou, K. (2017). **Effect of Drug Loading Method and Drug Physicochemical Properties on the Material and Drug Release Properties of Poly (Ethylene Oxide) Hydrogels for Transdermal Delivery**. *Polymers*, 9(12), 286.

Yan, G., Zhuo, R & Zheng, C. (2007) **Study On The Anticancer Drug 5-Fluorouracil-Conjugated Polyaspartamide Containing Hepatocyte-Targeting Group**. *Journal of Bioactive and Compatible Polymers*, 16, pp. 277-293.

Yancik, R., 2005. **Population Aging And Cancer: A Cross-National Concern**. *Cancer Journal (Sudbury, Mass.)*, 11(6), Pp. 437-441.

Yang F, Jin C, Jiang Y, Li J, Di Y, Ni Q & Fu D. (2011) **Liposome Based Delivery Systems In Pancreatic Cancer Treatment: From Bench To Bedside**. *Cancer treatment reviews*, 37(8), pp. 633-642.

Yasser H . **Polymeric Micelles Of Biodegradable Diblock Copolymers: Enhanced Encapsulation Of Hydrophobic Drugs.** *Materials*, 11(5), pp. 688.

Young, R.J. & Lovell, P.A. (2011) **Introduction to polymers.** 3 edn. Boca Raton, Fla.: Crc.

Yuk, soon hong|oh, keun sang|koo, heebeom|jeon, hyesung|kim, kwangmeyung|kwon, ick chan, 2011. **Multi-core vesicle nanoparticles based on vesicle fusion for delivery of chemotherapeutic drugs.** *Biomaterials*, 32(31), pp. 7924-7931.

Z Iatridi ,Z., & Tsitsilianis,C, 2011. **Water-Soluble Stimuli Responsive Star-Shaped Segmented Macromolecules.** Basel: Mdpi ag.

ZAKARIA, A.D., SALAM, N.F.A., ZAIN, W.Z.W. & HASHIM, M.N., 2013. **A Multidisciplinary Approach in Management of Breast Cancer: Case Study and Literature Reviews.** *Journal of Cancer Therapy*, 4(7), pp. 7-11.

Zakaria, A.D., Salam, N.F.A., Zain, W.Z.W. & Hashim, M.N., 2013. **A Multidisciplinary Approach In Management Of Breast Cancer: Case Study And Literature Reviews.** *Journal Of Cancer Therapy*, 4(7), Pp. 7-11.

Zuccala, E. (2016). Clocking up resistance. **Nature Reviews Cancer**, 16(6), 343–343. Doi:10.1038/nrc.2016.50 .

Zuo, Z., Chen, K., Yu, Z., Zhao, G., Shen, S., Cao, Z., Luo, Y., Wang, Y. & Wang, J. (2016) **Promoting tumor penetration of nanoparticles for cancer stem cell therapy by TGF- $\beta$  signaling pathway inhibition.** *Biomaterials* 82, pp.48-59.